VAPOR-LIQUID EQUILIBRIUM MEASUREMENTS OF NITROGEN-ARGON MIXTURES

BY

CHRISTOPHER D. HUMMEL

A thesis submitted in partial fulfillment of

the requirements for the degree of

MASTER OF SCIENCE

(MECHANICAL ENGINEERING)

at the

UNIVERSITY OF WISCONSIN-MADISON

2016

This thesis has been approved by

Professor John M. Pfotenhauer, Professor of ME	**Date**
Professor Franklin K. Miller, Assistant Professor of ME	**Date**

Abstract

This thesis describes the design of an experimental facility used acquire high-accuracy vapor-liquid equilibrium (VLE) data in binary nitrogen-argon mixtures. Of specific interest are mixtures containing greater than 80% nitrogen, at pressures of less than six bar. VLE data consists of compositions in both the liquid and vapor phases as functions of temperature and pressure. The uncertainty in each of the three types of measurements has been quantified and is presented in this work.

The uncertainty in the temperature measurement varies approximately linearly from 29 to 33 milliKelvin in the temperature range of 75 to 105 Kelvin. The uncertainty in the pressure measurement varies approximately linearly from 2.6 to 3 millibar in the pressure range of one to six bar. The uncertainty in the compositions comes from two sources: the uncertainty in the calibration of the gas chromatograph (GC) and the sample standard deviation. The GC calibration procedure is detailed and the composition uncertainty as a result of calibration amounts to ±0.00312% of the reported composition. The composition uncertainty from the sample standard deviation is dependent on how repeatable the GC injections are for each sample. The sampling uncertainty was the dominant source of uncertainty in the reported composition data.

A detailed experimental procedure is included to provide a means for acquiring repeatable results in the future. This procedure includes techniques for reaching an isothermal equilibrium condition in the VLE cell. It also includes the technique used for taking and measuring vapor and liquid samples from the VLE cell.

VLE data was taken in three separate runs of the experiment. The first run in October 2015 did not provide useful VLE data but did provide much needed insight into the complex operation requirements of the system. The second run in February 2016 provided VLE data for three separate mixtures at a range of controlled temperatures from 84 to 98 Kelvin. The data from the February run is characterized in temperature-composition plots and relative volatility plots. The last run took place in April 2016. This run focused on the repeatability of the sampling technique. The liquid composition data showed considerably more scatter than the vapor data, suggesting room for improvement in the liquid sampling technique.

Comparing the VLE results to past work with nitrogen-argon mixtures, there is room for improvement in the liquid sampling technique as well as the temperature and pressure measurements.

Contents

Table of Figures

List of Tables

1. Introduction

Vapor-liquid equilibrium (VLE) data is critical to many chemical engineering fields. Distillation is a mixture separation process by selective evaporation and condensation. Well understood VLE properties enable a distillation process to be more efficient and more effective (Perry & Green, 2008). Emission monitoring is an important part of responsible chemical manufacturing and processing. Knowing VLE properties of volatile compounds helps to pinpoint the most dangerous parts of a process (Elliott & Lira, 2012). VLE data is also useful in characterizing molecular interactions. These can be extrapolated modestly to correlate experimental data into equations of state for complex systems (Wichterle et al., 2004).

Vapor-liquid equilibrium data for nitrogen-argon mixtures, specifically with low argon concentration, are of interest to the air separation industry. Discrepancies between field measurements and predictive process modeling led to the research outlined in this thesis. The goal of this project was obtain concentration measurements of nitrogen-argon mixtures in vapor-liquid equilibrium. These include temperature, pressure, and compositions of both the liquid and vapor phases. Of specific interest were mixtures containing greater than 80% nitrogen in the pressure range from one to six bars, resulting in a temperature range of 77 to 100 Kelvin.

The design and construction of an experimental apparatus for obtaining high accuracy VLE data will be discussed. Detailed analyses are provided for the uncertainties of each part of the measurement. An experimental procedure is provided for future use of the apparatus. Experimental results and analyses are included as well.

2. Background

2.1 Vapor-Liquid Equilibrium Properties and Theory

When a single component substance, such as water, changes phase from liquid to vapor it does so at a constant temperature that is dependent on the pressure. This is defined by Gibb's Phase Rule shown below.

$$F = C - \Pi + 2$$

In the case of water boiling, the number of components, C, is equal to one. The number of phases, Π, is equal to two. That means the number of intensive properties, F, to fix the state is equal to one. In other words, temperature is dependent on pressure, and vice versa (Klein & Nellis, 2012).

However, if we take a two component mixture and put it into vapor-liquid equilibrium, it will now take two intensive properties to fix the state of this system. In other words, there is a range of temperatures possible for a mixture boiling at a specific pressure.

For a mixture that is in vapor-liquid equilibrium, the mole fraction in the liquid phase $(x_1, x_2, \dots, x_i)$ is typically different than the mole fraction in the vapor phase $(y_1, y_2, \dots, y_i)$. Each of these compositions may differ from the overall mole fraction $(z_1, z_2, \dots, z_i)$ (Elliott & Lira, 2012). The cause of the difference in phase compositions depends on the thermodynamic model used to solve the problem, but even in the simplest case (ideal gas behavior in the vapor and ideal solution in the liquid), the difference in phase compositions is still present (Klein & Nellis, 2012). The ideal model as well as more complex models will be discussed in the following sections.

Ideal Gas Model

Relating the liquid and vapor phases to one another can start to become complicated. To look at one component of the mixture specifically, the VLE K-ratio can be utilized. This is defined below.

$$K_i = \frac{y_i}{x_i}$$

The K-ratio is equal to the vapor phase mole fraction *(y_i)* divided by the liquid phase mole fraction *(x_i)*. If the mixture is an ideal solution that obeys the ideal gas law, the K-ratio can be solved using the equation below. This equation is known as Raoult's Law (Elliott & Lira, 2012).

$$K_i = \frac{y_i}{x_i} = \frac{P_{sat,i}}{P}$$

The saturation pressure is a fluid property based on temperature. For a mixture in vapor-liquid equilibrium that follows these ideal rules, the pressure (P) must be between the saturation pressures of each component of the mixture at the equilibrium temperature. The equation above shows that the mixture component with the higher saturation pressure will make up a larger portion of the vapor phase than it does the liquid phase. The equation also shows that a binary mixture with components of very similar saturation pressures will exhibit smaller differences in the liquid and vapor mole fractions compared to mixtures with very different saturation pressures.

The plot below is called a P-xy diagram. This plot is created for a binary mixture of nitrogen and argon assuming a constant temperature of 85 Kelvin, and ideal gas mixing parameters.

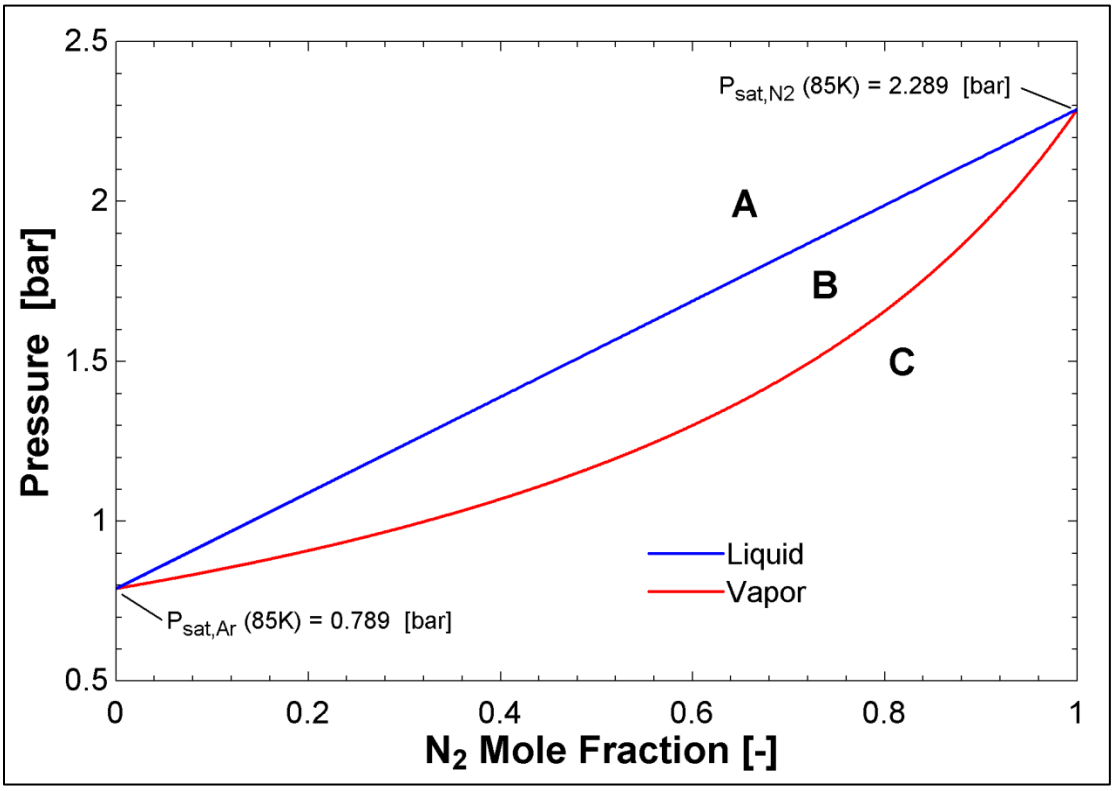

Figure 1: Pressure-composition (P-xy) plot for nitrogen-argon mixture at 85 Kelvin

Region 'A' on this plot is compressed liquid. Region 'C' is superheated vapor. In region 'B', the mixture is in vapor-liquid equilibrium. When the mixture is in region 'B', the composition of the liquid phase will follow the blue line, and the composition of the vapor phase will follow the red line.

We can zoom into this plot to follow what would happen to a mixture of 85% nitrogen and 15% argon as it is compressed from 1.6 bar to 2.2 bar.

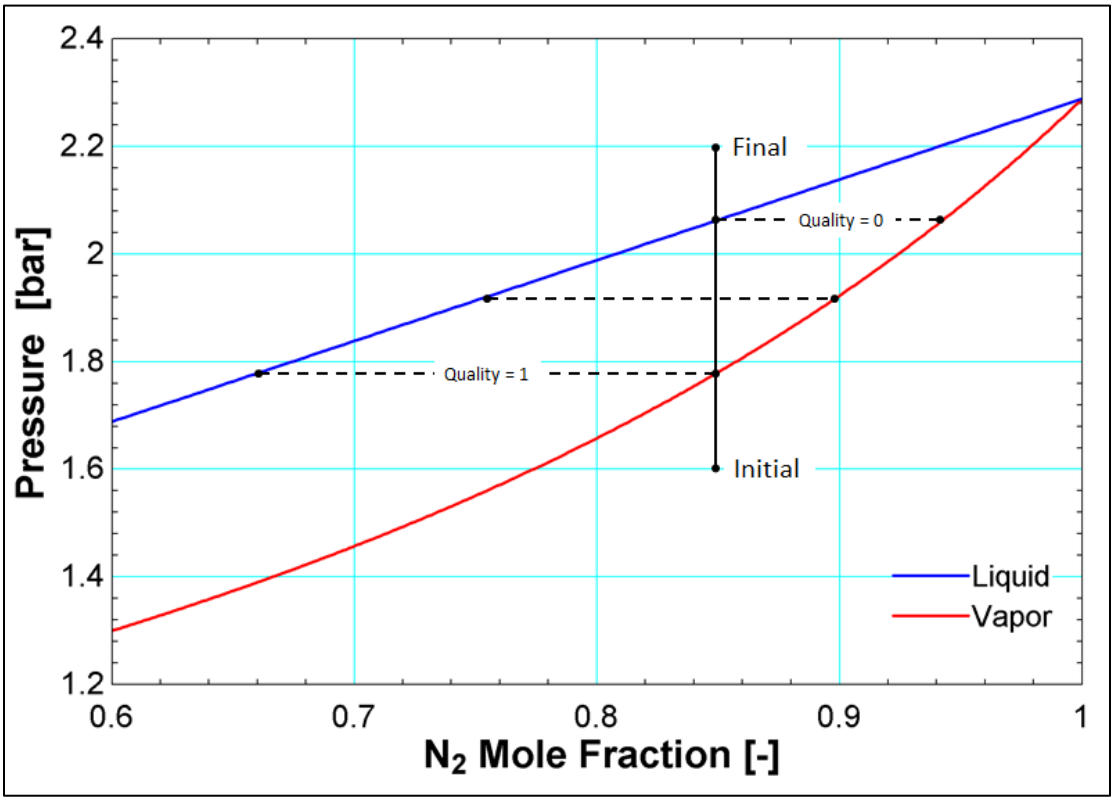

Figure 2: Isothermal compression of 85% nitrogen, 15% argon mixture at 85 Kelvin

In this process, the mixture begins as a superheated vapor. As it is compressed, it will remain a superheated vapor until it reaches the first horizontal dashed line. At this point, the mixture is now in vapor-liquid equilibrium.

Now the mixture is a saturated vapor (quality is equal to one). The composition of the vapor phase is still equal to the overall composition (85% nitrogen), but the first drop of liquid will have a different composition with a lower nitrogen percentage.

As the pressure is increased further, more vapor will convert to liquid, decreasing the quality of the mixture. The vapor composition will deviate from the overall composition, and the liquid composition will approach the overall composition.

The last point of vapor liquid equilibrium is similar to the first. With a quality of zero, the mixture is now a saturated liquid with the liquid composition equal to the overall composition. The last bit of vapor will have a composition with a higher nitrogen percentage compared to the overall composition. As the pressure is further increased, the mixture now becomes a compressed liquid.

Deviations from Ideal Model

The ideal gas model for vapor-liquid equilibrium is a good place to start but not a good place to end. Fugacity is a property that has equivalent units to pressure, but it takes into account the deviations from ideal gas behavior (Klein & Nellis, 2012). The K-ratio for this behavior is shown below.

$$K_i = \frac{y_i}{x_i} = \frac{f_{sat,i}}{f_i}$$

Other mixtures may have components that interact with each other under certain conditions. Using different equations of state for property evaluations may help account for this. Other mixtures may require activity coefficients (γ_i) along with the liquid terms to deal with azeotropic behavior (Elliott & Lira, 2012). Activity coefficients reflect interactions between the components that make up the mixture. They are often not a constant value as the liquid and vapor phases are varied. The K-ratio that takes this into account is shown below.

$$K_i = \frac{y_i}{x_i} = \frac{\gamma_i f_{sat,i}}{f_i}$$

Not surprisingly, there is no general model that works for all types of mixtures. For those applications which require very high accuracy, empirical data is used to characterize adjustable parameters in complex equations of state (Elliott & Lira, 2012). REFPROP is a commercially available program from the National Institute of Standards and Technology (NIST). This program provides high accuracy property data for both pure components and mixtures (Lemmon, Huber, & Mclinden, 2010). Although ideal gas mixture models were used in the design phase of this experiment, the experimental results are all plotted next to theoretical results obtained using REFPROP. The plot below shows two nitrogen-argon P-xy diagrams at different isotherms. The results from the ideal gas model and REFPROP are plotted next to each other.

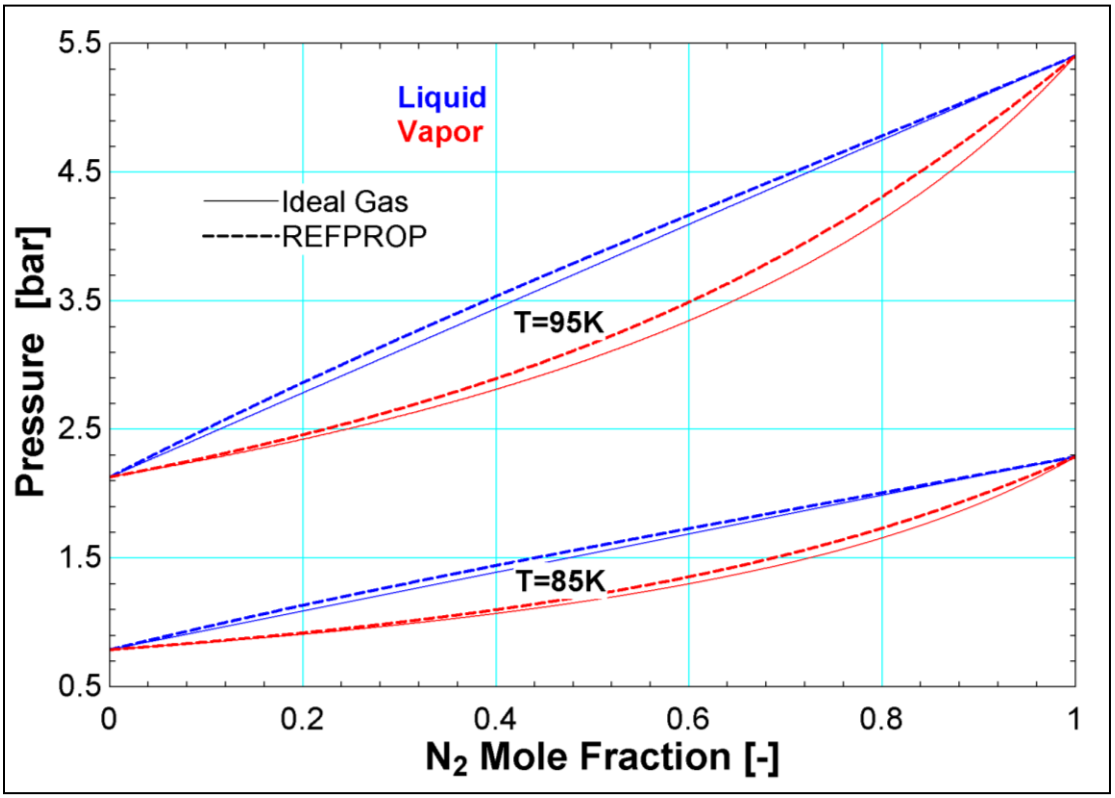

Figure 3: P-xy plots at separate isotherms using ideal gas model and REFPROP

The compositions calculated using REFPROP show some deviation at 85 Kelvin. As the temperature is increased to 95 Kelvin, the deviation between compositions becomes even more pronounced.

Characterizing VLE Data based on Composition

Vapor-liquid equilibrium data can be characterized in a number of ways. Up to this point, the data has been put into pressure composition plots: where temperature is set and pressure is a calculated value. Another common method is a temperature composition plot (T-xy). A T-xy diagram for a nitrogen-argon mixture in a similar range is shown below.

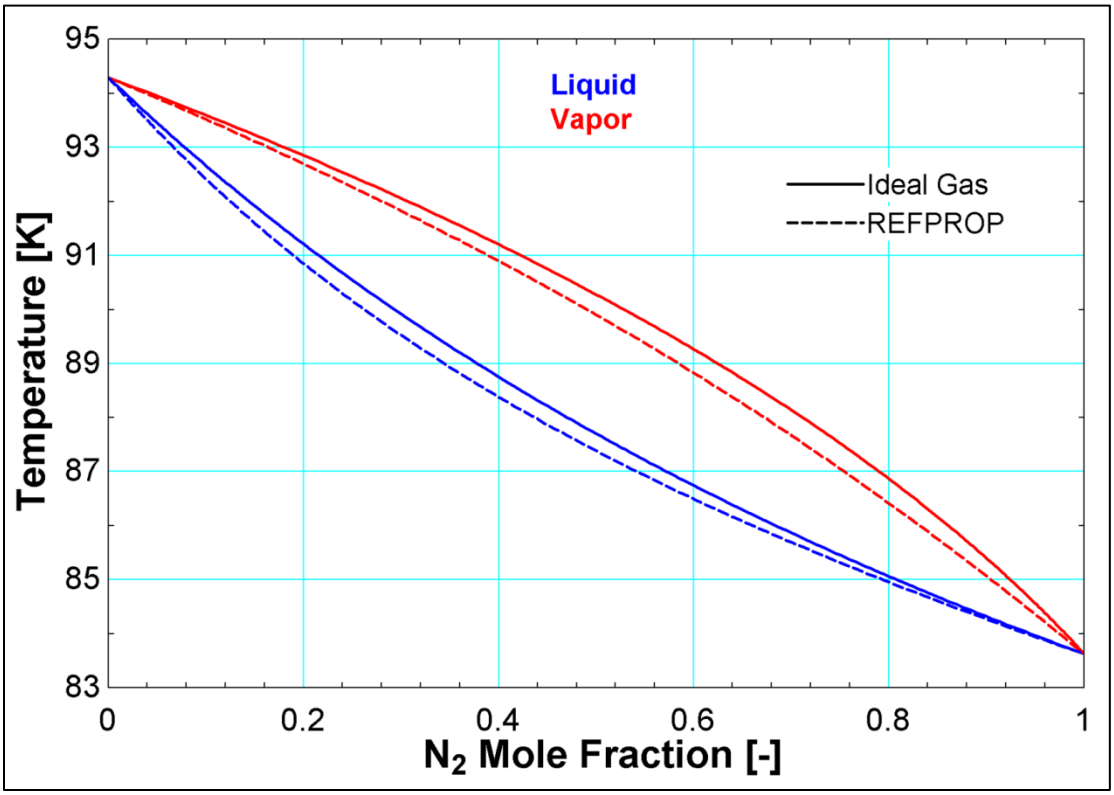

Figure 4: Temperature-composition (T-xy) plot for nitrogen-argon mixture at 2 bar

This plot is made by holding pressure constant instead of temperature. Compared to the P-xy plots shown previously, the slopes of all composition lines have flipped. Also, the liquid composition lines are now below the vapor composition lines.

Composition diagrams are another common method of characterizing VLE data. These simply plot the liquid and vapor phases against other. These diagrams can be created holding either pressure or temperature constant. An example is shown below.

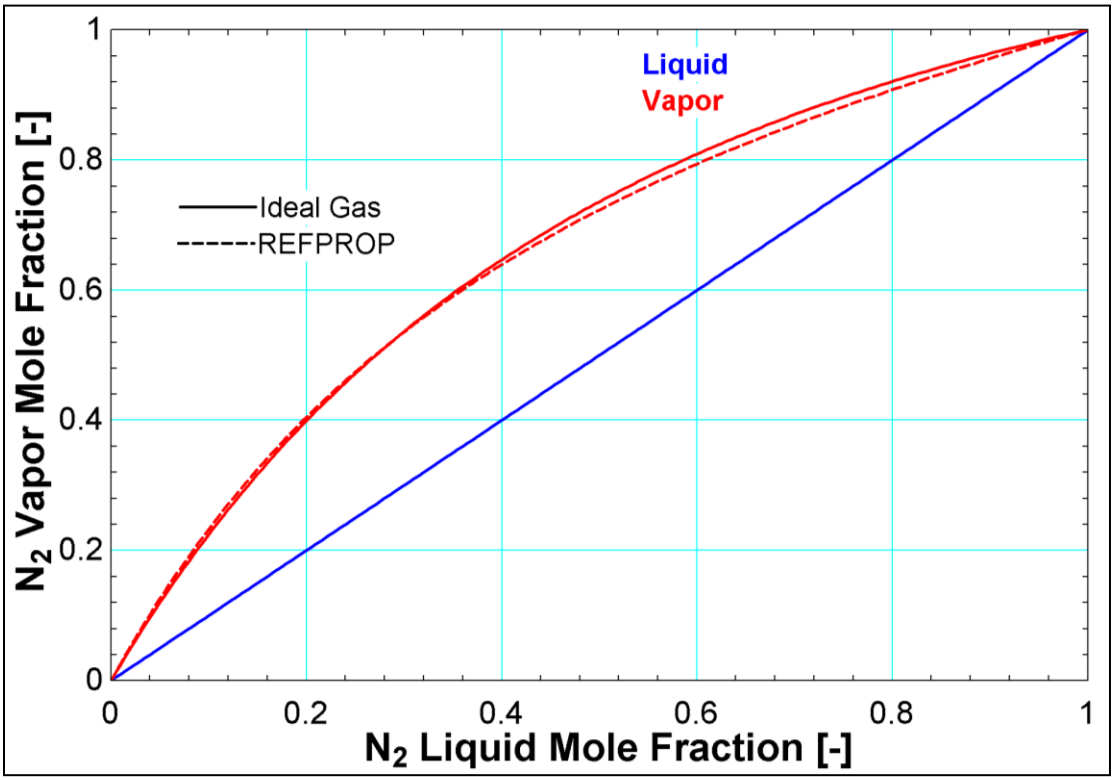

Figure 5: Composition diagram for nitrogen-argon mixture at 2 bar

Pressure-composition, temperature-composition and composition diagrams all help to provide an idea of how a binary mixture will behave. However, their use is limited since one intensive property (either pressure or temperature) must be held constant.

Other Methods of VLE Data Characterization

A P-xy diagram may be used to find the composition of liquid air that will condense on a very cold surface at ambient pressure. This is a single data point that may be of interest to someone who is transferring a liquid cryogen. However, this single data point is of little use to someone attempting to optimize an air separation process. In fact, changing the pressure on a fixed amount of air in vapor-liquid equilibrium will also have an effect on its temperature (and vice versa). For processes like air separation, it is important to see how the liquid composition changes with respect to temperature and pressure to find when it is best to extract one component from the mixture.

Relative volatility is a VLE property that is used by chemical engineers in these types of processes. It is defined by the variable 'α' and it compares two components of a mixture to each other. It uses the K-ratios of each component which have already been defined. For a binary nitrogen-argon mixture, the equation for relative volatility is shown below.

$$\alpha = \frac{K_{N2}}{K_{Ar}} = \frac{y_{N2}/x_{N2}}{y_{Ar}/x_{Ar}}$$

Typically, the component with the higher K-ratio is chosen to be in the numerator to make the value of relative volatility greater than one. Note that for a ternary mixture, three separate relative volatility terms are required to relate all three components to each other.

The component with the higher K-ratio is deemed the more volatile component. As previously stated, this component will occupy a larger portion of the vapor than it will of the liquid. Plotting the relative volatility against temperature or pressure allows one to determine which conditions maximize or minimize this difference; useful information for separation processes.

Relative volatilities of nitrogen-argon mixtures plotted against pressure are shown below. Note that in order to create this plot, one composition parameter must be set. For this result, the liquid phase mole fraction of nitrogen was held constant.

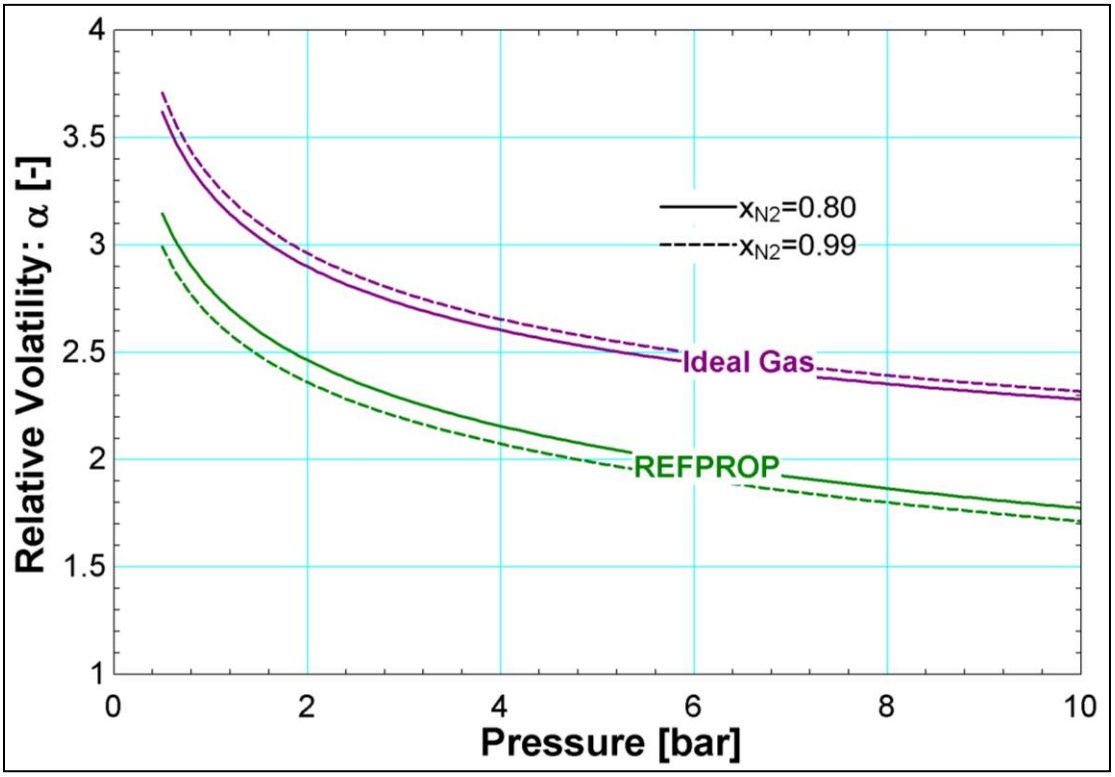

Figure 6: Relative volatility of nitrogen-argon versus pressure

The dashed and solid lines respectively represent the upper and lower bounds of nitrogen composition addressed by the present experiment (lower: 80% nitrogen, upper: infinite dilution of argon). The difference in the relative volatility over the composition range of this experiment is pretty small. However, there is a more significant difference in the relative volatilities

calculated from REFPROP compared to the results from the ideal gas solution. The relative positions of the dashed and solid lines are flipped depending on how the volatilities are calculated. The ideal gas solution shows an increase in relative volatility as the nitrogen composition is increased, while REFPROP shows the opposite.

When it comes to experimental VLE data, filling in a P-xy or a T-xy diagram becomes tedious because these parameters have to be controlled very precisely. Unless the VLE mixture is modified (by either adding or removing mass), only one data point can be taken at each temperature or pressure. However, with a relative volatility plot, precise control is not as critical and more VLE data points can be analyzed at once. Relative volatility plots will be used in this thesis to characterize data taken in a past experiment as well as the present experiment.

2.2 Gas Chromatography

The gas chromatograph (GC) is responsible for providing the composition data which is dependent on temperature and pressure. This section will briefly describe the different components of a GC and how they work together to separate gas mixtures. The diagram below is a simplified schematic of a gas chromatograph.

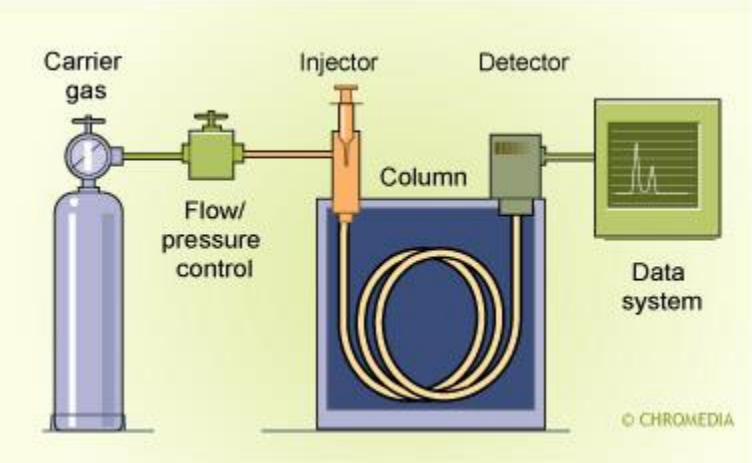

Figure 7: Simple schematic of gas chromatography station (Snow, 2016)

The GC fully separates the mixture so that each component is represented by its own separate and discernible peak. This result is called a chromatogram and it is shown on the 'Data system' in the graphic above. If no mixture is injected into the GC, the chromatogram should only display a steady baseline. This baseline is created by the carrier gas. To ensure that it remains steady, the 'Flow/pressure control' is used. The carrier gas flows through the column and detector at a constant rate.

A sample of the mixture of interest is injected into the carrier gas flow stream through the injector port. It flows along with the carrier gas through the column and detector.

The column consists of a long (30-50 meter) capillary tube where the various components of the mixture interact with the walls differently. This component-dependent interaction causes the mixture to separate and each component will take a different amount of time to reach the detector. The amount of time it takes to reach the detector from when the mixture is injected is called the retention time. The carrier gas flow rate, type and length of column, as well as the column oven temperature affect the retention time. But if these variables are kept constant, the retention time for each component will be the same regardless of sample composition.

The detector used in this experiment was a thermal conductivity detector (TCD). A TCD consists of a hot filament in a constant temperature-controlled cell. There is a temperature-dependent resistance across the filament that is measured with a voltage (Grob & Barry, 2004). With only the carrier gas flowing through the detector at a constant flow rate and temperature, the measured TCD voltage will be constant. If another gas with a different thermal conductivity than the carrier gas flows through the detector, the temperature of the filament will change, causing a difference in the TCD voltage.

If the conductivity of the sample component is less than the conductivity of the carrier gas, the voltage change will be positive. Once the 'plug' of sample component has made it fully through the detector, the TCD voltage will go back to its baseline value. The area under the voltage peak that has been created is analogous to the volume of that component within the sample. If a binary mixture has been properly separated in the column, the areas of the two resulting peaks will correspond to the composition of the mixture. A chromatogram of an experimental result is shown below.

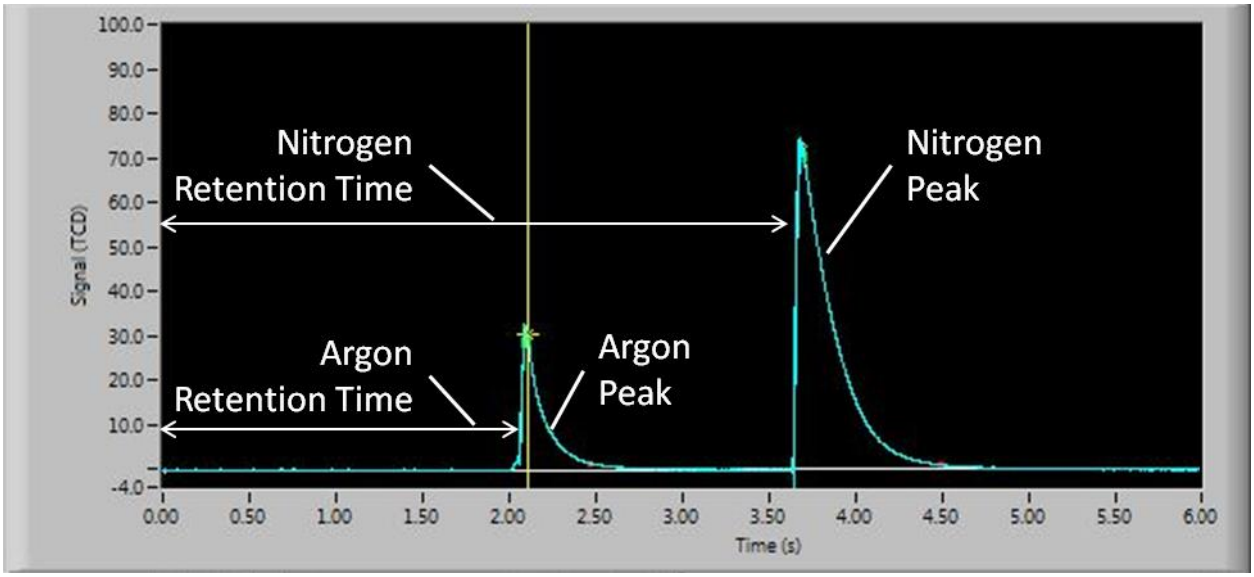

Figure 8: Labelled chromatogram of approximately 80% nitrogen, 20% argon mixture

Argon is represented by the first peak, and nitrogen is represented by the second. The last part needed to turn this result into a composition is a response factor (RF) for each gas. The response factor converts the peak area to a volume of the component. If each component behaves as an ideal gas with consistent temperature and pressure when flowing through the TCD, the volume is directly proportional to the number of moles of that substance. If the moles of each component are known, then the molar composition can easily be calculated.

$$RF_i = \frac{(Moles)_i}{(Integrated\ TCD\ Area)_i}$$

$$MolarComposition_i = \frac{(Area_i)RF_i}{\sum_{i=1}^{n_{components}}(Area_i)RF_i}$$

Response factors can be predicted based on properties of the compound and the carrier gas (Eugene. Rosie, 1971). However, the assumptions that go into these predictions are not accurate for every compound, so experimental data is more commonly used. It has been shown that response factors can also change slightly depending on the GC method, or even the GC itself (Gislason & Wharry, 2000). For this reason, if high accuracy composition data is required, it is best to calibrate the gas chromatograph specifically with the gases of interest using a consistent GC method. The response factors used in the data presented in this experiment were found through a calibration method that is detailed in a later section of this thesis.

2.3 VLE Experiments

Due to the non-intuitive behaviors of many mixtures, experimental vapor-liquid equilibrium data is necessary in order to generate curves that can be used to describe the mixture properties (Elliott & Lira, 2012). If the components of interest are not volatile or reactive, the VLE apparatus and method of experimentation typically falls into one of two categories: static or flow.

Static Systems for VLE Measurements

Shown below is a static apparatus for attaining vapor-liquid equilibrium.

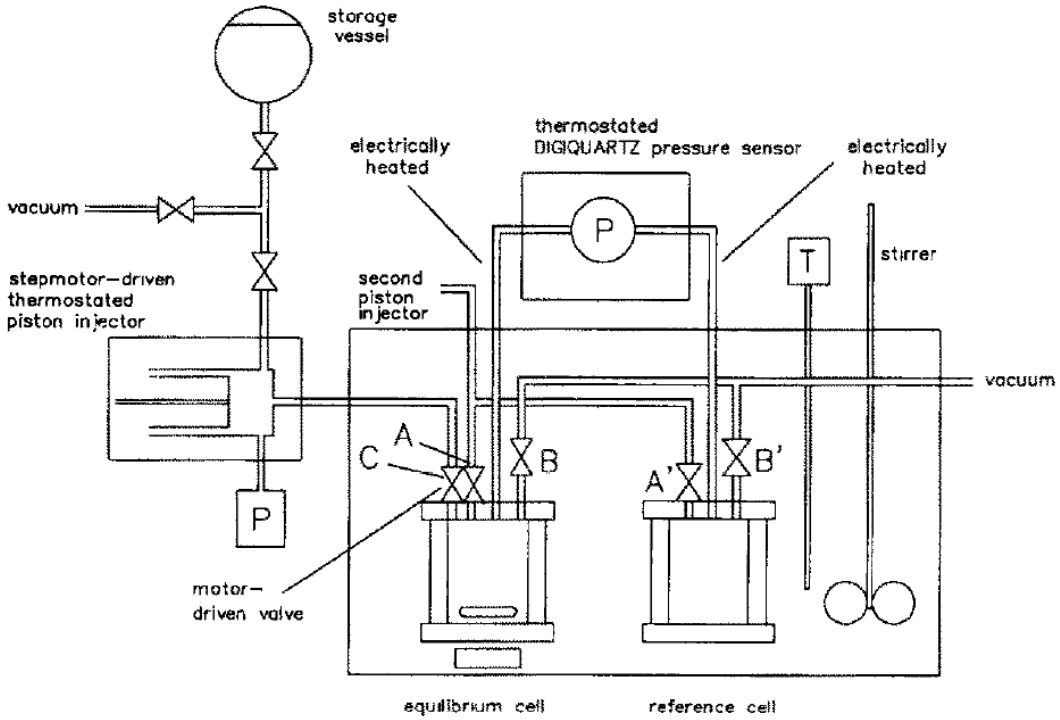

Figure 9: Static VLE experimental apparatus (Rarey & Gmehling, 1993)

In static measurements, a known amount of mixture is charged into the equilibrium cell which is temperature controlled (Wichterle et al., 2004). There is no direct method for pressure control with this configuration. After equilibrium is attained, vapor and liquid samples are taken. At the same temperature, the system will come to equilibrium again but at a lower pressure. One advantage of this system is the minimal usage of components that make up the mixture. Static systems can be scaled smaller than flow systems (Wichterle et al., 2004).

Flow Measurements for VLE Measurements

There are more variations on flow (or circulation) systems for VLE measurements. A simple schematic of a vapor phase recirculation system is shown below.

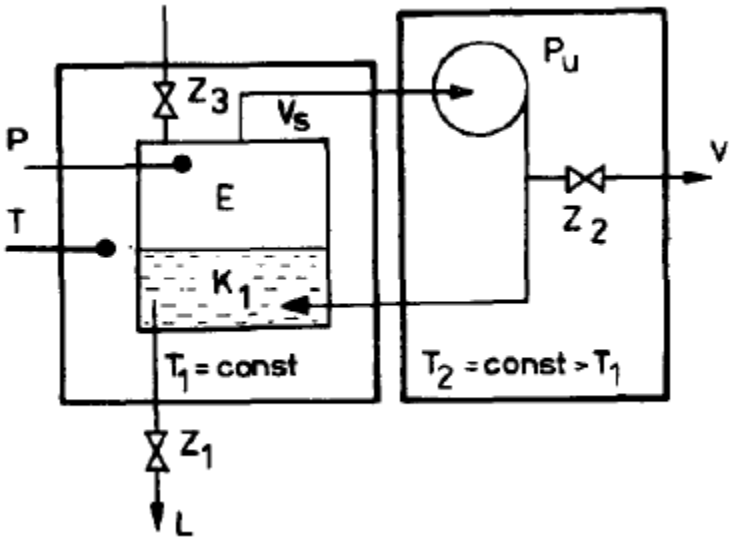

Figure 10: Flow VLE experimental schematic (Malanowski, 1982)

Under ideal conditions for this setup, the temperature of the equilibrium cell is held constant and there is no pressure drop in the recirculation loop. If the system runs continuously under these ideal conditions, the vapor composition will be the same at every point in the system. In practice, this condition is very difficult to achieve because the flow through the equilibrium cell usually disrupts the equilibrium. For this reason, the device being used to circulate the mixture is typically turned off and the system is allowed to become steady before the VLE samples are drawn from the equilibrium cell.

Methods for circulation of the liquid phase exist but these are more common in high temperature VLE experiments and will not be discussed in this report.

2.4 Previous Work with Nitrogen-Argon Mixtures

A thorough analysis of mixtures containing nitrogen, argon and oxygen in vapor-liquid equilibrium was published by Wilson et al in April 1964. This experiment was funded by Air Products and Chemicals and data was taken from July, 1962 to April, 1964 (Wilson et al., 1964).

Test Apparatus and Procedure

The figure below depicts their vapor-liquid equilibrium apparatus.

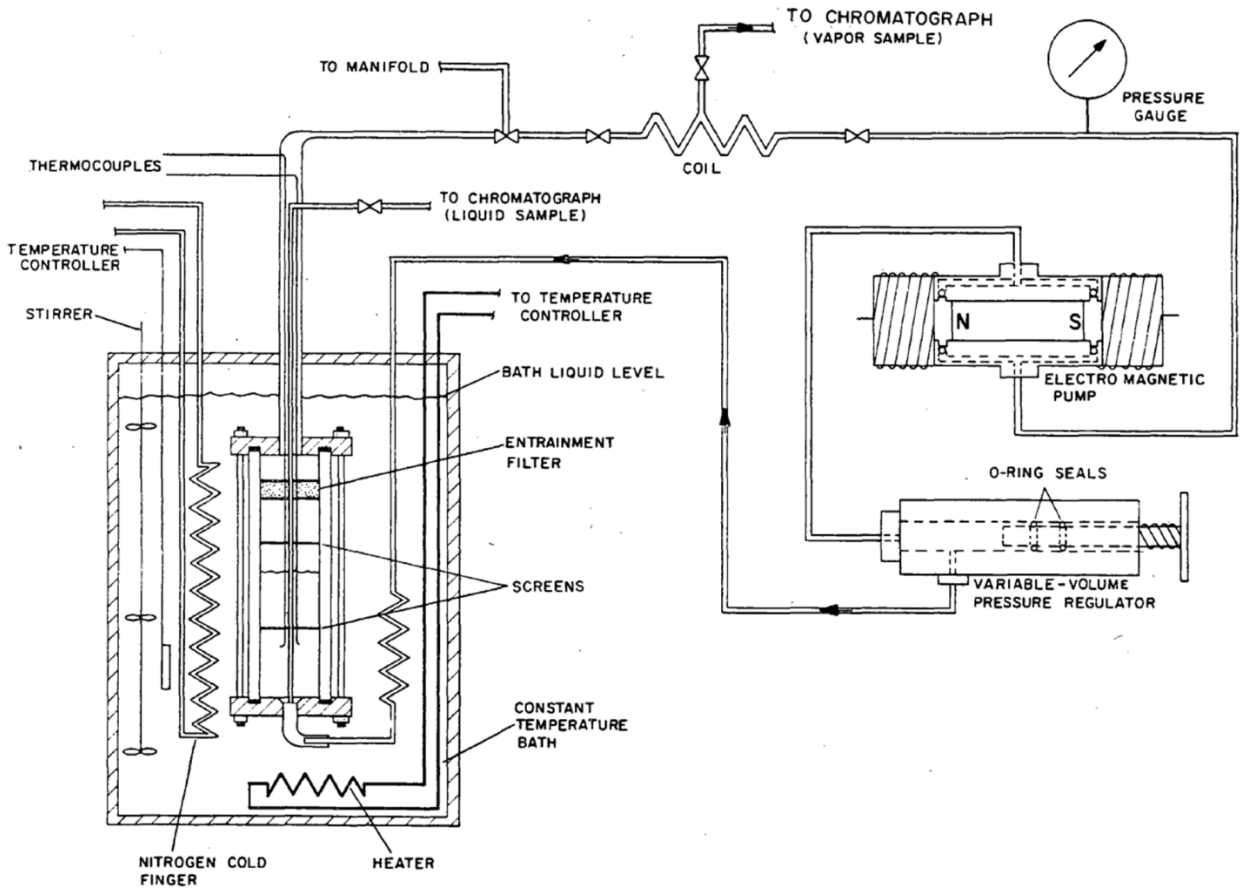

Figure 11: VLE experimental apparatus used by Wilson et al. (1964)

The temperature of their VLE cell was controlled with a pressurized liquid cryogen bath. This bath was cooled with the 'nitrogen cold finger' which consisted of an adjustable flow rate of liquid nitrogen. The bath was heated with a resistive heater. The temperature was controlled to within ±0.01°R (Wilson et al., 1964) by connecting the heater to a proportional controller based on a temperature reading of a platinum resistance thermometer submerged in the bath.

The electro-magnetic pump was used to circulate the mixture from the top of the equilibrium cell to the bottom of it. When equilibrium was achieved, portions of the liquid and vapor were removed simultaneously from the equilibrium cell.

A total of 1962 VLE samples were taken with this apparatus. Compositions of the liquid and vapor were analyzed for each sample. The samples taken were of the ternary mixture, as well as the three possible binary mixtures. The pressures ranged from one to 26 atmospheres, the temperatures ranged from 77 to 140 Kelvin.

Pressure and Temperature Measurement Analysis

The pressure measurement came from a gauge calibrated by the manufacturer. This was read directly to the nearest 0.1 psi with a hysteresis error of ±0.005 psi (Wilson et al., 1964). Based on these values, the uncertainty of their pressure measurement is calculated below.

$$u_P = \pm\sqrt{\left(0.5 * (0.1\ [psi])\right)^2 + (0.005\ [psi])^2} = \pm 0.0502\ [psi]$$

A copper-constantan thermocouple immersed in the liquid portion of the equilibrium cell was used for the temperature measurement. An ice bath was used as the warm end reference junction. Seven calibrations were performed on this thermocouple through the course of the experiment using vapor pressures of argon, oxygen and nitrogen. A polynomial fit based on a least squares analysis from the calibrations was performed. The deviation from this fit is plotted as a function of the thermocouple reading and of the temperature. A third scale showing the temperature in Kelvin has been added to this plot for consistency in this report.

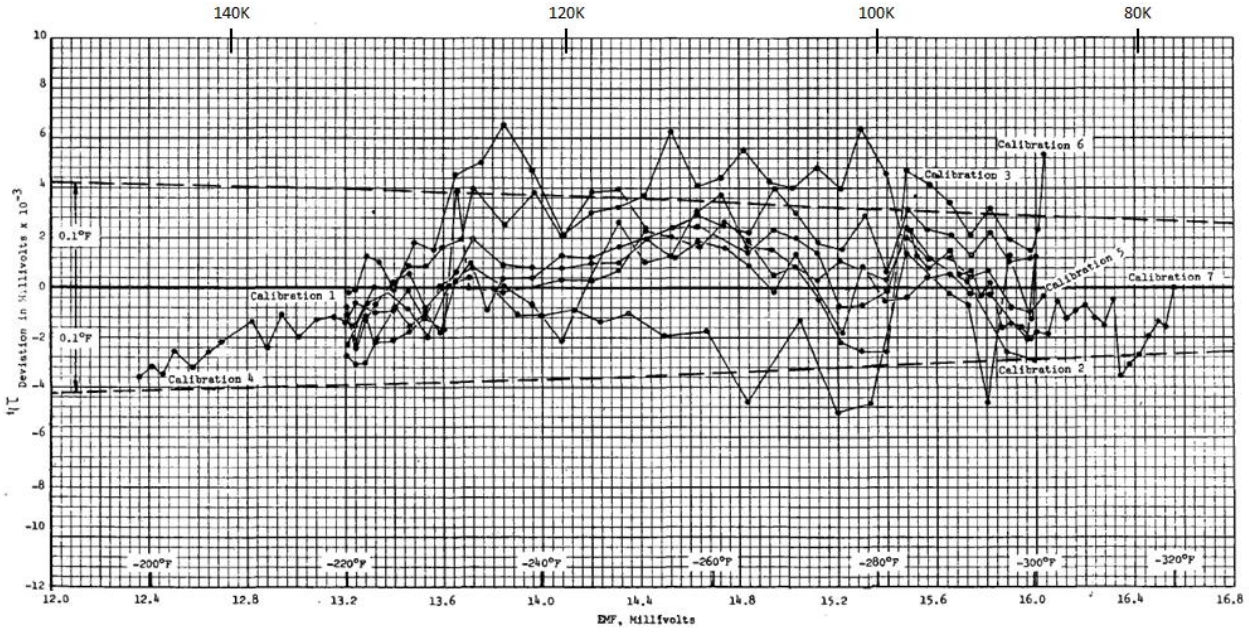

Figure 12: Temperature measurement deviation from polynomial fit from Wilson et al. (1964)

The two dashed lines in the plot above represent a temperature deviation of ±0.1°F from the polynomial fit. Focusing specifically on the region below 100 Kelvin, the majority of their calibration data lies within these dashed lines. Counting the points that lie inside and outside of the dashed lines leads to a confidence interval of 88%. This value is less than the traditional 95% confidence interval that is typically associated with measurement uncertainties. This plot is the only analysis of the temperature measurement provided in the report by Wilson et al. Raw data

for this plot is not included, limiting the potential to calculate a more appropriate temperature uncertainty than ±0.1°F.

Nitrogen-Argon Vapor-Liquid Equilibrium Concentration Data

Analysis of the data provided by Wilson (1964) will be limited to only the points that lie within our range of interest. Pulling the points that are binary nitrogen-argon mixtures with a minimum nitrogen composition of 80% and with a maximum pressure of six atmospheres leads to the data shown in the table included in Appendix Section 9.1.

The relative volatility was calculated for each data point. This result is plotted below.

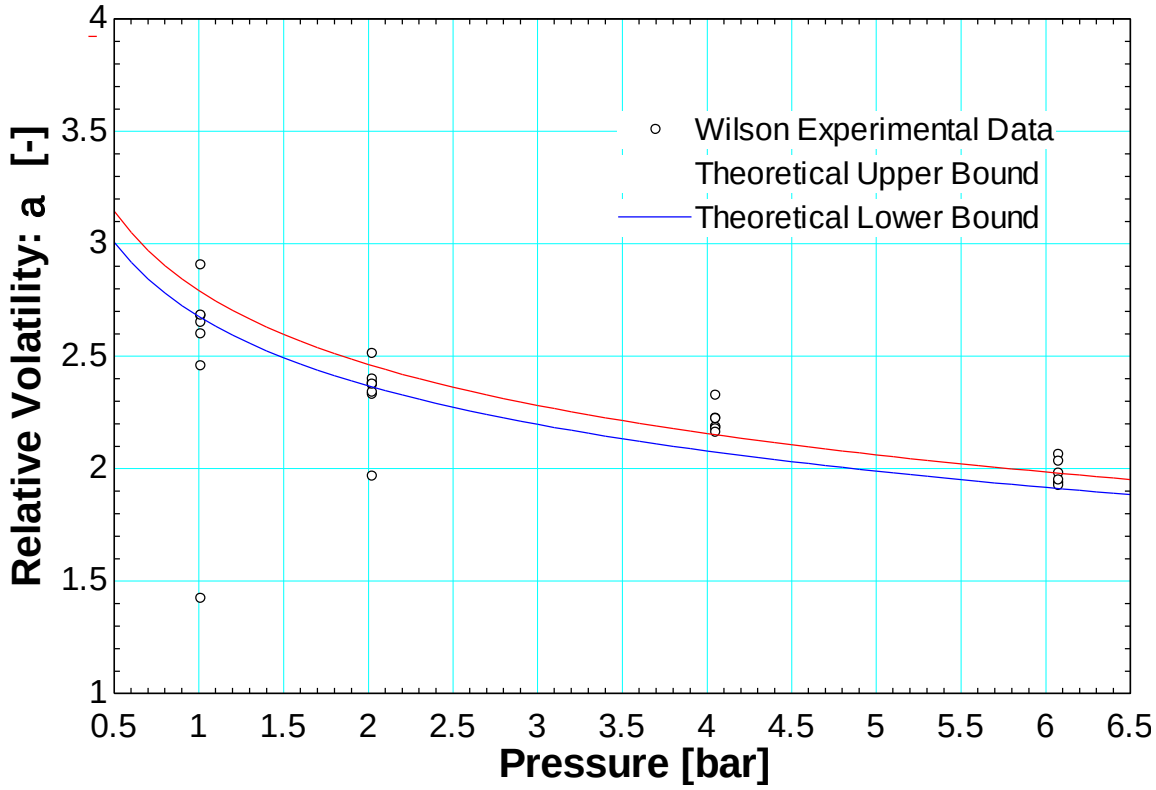

Figure 13: Relative volatility of Wilson (1964) VLE data points with >80% N2 and under 6 atms

The downward trend as pressure increases is the expected result. This data should not form a single line because volatility is not dependent only on pressure, but composition also. Other than the outliers at one and two atmospheres, the data points for each pressure are pretty close to each other, perhaps converging better as pressure is increased.

The Wilson (1964) experiment as a whole was effective at rapidly obtaining a large amount of data. They had a dual gas chromatograph setup for rapid sample analysis, a single controller for obtaining steady equilibrium temperature, no moving parts in the cryogenic zone that might need

repair, and multiple technicians running the experiment full-time. However, there is room for more analysis into the uncertainties of the temperature and concentration measurements.

3. Description of Test Rig and Components

This section will describe the components that are in the cold zone during the present experiment. All of these components will be referenced in upcoming sections. The considerations during fabrication will also be discussed.

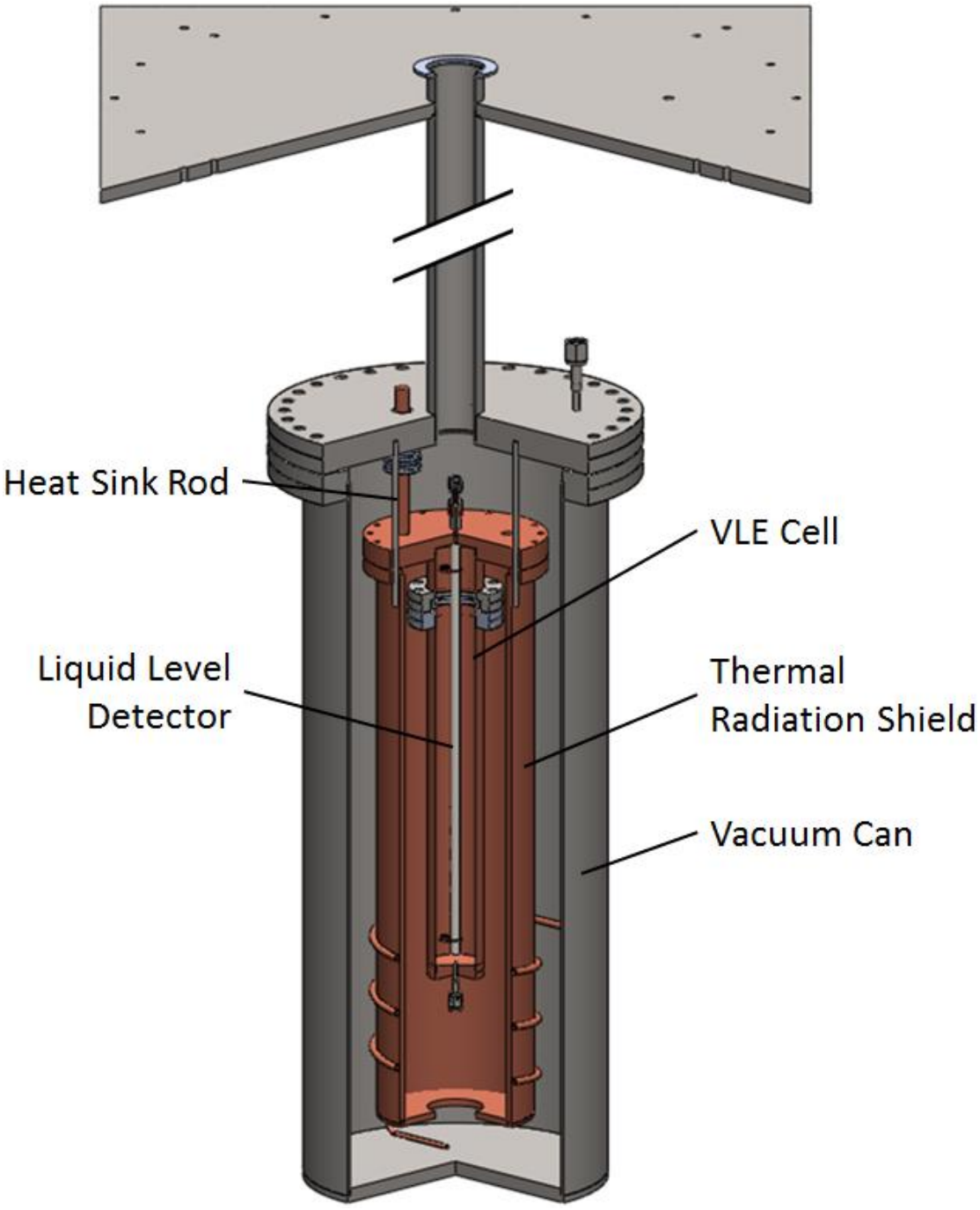

Figure 14: Major components of test rig used in experiment

3.1 Vapor-Liquid Equilibrium Cell

The vapor-liquid equilibrium (VLE) cell is the central cylinder in the graphic above. This cylinder is made of two inch diameter SCH40 copper pipe and is approximately fifteen inches tall. There is an inlet port to the VLE cell on the bottom and an outlet port on the top for circulation of the test mixture. There is another opening in the center of the bottom plate where the liquid sample solenoid valve is attached.

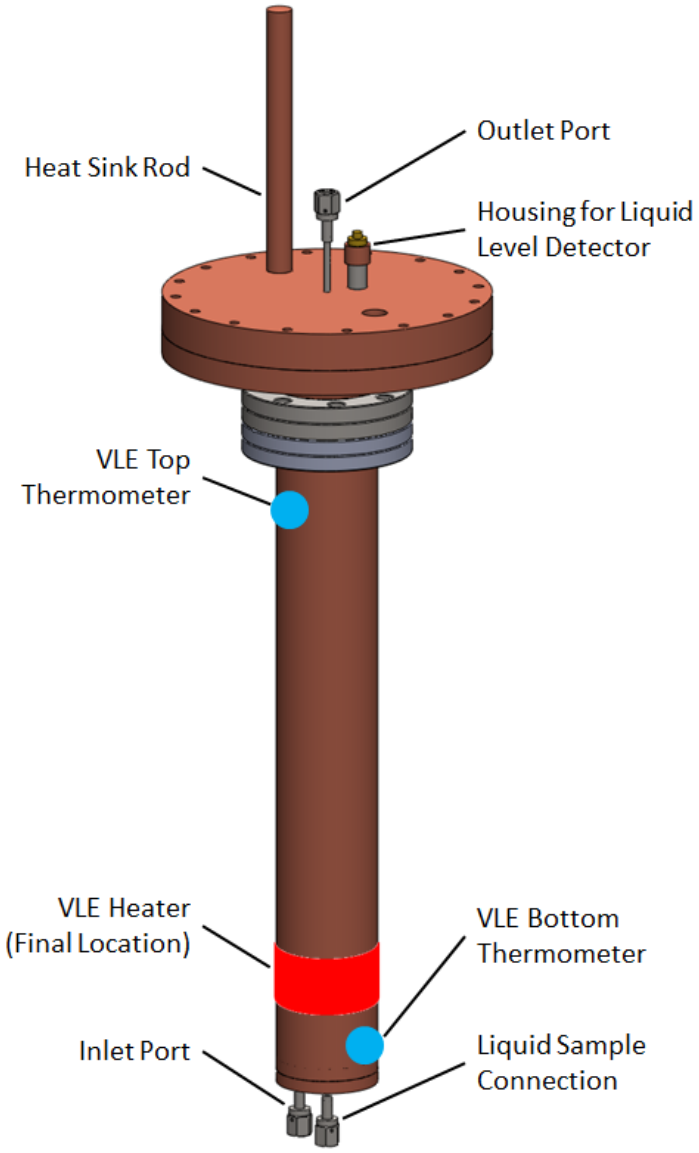

Figure 15: Locations of features associated with VLE cell

The two calibrated thermometers are attached here, one on the top and one on the bottom. Each thermometer is attached by first coating non-conductive paper with VGE7031 varnish to the surface of the VLE cell which has been adequately cleaned with methanol. The thermometer is

placed on the paper and held in position with a wire twisted around the back of the cylinder. Shrink wrap was added to this wire to cushion the contact point between the wire and the thermometer and to provide another layer of electrical isolation. Once in position, the thermometer, the place-holding wires, and a portion of the thermometer leads are all coated with VGE7031 varnish again to provide better thermal communication between the VLE cell and the platinum RTD. The thermometer attached to the top of the VLE cell in its final mounted position is shown below.

Figure 16: Calibrated thermometer in final mounted position on VLE cell

The VLE cell also had a PID controlled heater based on the bottom temperature. This was simply a resistive heater made by wrapping a thin-gauge stainless steel wire around the bottom of the VLE cell. This wire was electrically isolated from the VLE cell using non-conductive paper and varnish. This heater was powered by the Cryo-Con temperature controller which put out its maximum power into a 50 ohm load. The length of this wire heater was set such that the wire's resistance would be approximately 50 ohms when the temperature of the wire was 80 Kelvin. The leads for this heater were varnished into position on the VLE cell. Kapton tape was wrapped around these leads to provide additional stability for the thicker gauged wire.

3.2 Thermal Radiation Shield

The thermal radiation shield (TRS) is the next cylinder outward from the VLE cell. The purpose of this component is to stay at a similar temperature to the VLE cell in order to minimize radiation heat loss from the cell. The TRS is made of five inch diameter SCH40 copper pipe and

is approximately 21 inches tall. Piping wrapped around the TRS transfers the test mixture from the pipe heater to the VLE cell. The thermal radiation shield and its associated features are shown in the figure below.

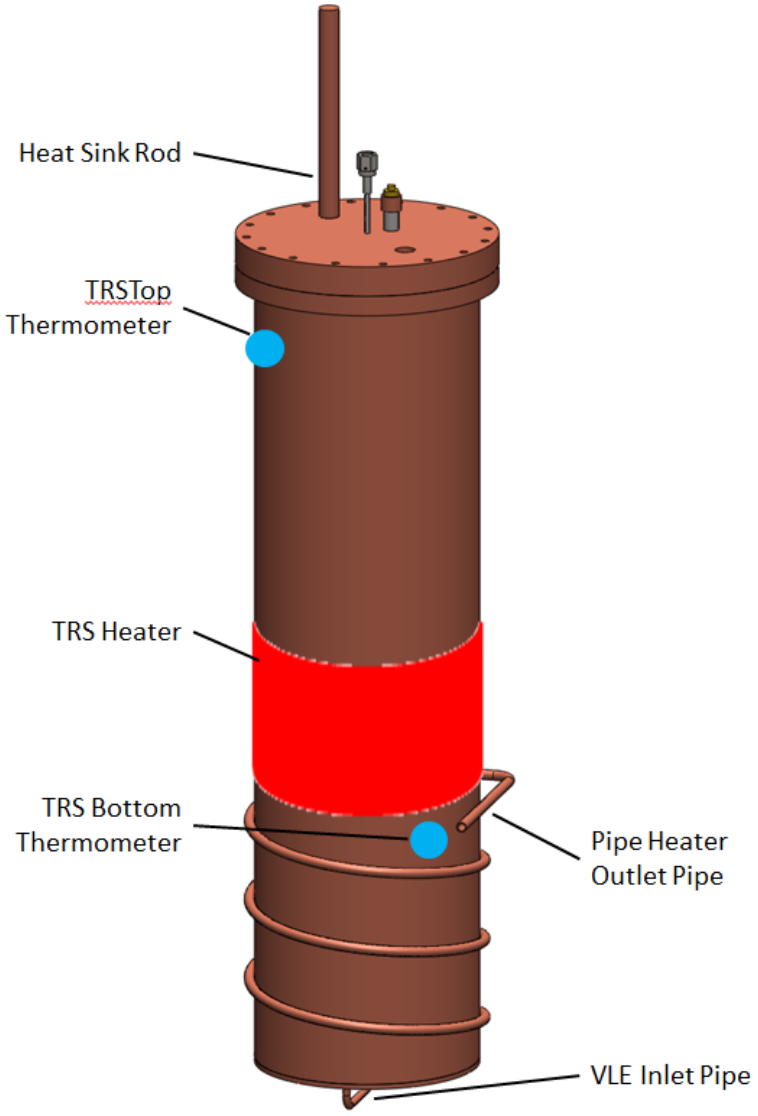

Figure 17: Locations of features associated with thermal radiation shield

Similarly to the VLE cell, the TRS has two thermometers and a heater attached to it. The TRS heater is controlled based on the value of the TRS top temperature. This heater was mounted in the same way as the VLE heater. It can be seen in the picture above approximately in the middle of the shield. The thermometers attached to the TRS were varnished on in the same way as the thermometers on the VLE cell. The only difference is they are held in place with tape instead of wrapped wires.

Attached to the top of the thermal radiation shield is the copper heat sink rod. This rod provides thermal communication to the liquid nitrogen bath that is surrounding the vacuum can. It is simply a half inch diameter copper rod. This is the primary means of dropping the temperature of the VLE and the TRS when the experiment is running.

3.3 Vacuum Can and Support Flange

The vacuum can is the outermost cylinder in Figure 14. This component is made of stainless steel. It is approximately eleven inches in diameter and 27 inches tall. The support flange is a square piece of half inch plate steel.. The figure below shows these components.

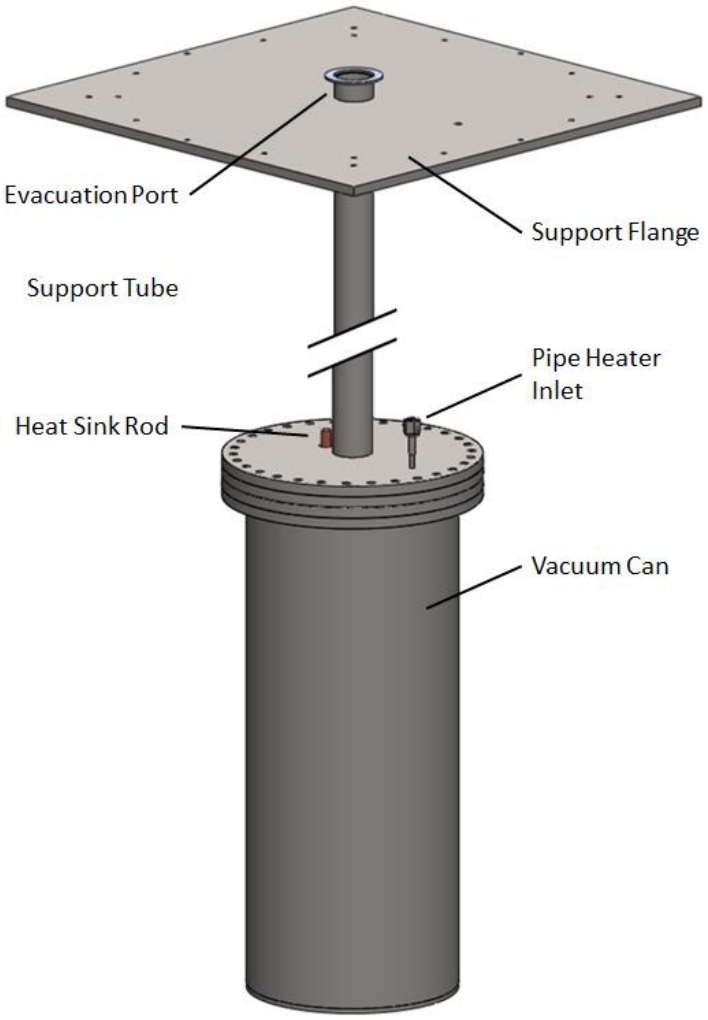

Figure 18: Vacuum can, support flange and associated features

The vacuum can completely encloses the VLE cell and the TRS and provides a seal so that the space inside can be evacuated. When the experiment is running, the vacuum can is completely submerged in liquid nitrogen. The support flange holds the weight of the vacuum can and

everything inside of it. The support flange rests atop the dewar used in this experiment. The flange and vacuum can are connected by the support tube. This tube is of sufficient length to prevent icing on the top of the support flange. This tube also houses the piping and wiring that run from ambient to the cold zone, as well as providing a means to evacuate the vacuum can.

3.4 Liquid Level Detector

By the definition of VLE, when it has occurred, there will be a liquid-vapor interface. Due to the density difference between the two phases, below the interface will be liquid; above it will be vapor. If this interface exists, and the temperature and pressure are steady, it can be concluded that the cell is in vapor liquid equilibrium.

The liquid level detector provides the means for confirming a vapor-liquid interface inside of the VLE cell. This is achieved by two silicon diodes wired in series with each other. These diodes are typically used for temperature measurements in cryogenic experiments. There is a temperature-dependent voltage drop across them when a certain current is applied. That effect is shown in the plot below.

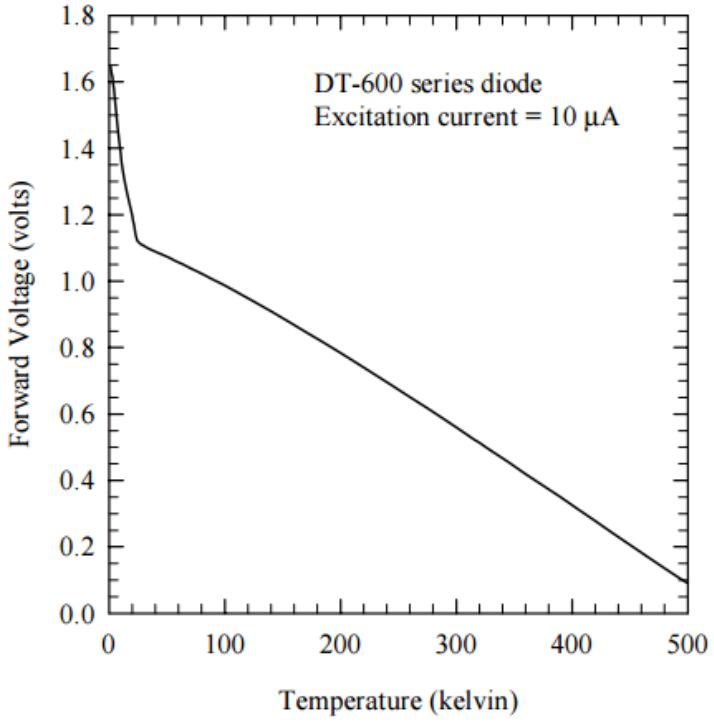

Figure 19: Standard response of silicon diode thermometer (Courts, 2002)

This is the result that occurs when the recommended excitation current of 10 microamps is applied. This is the recommended amount so that self-heating of the diode does not occur which would affect the temperature. The self-heating effect is carefully exploited by the liquid level detector. The figure below shows the detector and its expected responses.

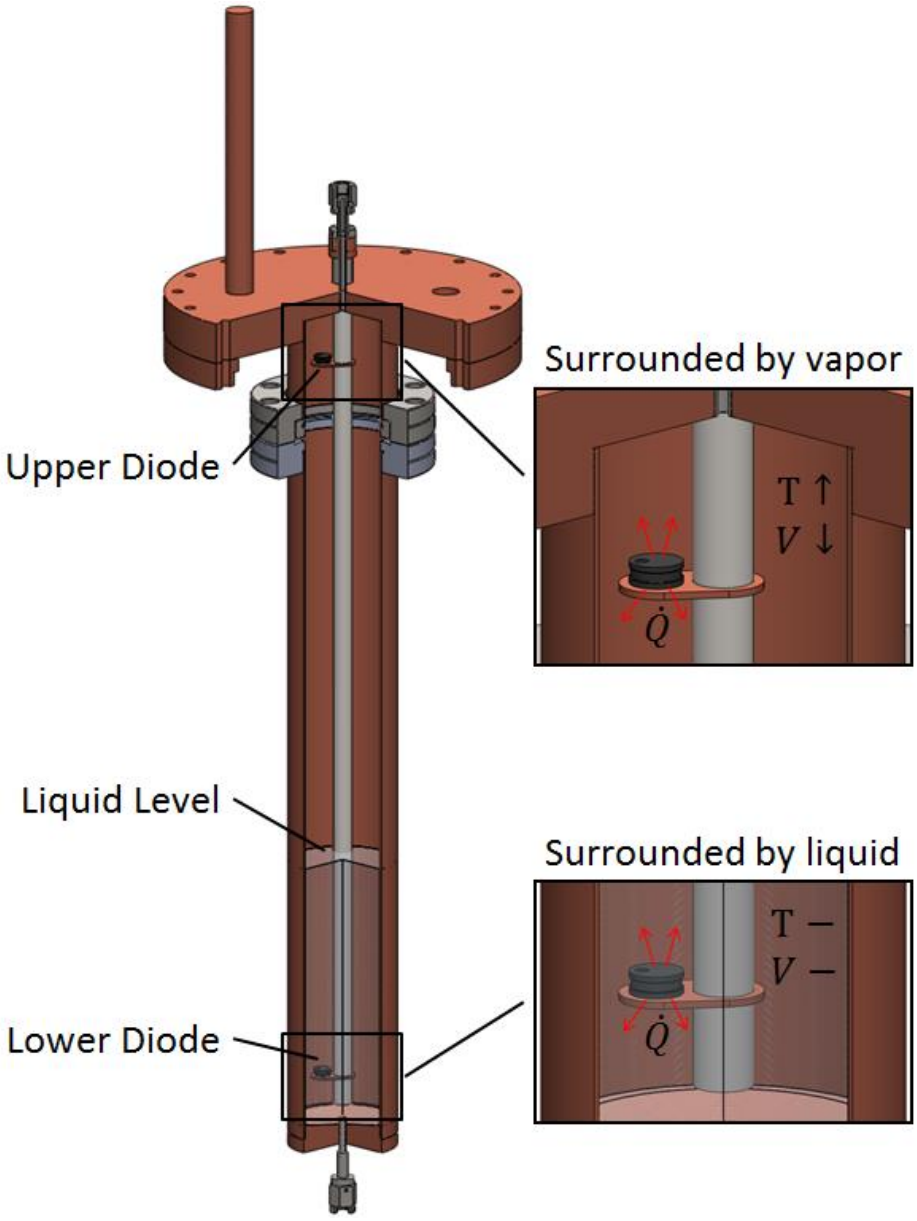

Figure 20: Liquid level detector expected response when liquid level is present

When it was necessary to verify a VLE condition, a current of 100 milliamps was applied to the upper and lower diodes. Since the vapor has a much lower specific heat than the liquid, the temperature of a diode surrounded in vapor will increase resulting in a drop in the measured voltage. A diode surrounded in liquid will still heat that liquid but the temperature and measured voltage of the diode will remain steadier compared to the diode surrounded by vapor.

The figure below shows the liquid level detector response for two different scenarios.

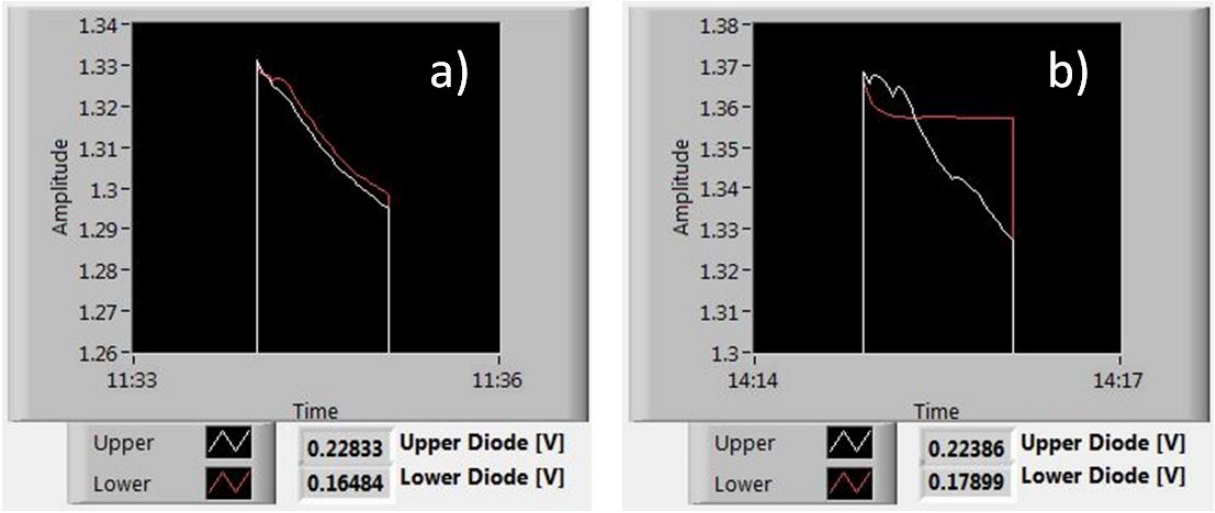

Figure 21: a) level test with all vapor in VLE cell b) level test with liquid level in VLE cell

Both of these responses were recorded after the VLE pressure and temperatures were steady. In scenario 'a)' there was no liquid present in the VLE cell. Therefore, each diode experienced self-heating, raising their temperature and dropping the measured voltage. In scenario 'b)' there was a liquid level between the two diodes. The lower diode's temperature was relatively steady, while the upper diode experienced self-heating, dropping its measured voltage.

Experimentally, it was better to perform this level test after taking a sample instead of before since performing the test would disturb the equilibrium condition.

The liquid level detector consisted of two DT-470 silicon diodes purchased from Lake Shore Cryotronics. These diodes were mounted to a small copper plate that was welded to a thin-walled stainless steel tube. The stainless steel tube was mounted to the top of the VLE cell using Stycast 2850 epoxy. The current and voltage leads for the two diodes were run through this epoxy. The lower diode was approximately one inch from the bottom of the VLE cell and the upper diode was approximately one inch below the top of the VLE cell.

3.5 Liquid Sample Solenoid Valve

The liquid sample solenoid valve is not shown in Figure 14 but it was a crucial component in this experiment. It is attached to the center of the bottom of the VLE cell. The requirements of this valve were that it could function and remain leak-tight at cryogenic temperatures. This proved to be a difficult product to find since most solenoid valves are not made for applications with such stringent leak rate requirements.

Clark-Cooper manufactures and tests their valve in-house to meet their leak-rate specifications. Below is a picture of the solenoid valve selected for this experiment.

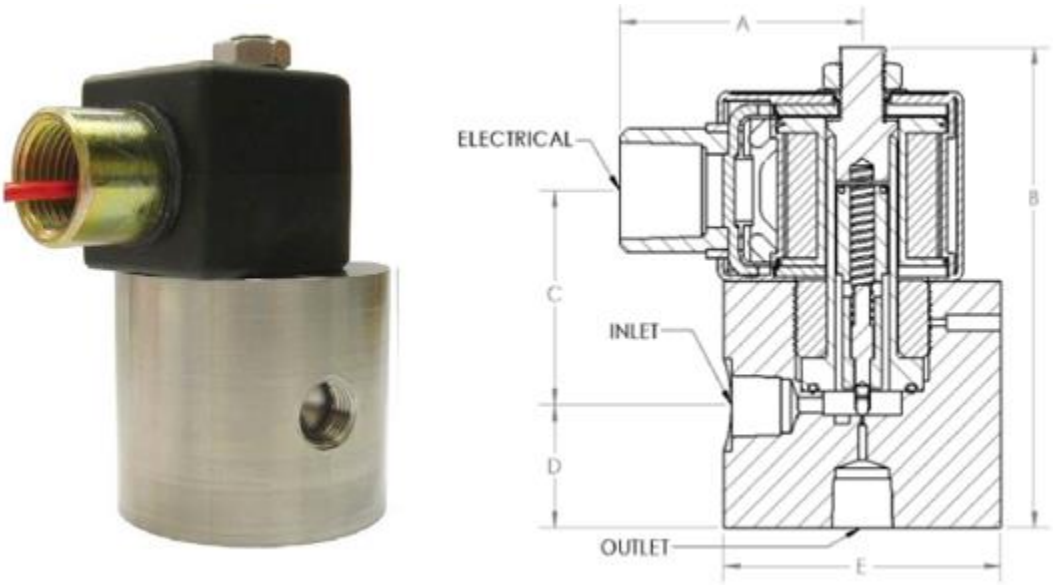

Figure 22: EH30 series cryogenic solenoid valve (Clark Cooper, 2014)

This valve is in the 'normally closed' orientation. It required a minimum of 12VDC signal, with a 22 watt power draw to open. Experimentally, this valve was opened and closed quickly to allow a rapid 'gulp' of the liquid portion of the test mixture in the VLE cell. This was achieved by simulating a timed square-shaped pulse in LabVIEW, amplifying it with a transistor and power supply and sending this to the valve. The circuit diagram is shown below.

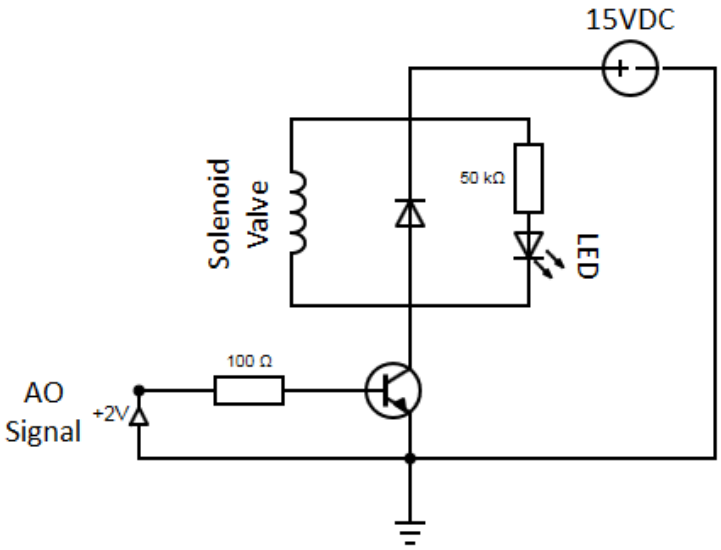

Figure 23: Electric diagram for valve operation and feedback

The LED is included as an indication that the circuit has been closed and the valve has pulsed open. The other diode in parallel with the solenoid valve is there to prevent generation of a back-emf after the valve has been closed.

3.6 Piping and Valving in Ambient

Shown below is the piping and instrumentation diagram for the whole system. This diagram will be referenced later in section 5: Experimental Procedure.

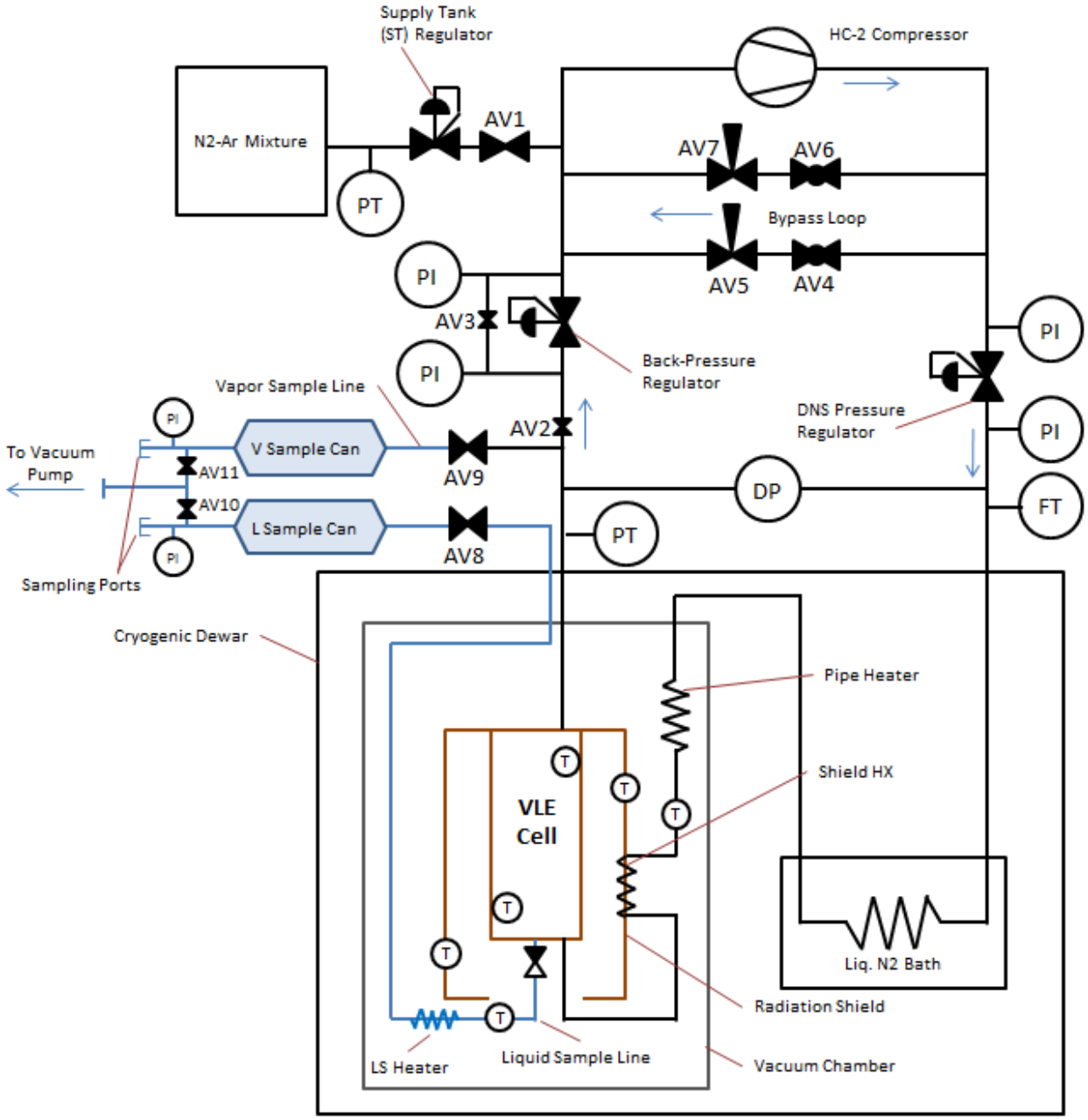

Figure 24: Piping and instrumentation diagram for experiment

The denotation ‘AV’ stands for ‘ambient valve’. All of these valves can be operated manually at any time. Starting at the supply tank (N2-Ar Mixture), when the ST regulator and AV1 are opened, the test mixture flows into the suction side of the compressor. Only one of the bypass throttle valves within the bypass loop is needed. With the compressor running and appropriate settings on the bypass valves, it is possible to maintain a steady high pressure at the compressor outlet and a steady low pressure at the compressor suction. The pressure in the liquid nitrogen bath and VLE cell should be at an intermediate value between the compressor inlet and outlet pressures. Therefore mass can be added or removed from the VLE cell by use of the DNS pressure regulator or the back-pressure regulator bypass valve (AV3).

The mixture enters the vacuum can at the temperature of the liquid nitrogen bath. The temperature of the mixture in the VLE cell is controlled by the heaters on the VLE cell and the thermal radiation shield (TRS).

The labelled pictures below show the locations of the diagram components in the lab.

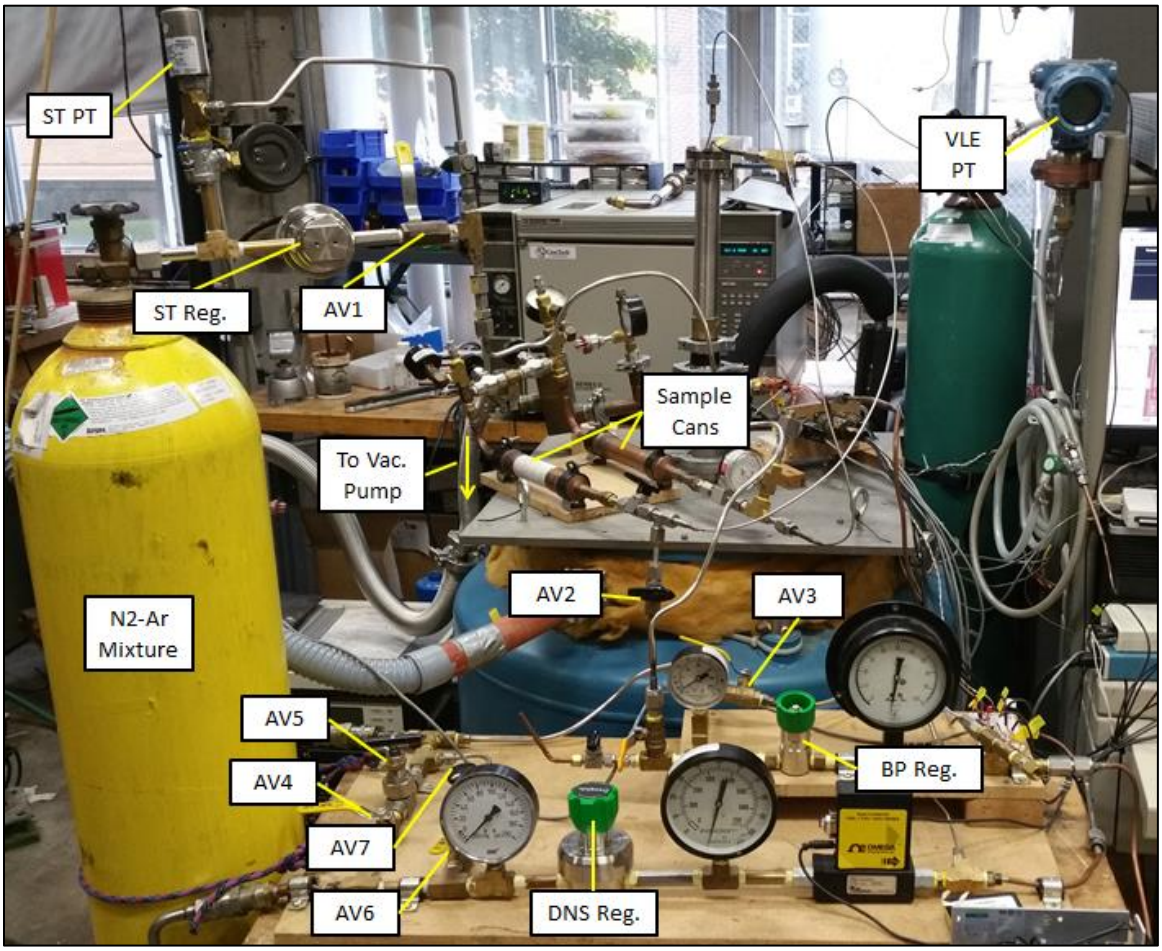

Figure 25: Location of components that control and monitor pressure and flow

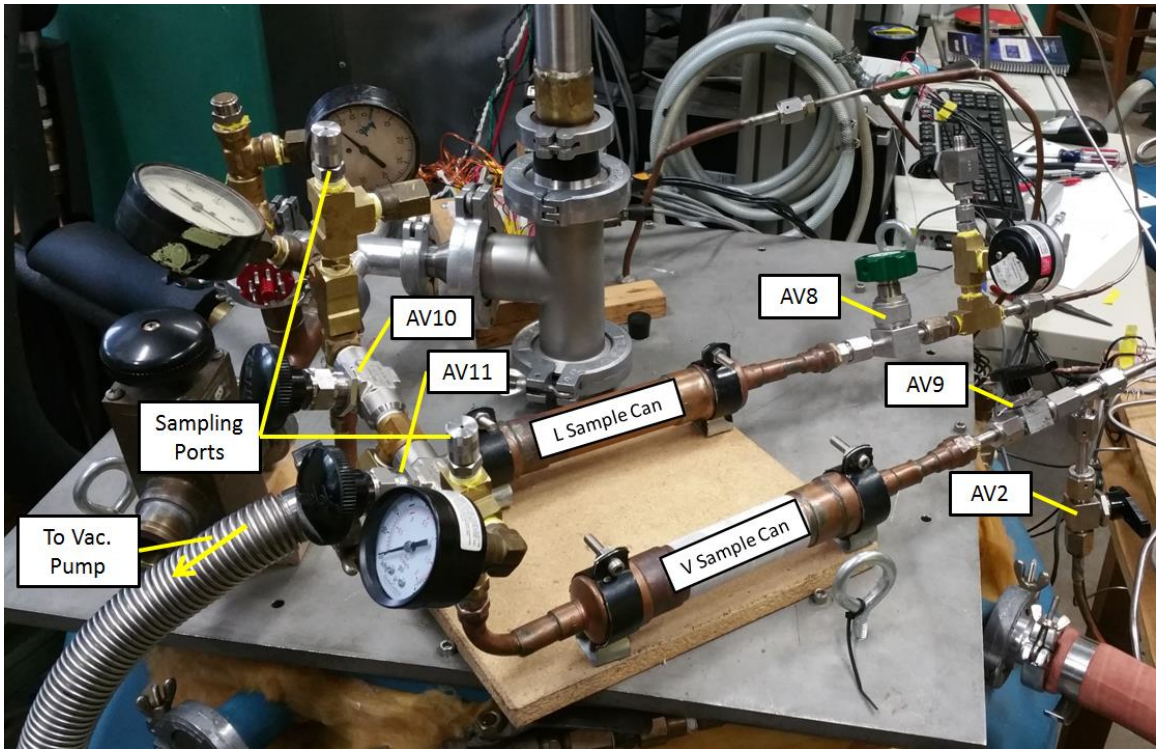

Figure 26: Location of components related to GC sampling

4. Analysis of Instrumentation and Measurement Accuracy

4.1 Gas Chromatograph

The gas chromatograph is a crucial part of this experiment. A refurbished Hewlett-Packard model 5890 Series II was purchased specifically for this experiment. The GC came equipped with a thermal conductivity detector. A Restek Msieve 5A capillary column was installed inside of the GC. This column was selected for its ability to separate permanent gases above ambient temperature.

Calibration Procedure

A properly calibrated gas chromatograph will separate a mixture and create a peak for each component in that mixture. The area of each peak can be calculated by integration. However, in order to convert these peak areas to composition values for the mixture, it is necessary to know how each gas interacts separately with the thermal conductivity detector (TCD). The plot below shows a GC run of a nitrogen-argon mixture. This data is recorded using LabVIEW and integrated using tools within OpenChrom which is an open source chromatogram analyzer.

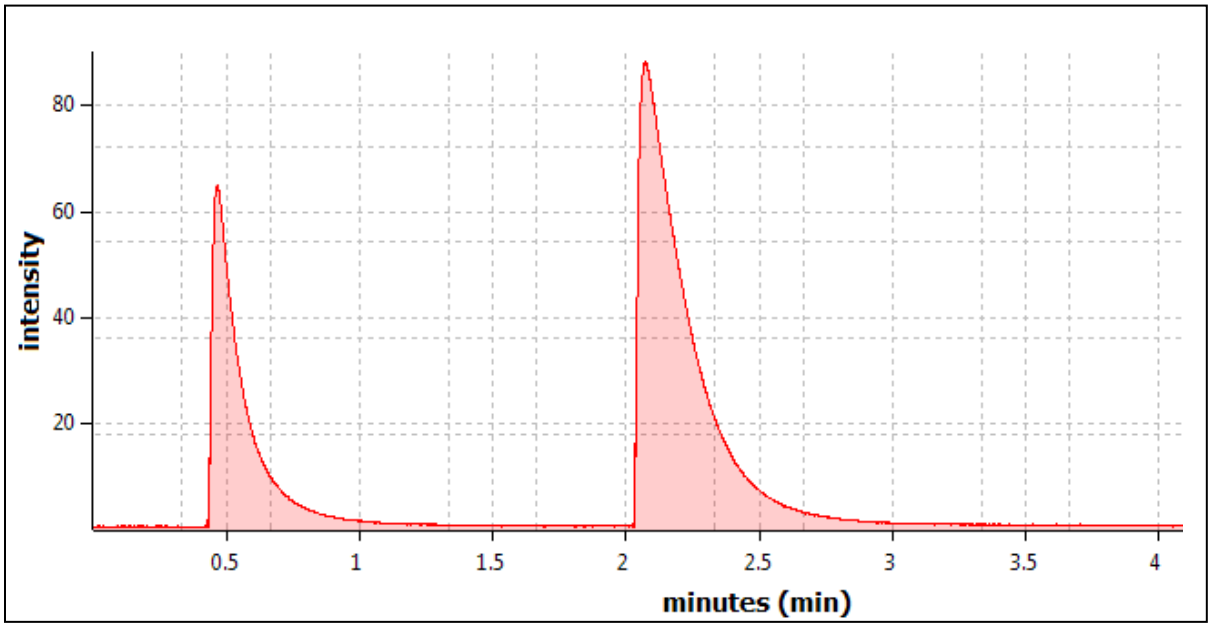

Figure 27: Sample chromatogram of nitrogen-argon mixture after it has been transferred to OpenChrom

The first peak to come out is argon, the second is nitrogen. The area percentage (AP) for each peak is represented by the equation below.

$$AP_i = \frac{Area_i}{Area_{total}}$$

Each area percentage needs to be multiplied by a factor (specific to each component) in order to convert it to a composition for that component of the mixture.

Theoretical Calibration Data

Theoretical data for this multiplier exists for many gases and compounds. Our GC calibration was compared with the results published in the Analytical Chemistry journal by Rosie and Grob (1957). The experiment performed by Rosie and Grob (1957) calculated relative molar responses (RMR) for many different compounds and gases. The definition of the RMR value is response units per mole of compound. The results for nitrogen and argon are shown below.

Table 1: RMR values for nitrogen and argon from Rosie and Grob (1957)

	Theoretical Relative Molar Response
Nitrogen	**42**
Argon	**44**

The RMR value for each gas on its own is not as important as their value relative to each other. These results predict that the integrated area of a TCD response to one mole of nitrogen will be equal to that of one mole of argon when multiplied by a factor of 44/42.

$$\left(\frac{IntegratedArea}{mole_{N2}}\right)(42) = \left(\frac{IntegratedArea}{mole_{Ar}}\right)(44)$$

The response factor (RF) is the value that is multiplied by the integrated area from the TCD to attain the composition (molar amount) of each component. The response factor is equal to the inverse of the RMR.

$$RF = \frac{Const.}{RMR}$$

The value of interest when calibrating for a mixture of gases is the result when one RMR is divided by the other.

$$\frac{RMR_{Ar}}{RMR_{N2}} = \frac{(44)}{(42)} = \mathbf{1.0476}$$

This result is calculated from the data presented by Rosie and Grob (1957). This value will come up later when validating our calibration results.

Calibration Procedure

With ideal gas assumptions, the number of moles of any gas is equal when temperature, pressure, and volume are constant. Therefore, under consistent atmospheric conditions, an injection needle filled to the same volume will have the same number of moles of pure argon as it will have of pure nitrogen. If this pure gas sample is injected into the GC, however, the TCD response will be different for pure argon when compared to pure nitrogen. The goal of calibrating a gas chromatograph is to find the relation between the TCD response and the amount of gas injected for each component. That relation for each component is analogous to the response factor of that component. It is also important calibrate using the same GC method (oven temperature, detector temperature, carrier gas flow rate, etc.) that will be used experimentally.

Our calibration procedure consisted of taking different sample volumes of each pure component (nitrogen and argon) and injecting each sample through the gas chromatograph, integrating and recording each response.

Ten samples of each gas were taken at injection volumes of 50, 40, 30, 20 and 10 µL. The injection needle used for this process is shown below.

Figure 28: Hamilton gastight syringe used for injecting samples into GC

The resolution on the needle shown above is one microliter. Ultra-High-Purity (99.9995% purity) tanks of nitrogen and argon were used for this calibration process. The pure gas was put into a previously evacuated sampling canister. This sampling canister has a septum port which was pierced in order to fill the injection needle to the desired volume. This is the same sampling canister that is used to take the VLE composition measurements. Other than the final volume of the injection, the sampling procedure for calibrating was the same as the procedure for taking experimental data.

Calibration Results

The plot below shows ten argon samples with injection volume of 30 µL. The area of each peak is included in the 'Peak Results' tab, next to the plot.

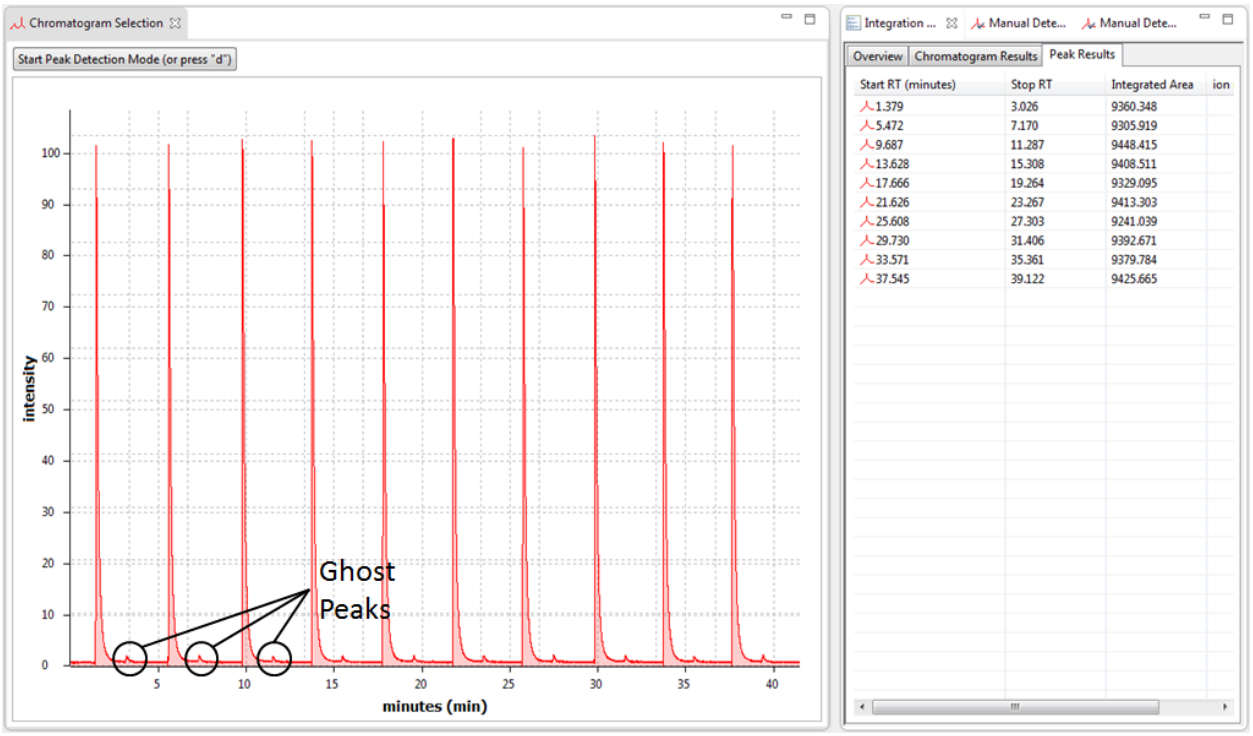

Figure 29: Integration results for ten 30 microliter samples of nitrogen

Note that after each argon peak, there is a much smaller peak; three of these are called out in the figure above. The cause for this 'ghost peak' is imperfect injection technique. There was some leakage into either the injection needle or the sampling canister during the process. For this set of argon samples, the ghost peak occurs where nitrogen would come out of the GC. For the nitrogen samples, a smaller ghost peak occurs where argon would come out. However, this ghost peak is likely oxygen but it is difficult to tell the two apart since they have very similar retention times.

A similar plot to that shown in Figure 29 for each gas (nitrogen, argon) at each injection volume (50µL, 40µL, etc.) was integrated. When the integrated area for each gas is plotted against the injection volume, the slope of each line is equivalent to some factor times the RMR for the gas. This plot is shown below.

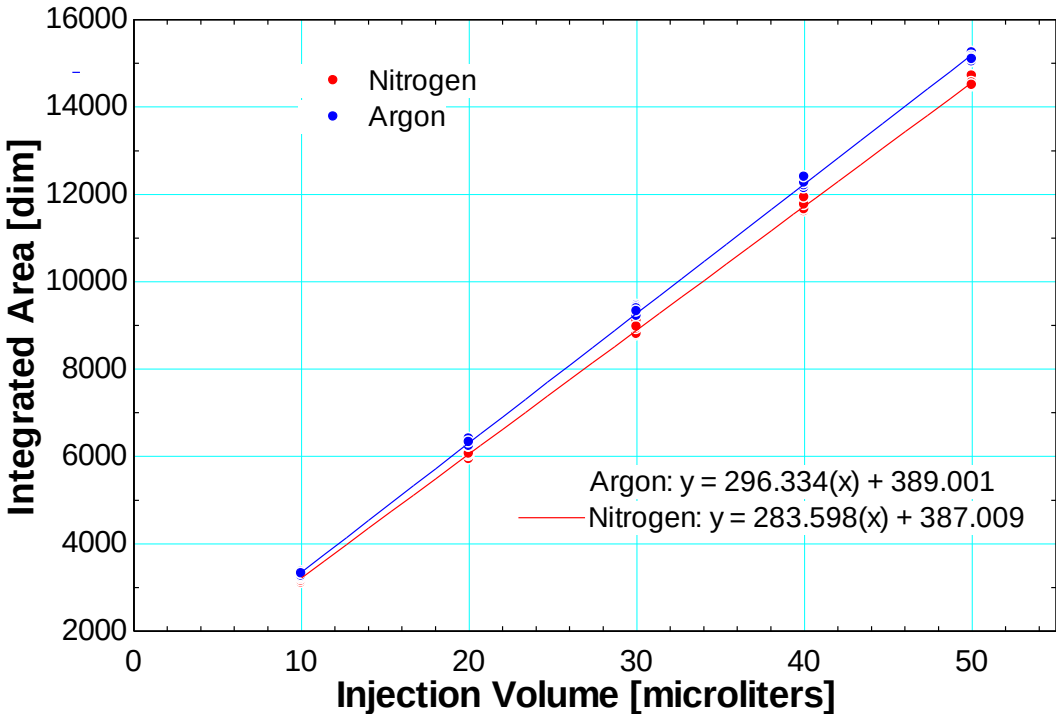

Figure 30: Integrated area versus injection volume. Slope should be equal to relative molar response

A linear best fit has been applied to each set of points. Ideally, this line should intersect at zero. This would mean that if an injection volume of zero is put into the GC, the TCD response will show no peak that can be integrated. But due to the imperfections described above, this wasn't the case. The table below compares the experimental and theoretical sets of relative molar responses.

Table 2: RMR data for argon and nitrogen

	Theoretical	Experimental
Argon	44	296.3338
Nitrogen	42	283.5975
A/N	**1.0476**	**1.0449**
Percent Error	0.00%	-0.26%

The experimental results show a slightly lower RMR for argon relative to nitrogen (A/N) compared to the theoretical RMRs. The experimental RMR ratio is very close to the theoretical one. To see how these results impact the composition measurements, the RMRs must be converted to response factors. This is done in the next section.

Uncertainty Associated with Calibrated Response Factors

An easy way to convert the relative molar responses to response factors is to invert the axes and calculate a new set of slopes.

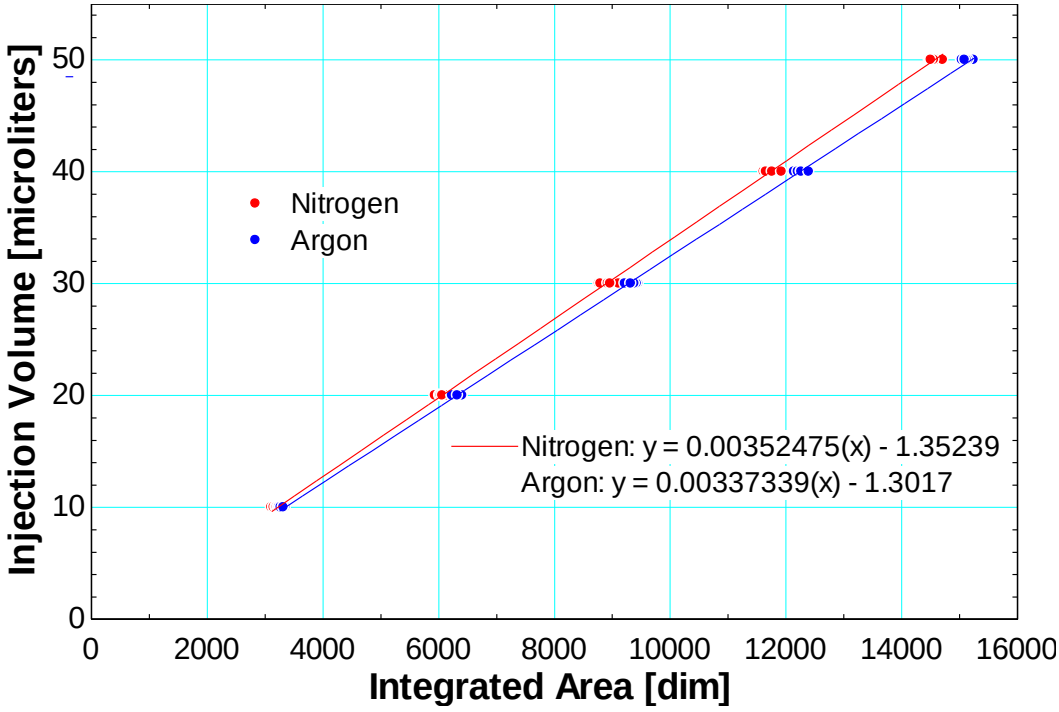

Figure 31: Injection volume versus integrated area. Slope should be equal to response factor

Linear regression was used to calculate the slope and intercept of each line in the plot above. This process was done manually in order to see how uncertainty from the calibration propagated through to the resultant response factors. The equations and EES code for this process are included in Appendix Section 9.2.

One source of uncertainty in the gas chromatograph calibration comes from the injection volume. This uncertainty is equal to half of the resolution of the injection needle's tick marks.

$$u_{injectionVolume} = \pm 0.5(1\ [\mu L]) = \pm 0.5\ [\mu L]$$

This uncertainty was applied to every injection volume and propagated through to find the uncertainty in the slopes of the lines shown in Figure 31. The results are summarized in the table below.

Table 3: Uncertainty results for each response factor

	Theoretical	Experimental		
	RF Value	**RF Value**	Uncertainty	
			Absolute	Percentage
Argon	1/44	0.00337339	1.687E-05	0.50%
Nitrogen	1/42	0.00352475	1.763E-05	0.50%
A/N	**0.9545**	**0.9571**	-	-
Percent Error	0.00%	0.26%	-	-

Once the response factors, as well as their uncertainties, have been determined, the uncertainty in the composition can be calculated. Recall the equation that converts area percentages to compositions. The generalized form of this equation is shown below.

$$Composition_i = \frac{RF_i \cdot AP_i}{\sum RF_i \cdot AP_i}$$

In order to determine the uncertainty in the composition, an uncertainty propagation table was created using EES. The nitrogen area percentage was varied from zero to one in order to span all binary nitrogen-argon mixtures.

The uncertainty as a function of the calculated nitrogen composition is shown below.

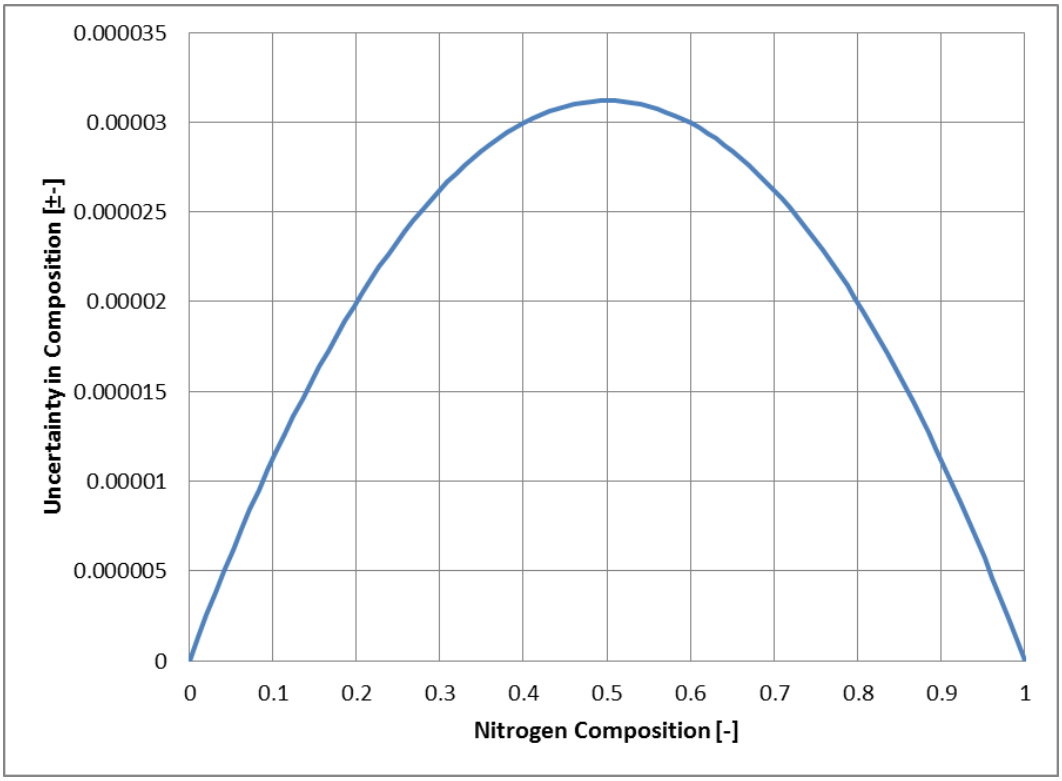

Figure 32: Composition uncertainty resulting from calibration

The uncertainty result shown above affects the argon concentration in the same way. The largest uncertainty in composition occurs when the composition is equal at 50% nitrogen and argon. On either end of the plot (nitrogen composition equal to 100% or 0%), the uncertainty in this composition is equal to zero. That result is expected since it would only occur when a pure sample is integrated from the GC.

To be conservative, the maximum uncertainty value in the plot above is added to the composition measurements reported in this thesis. The value is shown below.

$$u_{comp,Calibration} = \pm 0.000031195 = \pm 0.00312\%$$

It is important to note that there is one more source of uncertainty in the composition for each specific set of GC measurements. This is the uncertainty associated with the standard deviation of the set of five samples taken. This is not a fixed value, but instead is dependent on how repeatable the area percentages were between each set of samples. The equation for this is shown below.

$$u_{comp,AreaPercentage} = \frac{\sigma_{AP}}{\sqrt{N_{samples}}} = \frac{\sigma_{AP}}{\sqrt{5}}$$

The total uncertainty in composition comes from combining these two sources of uncertainty. The equation below demonstrates how this is done.

$$u_{comp,TOTAL} = \sqrt{\left(u_{comp,Calibration}\right)^2 + \left(u_{comp,AreaPercentage}\right)^2}$$

The uncertainty resulting from the variance in the five samples for each VLE composition is the dominant factor in the total uncertainty in reported composition.

4.2 Temperature Measurements and Controller

Thermometer Specifications

Temperature measurements were taken with platinum resistance temperature detectors (RTDs). These were selected because of their high accuracy in the temperature range from 77 to 100 Kelvin. A total of six PT-111 sensors were purchased from Lake Shore Cryotronics.

Figure 33: Platinum RTD model PT-111 (Lake Shore Cryotronics, 2016)

The two thermometers that were attached to the VLE cell required the highest accuracy. These came calibrated from Lake Shore; however their calibration was verified and adjusted. The adjustment process and its results are detailed in the following section.

The remaining four thermometers were not calibrated. Instead, the standard PTC100 curve was used to convert their resistance output to a recorded temperature.

Calibration Procedure

The two thermometers attached to the VLE cell came with the best calibration available from Lake Shore. Each thermometer had its own calibration curve that was specified to be accurate within 10 milliKelvin at 50 Kelvin and 11 milliKelvin at 100 Kelvin of the absolute temperature. The calibration curve is a fitted Chebychev polynomial based on 13 coefficients for the temperature range of 18-120 Kelvin. The temperature can be computed using the equation below.

$$Temperature\ [K] = \sum_{i=0}^{12} A_i * \cos\left(i * arccos\left(\frac{(\log(R\ [\Omega]) - ZL) - (ZU - \log(R\ [\Omega]))}{ZU - ZL}\right)\right)$$

The values of ZU, ZL and the A_i coefficients are provided by Lake Shore's calibration. The calibration from Lake Shore took place on August 7, 2014.

There can be drift in the thermometer's measurement stability over time. This drift can come from thermal cycling, or mechanical shock among other things.

For this reason, the original calibration from Lake Shore was modified with a two-point calibration carried out in the lab. Liquid nitrogen was used for the low temperature point. This temperature was determined using the ambient pressure reported by a Rosemount pressure transducer (discussed in a later section). The high temperature point was achieved using a distilled ice water bath. The resistance measurement of the thermometer came from a Cryo-Con Model 24C temperature controller (discussed in a later section). The two thermometers were arbitrarily named T46 and T47. The results of the calibration are summarized below.

Table 4: Two-point calibration data

	Actual Temperature [K]	Resistance [Ω]	Expected Temperature [K]	DELTAT [K]
T47	77.0955	20.10686	77.21942	-0.12392
	273.15	99.91473	273.0679	0.0821
T46	77.0955	20.11194	77.22048	-0.12498
	273.15	99.86235	273.0736	0.0764

The actual temperature is the temperature of either the liquid nitrogen bath or the DI ice water bath. The resistance is an averaged value recorded using the Cryo-Con temperature controller. The expected temperature is defined as the temperature that would result from plugging the measured resistance into the given Chebychev polynomial equation. The temperature difference is defined as the difference between the actual and expected temperatures.

To modify the calibration that came from Lake Shore, a linear interpolation of the difference between the actual and expected temperatures (ΔT) was added to the expected temperature. Thus, the original shape of the Chebychev polynomial did not change, instead there is a linear offset added to it so that it will fit the temperature versus resistance data points acquired from the calibration.

The calibration modification did add some new sources for uncertainty in the temperature reading. This is discussed in the following section.

Uncertainty

The platinum thermometers are read and controlled using a Cryo-Con Model 24C Temperature Controller. The LabVIEW VI communicates directly with the temperature controller via a local

area network (LAN) connection. Therefore the uncertainty associated with each temperature measurement comes from what is reported from Lake Shore, from the resistance measurement in the temperature controller and from the calibration modification. From the Lake Shore calibration, the absolute uncertainty associated with the temperature is equal to ±10 milliKelvin at 50 Kelvin and ±11 milliKelvin at 100 Kelvin. The component of the temperature uncertainty associated with the original calibration will be represented by a linear fit between those two data points.

$$u_{T,LS} = \pm(.00002(T) + .009)\ [K]$$

The next component of the uncertainty in the temperature measurement comes in the ability of the Cryo-Con controller to read the resistance. This is reported in the User's Guide for the 24C. The table from this manual is shown below.

Range	Max/Min Resistance	Excitation Current	Resolution	Accuracy
PTC100 1mA	500Ω 0.01Ω	1.0mA	0.1mΩ	± (0.004 + 0.01%)Ω

Figure 34: Cryo-Con temperature controller measurement accuracy (Cryogenic Control Systems, 2016)

The measurement uncertainty in resistance was calculated in EES for the temperature range of 75-105 Kelvin. And the error in resistance was propagated to find the error in the resultant temperature. Temperature versus resistance with error bars is plotted below.

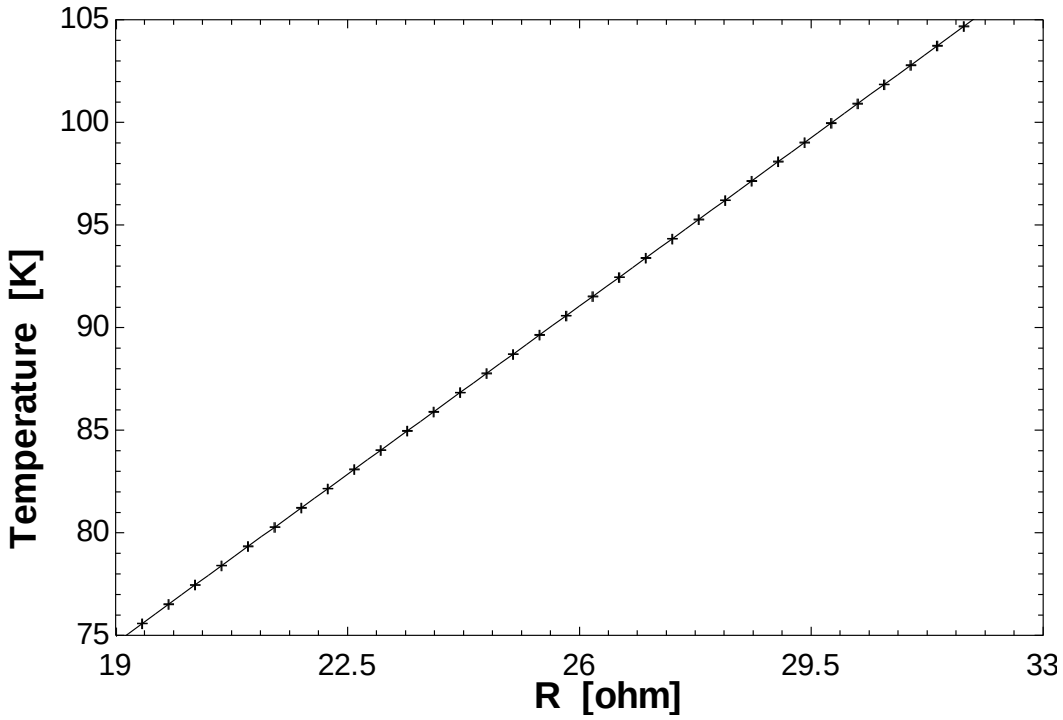

Figure 35: Temperature versus measured resistance of PT-111 with uncertainty included

The temperature uncertainty from the Cryo-Con varies approximately linearly from ±14 to ±17 milliKelvin in the temperature range of 75 to 105 Kelvin.

The uncertainty in the calibration modification method comes from several places. The low temperature is determined by the saturation curve of nitrogen. Since pressure was read using a barometric gauge, the uncertainty in the pressure reading is half of the resolution.

$$u_P = 0.5 * (1\ [mmHg]) = 0.5\ [mmHg]$$

There is uncertainty in the resistance readings at low and high temperature. This uncertainty comes from the Cryo-Con temperature controller and the number of samples taken. The equation for uncertainty in each resistance is shown below.

$$u_R = \sqrt{(.0001)^2 + \left(.004 + .0001(R)\right)^2 + \left(\frac{\sigma}{N_s}\right)^2}$$

$$R_{high} = 99.91473\ [\Omega], \qquad \sigma_{high} = .000207\ [\Omega] \quad \rightarrow \quad \boldsymbol{u_{R,high} = \pm .013991838\ [\Omega]}$$

$$R_{low} = 20.10686\ [\Omega], \qquad \sigma_{high} = .000691\ [\Omega] \quad \rightarrow \quad \boldsymbol{u_{R,low} = \pm .006011706\ [\Omega]}$$

These resistances, along with their uncertainties, make the slope of the line that characterizes the linear deviation from the Chebychev polynomial. The slope and intercept of this line were calculated in EES, and an uncertainty analysis was performed to find their associated uncertainties.

$$m_{calibration} = \frac{\Delta T_{high} - \Delta T_{low}}{R_{high} - R_{low}}$$

$$\Delta T_{high} = 273.15\ [K] - ExpectedT\left(R = R_{high}\right)$$

$$\Delta T_{low} = 77.0955\ [K] - ExpectedT(R = R_{low})$$

When this uncertainty is propagated through to the reported temperature, the uncertainty that comes from the calibration modification varies approximately linearly from 9 to 16 milliKelvin in the temperature range of 75 to 105 Kelvin.

The plot below shows all three sources of uncertainty that affect the temperature measurement. The values are reported in milliKelvin.

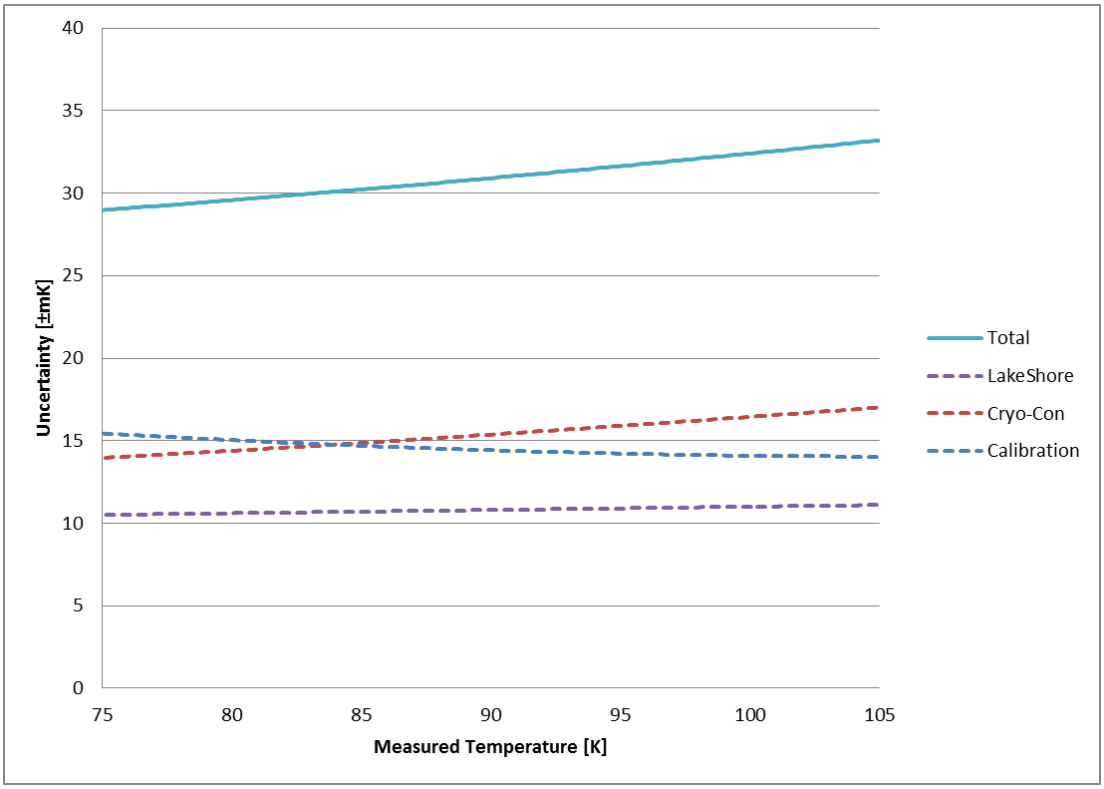

Figure 36: All uncertainties associated with temperature measurement as function of temperature

The total uncertainty is determined by taking the square root of the sum of each component squared.

$$u_{T,Total} = \sqrt{(u_{LakeShore})^2 + \left(u_{CryoCon}\right)^2 + (u_{calibration})^2}$$

From the plot above, it can be seen that the uncertainties associated with each source are on the same order of magnitude which means there is no quick or easy way to reduce the total uncertainty. The total uncertainty does vary with the measured temperature. In the temperature range of interest to this experiment, the uncertainty in the temperature measurement varies approximately linearly from ±29 milliKelvin at 75 Kelvin to ±33 milliKelvin at 105 Kelvin.

4.3 Pressure Measurement

Pressure Specifications

A Rosemount pressure transducer was used for the pressure measurement of the VLE cell. The transducer took a 15-40VDC input and converted it to a 4-20 mA output signal that scaled linearly to represent a pressure from zero to six bar.

Figure 37: Rosemount pressure transducer with digital display (Emerson Process Management, 2014)

The output amperage (4-20 mA) had to be converted to a voltage to be read by LabVIEW. This was done by using the circuit shown below.

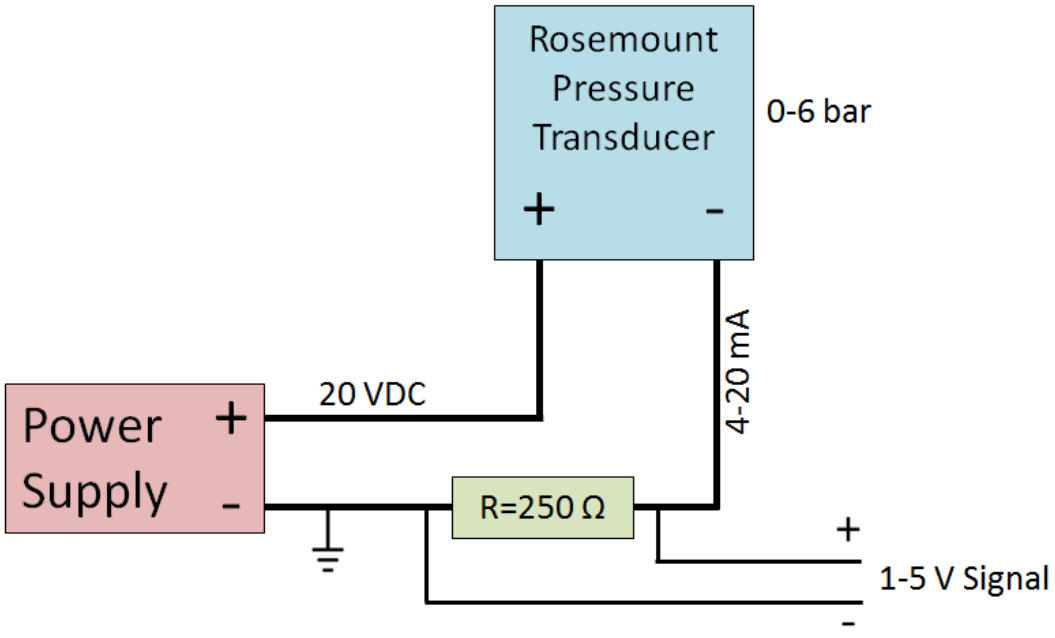

Figure 38: Electronic diagram with expected outputs for pressure measurement

Within LabVIEW, the 1-5 volt signal was converted to a pressure using the equation below.

$$Pressure\ [bar, absolute] = (Voltage\ [V] - 1\ [V])\frac{(6 - 0\ [bar])}{(5 - 1\ [V])}$$

There is also a digital readout on the transducer itself which displayed a value consistent with the calculated pressure in LabVIEW.

Uncertainty in Pressure Reading

The 'Ultra' performance model of the transducer was chosen because it had the highest absolute accuracy. The accuracy is reported from the manufacturer as ±0.025% of the full range of the transducer. The transmitter selected for this experiment has a full-scale range of 150 [psia], which is equivalent to 10.34 [bar]. The contribution to the uncertainty of the pressure measurement based on the device specification is shown below.

$$u_{P,Rosemount} = \pm(.025\%)(FullScaleRange) = (.00025)(10.34\ [bar]) = \pm .002586\ [bar]$$

Additional uncertainty in the pressure measurement comes from the resistance and the voltage used to read the 4-20 mA signal from the transducer. The uncertainty associated with the 250 ohm resistor came from the resolution in the multimeter reading of its resistance.

$$u_R = \frac{1}{2}(MultimeterResolution) = \frac{1}{2}(0.1\ [\Omega]) = 0.05\ [\Omega]$$

The uncertainty in the voltage reading comes from the resolution in the DAQ. The DAQ uncertainty is a function the voltage input range and the number of potential voltage inputs. Since the USB-6218 DAQ is a 16-bit device, the uncertainty associated with the voltage measurement is shown below.

$$u_V = \frac{1}{2}\left(\frac{InputRange}{2^{16}}\right) = \frac{1}{2}\left(\frac{5.5\ [V]}{2^{16}}\right) = 0.00004406\ [V] = 44.1\ [\mu V]$$

The pressure uncertainty as a result of the uncertainties in the resistance and voltage was computed using EES. The pressure versus measured voltage with error bars is shown below.

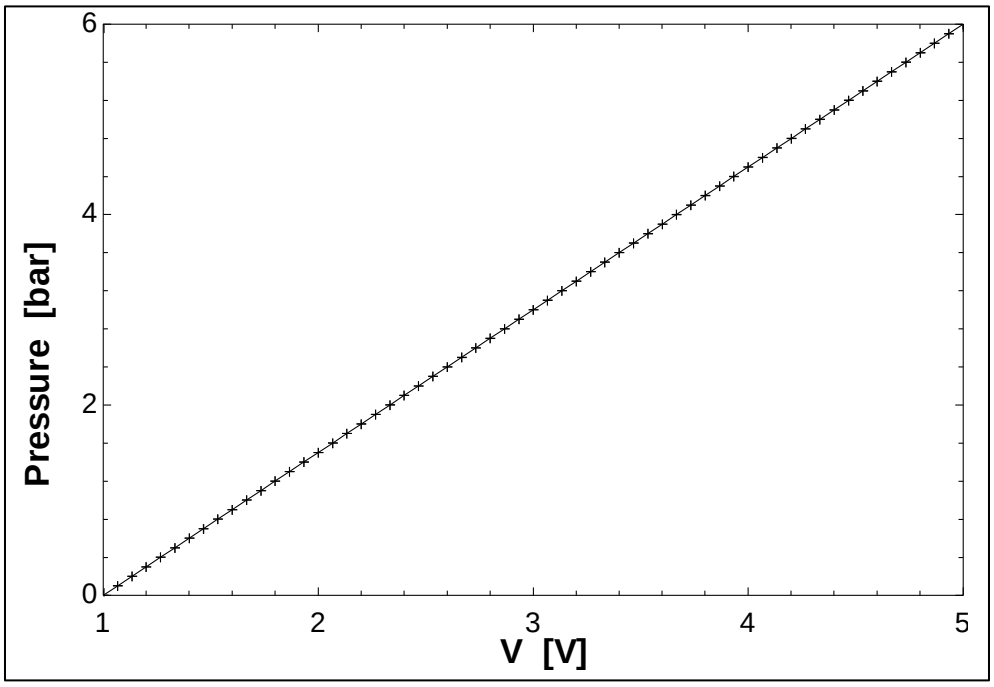

Figure 39: Pressure versus measured voltage with uncertainty included

The total uncertainty in the pressure measurement comes from adding the propagated uncertainty result to the absolute pressure uncertainty result provided by Rosemount. Each of these separate components of the uncertainty, as well as the total pressure uncertainty is plotted below.

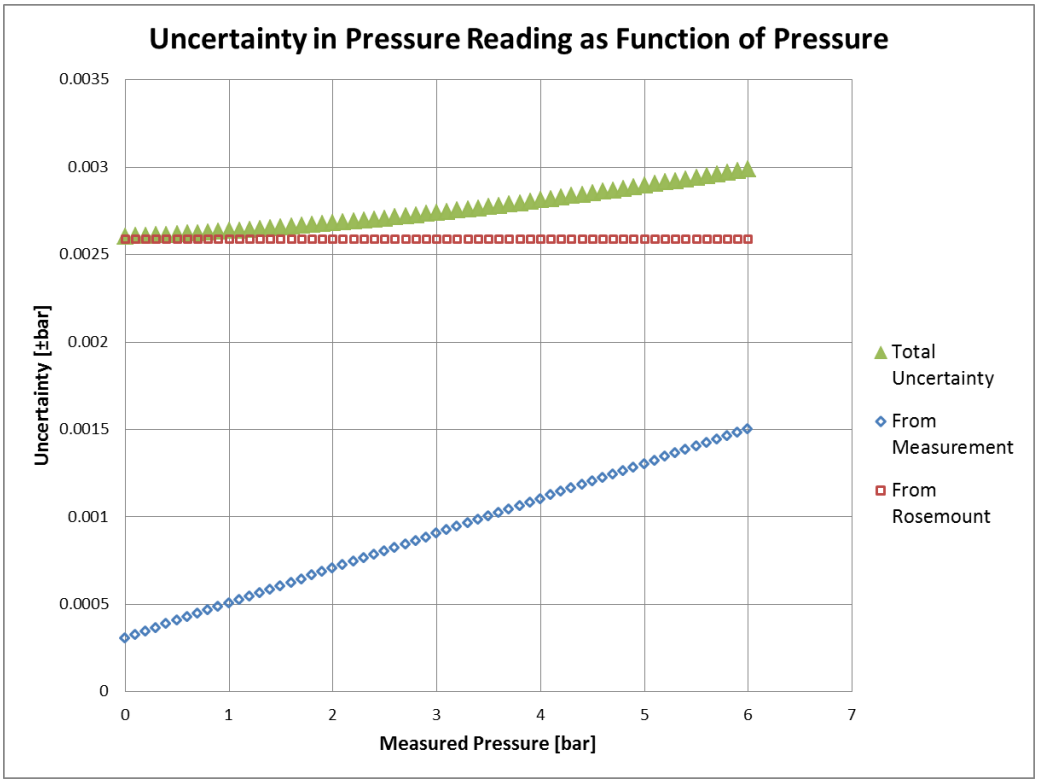

Figure 40: All uncertainties assoiciated with pressure measurement as a function of pressure

The linear best fit result of the total pressure uncertainty shown above will be added to all reported VLE pressures.

$$u_P = (6.485E-05 * (P) + 0.002564)[bar]$$

This corresponds to a pressure uncertainty of ±2.63 [mbar] at 1 [bar] (minimum experimental pressure), and ±2.93 [mbar] at 6 [bar] (maximum experimental pressure).

5. Experimental Procedure

The following procedure will reference the components in the piping diagram by their short names. The piping diagram is included in section 3.6: Piping and Valving in Ambient.

5.1 Start-Up

Creating the Base Mixture

The base mixture is the argon-nitrogen mixture that fills the supply tank. The same mixture determines the range of compositions that can be measured from taking the vapor and liquid samples. The mixture is made by use of partial pressures and the ideal gas law. For example, if an overall mixture of 80% nitrogen, 20% argon is desired with a target final tank pressure of 200

psia, the initially empty tank is filled first with argon to a pressure of 40 psia. Subsequently nitrogen is added until the final pressure of 200 psia is achieved. The target final tank pressure and composition must be chosen before mixing.

During charging of the VLE cell, the supply tank pressure drop provides a good estimate of the liquid level in the VLE cell at equilibrium conditions. The plot below shows an estimate of the VLE liquid level as a function of the pressure drop in the supply tank. The calculations to create this plot are included in appendix section XXX.

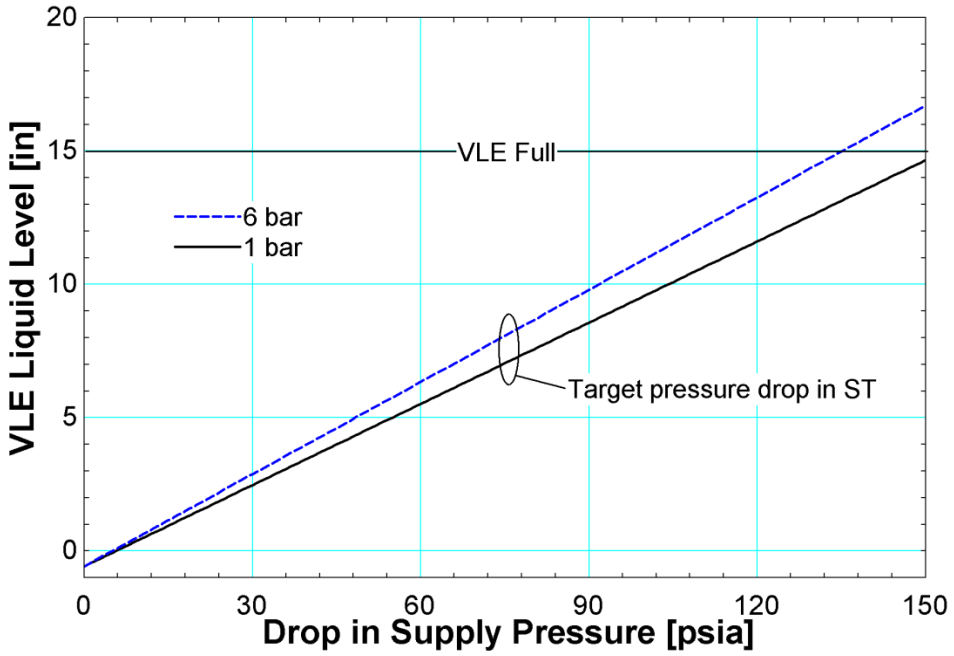

Figure 41: Approximate liquid level in VLE cell versus ST pressure drop

The target pressure drop is chosen so that the VLE cell is about halfway filled with liquid over the experimental range of pressures. To be conservative, the supply tank should be charged to a pressure that can fill the VLE cell halfway with liquid two separate times comfortably. For ease of mixing calculations and consistency, 200 psia was arbitrarily chosen as the target final pressure in all mixtures made.

The supply tank is first connected to the tank of the pure component (argon or nitrogen) along with a connection to a vacuum pump. Next, the supply tank and the piping that connects it to the pure component tank are evacuated with a turbomolecular vacuum pump. The pressure on the supply tank is monitored and logged with an Omega pressure transducer. Once the supply tank is ensured to be empty, the first component of the target mixture is added to the supply tank until its pressure is equal to the target final tank pressure times the target composition of that mixture component. The supply tank isolation valve is closed and the first pure component tank is

removed and replaced with the next pure component tank. The piping connecting these tanks is evacuated once again. Once this line is empty, the next component is added to the supply tank until the final target pressure is reached.

Sources for error in this mixing procedure include an imperfect pressure reading, potentially non-isothermal process of filling each gas, unaccounted volume of the piping connecting the tanks, and user error in adjusting the fill pressures. With the limited number of base mixtures ran for VLE data, tight control of this process wasn't absolutely necessary. Achieving a final composition within two percent of the target composition was deemed to be close enough. However, if many more mixtures are created with similar compositions, better control of this process may become necessary. The accuracy of the process could be improved by checking the composition after mixing and adding more of the component whose composition is lower than its target value.

Gas Chromatograph Setup

The gas chromatograph must have the helium carrier gas running through it with the thermal conductivity detector (TCD) on for at least twenty-four hours before it can be used for taking measurements. The helium tank pressure regulator must be initially turned all the way back, then open the helium tank. Monitor the pressure of the helium on the gas chromatograph pressure indicator. Adjust the pressure regulator on the tank until the pressure indicator reads 8 psig. Turn on the TCD either using the front panel of the GC or by using the LabVIEW vi for the GC. The TCD signal can either be monitored on the GC LCD display, or with the LabVIEW vi. This signal will asymptotically approach somewhere between zero and negative one. It will take about a day for the signal to become steady which is needed to have a consistent baseline for peak integration.

Liquid Nitrogen Fill

When all components are determined to be leak-tight, the start-up procedure described below was followed to prepare the system for experimental measurements.

Evacuate the vacuum can and then fill with pure nitrogen to speed up the cool-down process. Fill to somewhere less than one atmosphere so that no liquid forms inside of the vacuum can. Open the valve on the liquid nitrogen piping to begin filling the dewar from the tank outside which holds liquid nitrogen. If the piping from outside was not already cold, it may take close to an hour before any liquid nitrogen accumulates in the dewar. The liquid nitrogen level cannot be monitored until it reaches the top of the vacuum can. This point can be recognized by following the temperature of the top of the radiation shield (TRS Top). The time rate of change in this temperature will show a sudden decrease when the liquid nitrogen level in the dewar is above the top of the vacuum can. This point is circled in temperature versus time plot of the cool-down process below.

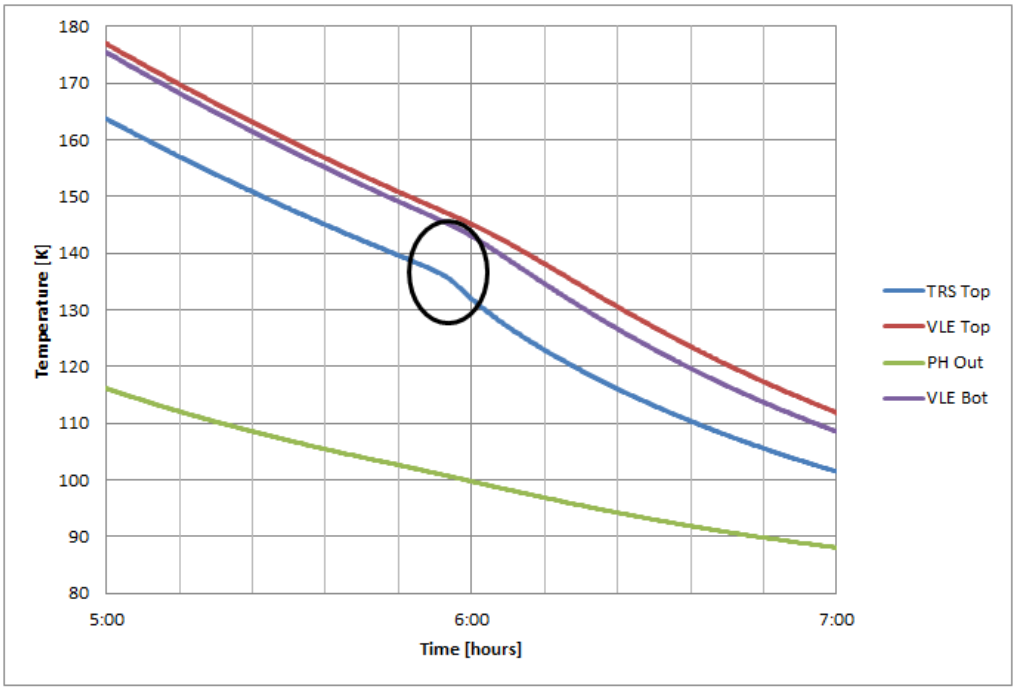

Figure 42: Temperatures plotted during cooldown. Circle denotes time when liquid nitrogen reaches top of vacuum can

Once the liquid covers the vacuum can, the liquid level in the dewar can be measured by inserting the wooden dipstick. The liquid nitrogen fill valve should be turned off when the liquid level is 18 inches above the top of the vacuum can. The process will take between three and four hours after the liquid nitrogen has reached the top of the vacuum can.

The liquid nitrogen level should be monitored daily by using the dipstick. It should be refilled before the liquid level reaches the top of the vacuum can. It takes about four to six days for the liquid nitrogen level to drop from 18 inches above the vacuum can to the level of the vacuum can.

Experimental Mixture Fill

If there is pure nitrogen in the vacuum can or process piping to speed up the cool-down process, it must be evacuated before filling the VLE. Close AV3 and close the DNS pressure regulator to minimize the amount of charge gas reaching the cold zone (Note that there will be some unavoidable leak through the DNS pressure regulator but as long as the VLE pressure remains below one atmosphere there will not be any liquefaction in the cold zone). Note the pressure of the supply tank before beginning this process. The pressure drop in the gas supply tank determines the liquid level in the cold zone.

Open AV1 and adjust the ST regulator so that the pressure in the bypass loop rises to 30 psig, then close the ST regulator. Close AV7 and AV5. Turn on the compressor. Slightly open AV5 so

that the pressure on the intake side of the compressor is around zero psig. Carefully open the ST regulator to add mass to the bypass loop. Adjust the AV5 as needed until the outlet of the compressor is operating at around 100 psig, and the suction side is slightly above zero psig.

Slowly open the DNS pressure regulator to start adding mixture to the cold zone. The differential pressure gauge can be used to see when there is flow entering the cold zone. Note that this filling process will affect the temperature of the VLE cell which will in turn affect the VLE pressure. This means that the DNS pressure regulator will have to be adjusted throughout the filling process. The filling process will also reduce the pressure on the compressor outlet. In order to counteract the pressure drop, open the ST regulator to maintain the bypass loop pressures at 100 and zero psig.

Once the ST pressure has dropped 75 psig from its starting point, close the ST regulator to stop adding mass to the system. At this point, the DNS pressure regulator should also be closed so that no more mass is going into the cold zone. If the bypass loop pressures are too high, open the DNS regulator to remove mass from this area in the system. If the bypass loop pressures are too low, slowly open AV3 to add mass to this area in the system.

If the compressor suction pressure is between zero and five psig, the compressor outlet pressure is between 90 and 110 psig, and the ST pressure has dropped 75 psig, then the VLE chamber will be approximately half full with liquid. Start-up of the experiment has been completed and it is now time to begin controlling temperatures.

5.2 Reaching Steady-State Conditions

Controlling Temperatures

The goal for steady-state vapor-liquid equilibrium is to have the VLE cell isothermal. By using the PID heater on the VLE cell in conjunction with the PID heater on the radiation shield, isothermal conditions can be established in the VLE.

The target temperature is the setpoint that is placed on the VLE heater. The VLE heater will adjust itself in order to maintain the temperature at the bottom of the VLE cell at this target temperature. If the radiation shield is also maintained at this target temperature, the system will reach steady-state but the VLE cell will not be isothermal. The VLE top temperature will be colder than the VLE bottom because it is closer to the heat sink rod than the TRS top thermometer which is controlling the TRS heater.

To compensate for the temperature difference, the setpoint for the radiation shield heater control can be set slightly higher than the target temperature in order to achieve isothermal conditions in the VLE cell. The table below shows the target temperature next to the radiation shield temperature setpoint that results in an isothermal VLE cell.

Table 5: Experimental TRS heater setpoints for isothermal VLE condition at target temperature

Target Temperature [K]	Radiation Shield Setpoint [K]	Temperature Difference [K]
84	84.35	0.35
86	86.45	0.45
88	88.55	0.55
90	90.63	0.63
92	92.724	0.724
94	94.9	0.9
96	97.02	1.02
98	99.19	1.19

With the system operating at steady-state and with the VLE cell isothermal, the heat load on the VLE heater will be very low. Almost all of the heat through the heat sink rod will be provided by the radiation shield heater.

With the VLE top and bottom temperatures equal to each other and steady, it is now time to take a composition measurement.

5.3 Taking VLE Sample

The following conditions have to be met before taking a sample:

Isothermal VLE: Temperatures of VLE top and bottom must be within 5 mK of each other

Steady-State: Both of the temperatures of the VLE cell must not have changed by more than five milliKelvin in a ten minute period. The pressure of the VLE cell must not have changed by more than one millibar for the same time period prior to taking a sample. This amount of time is chosen arbitrarily.

An example of both of these conditions being met is shown below. In this image, it can also be seen that the VLE heater power is much less than the radiation shield heater power.

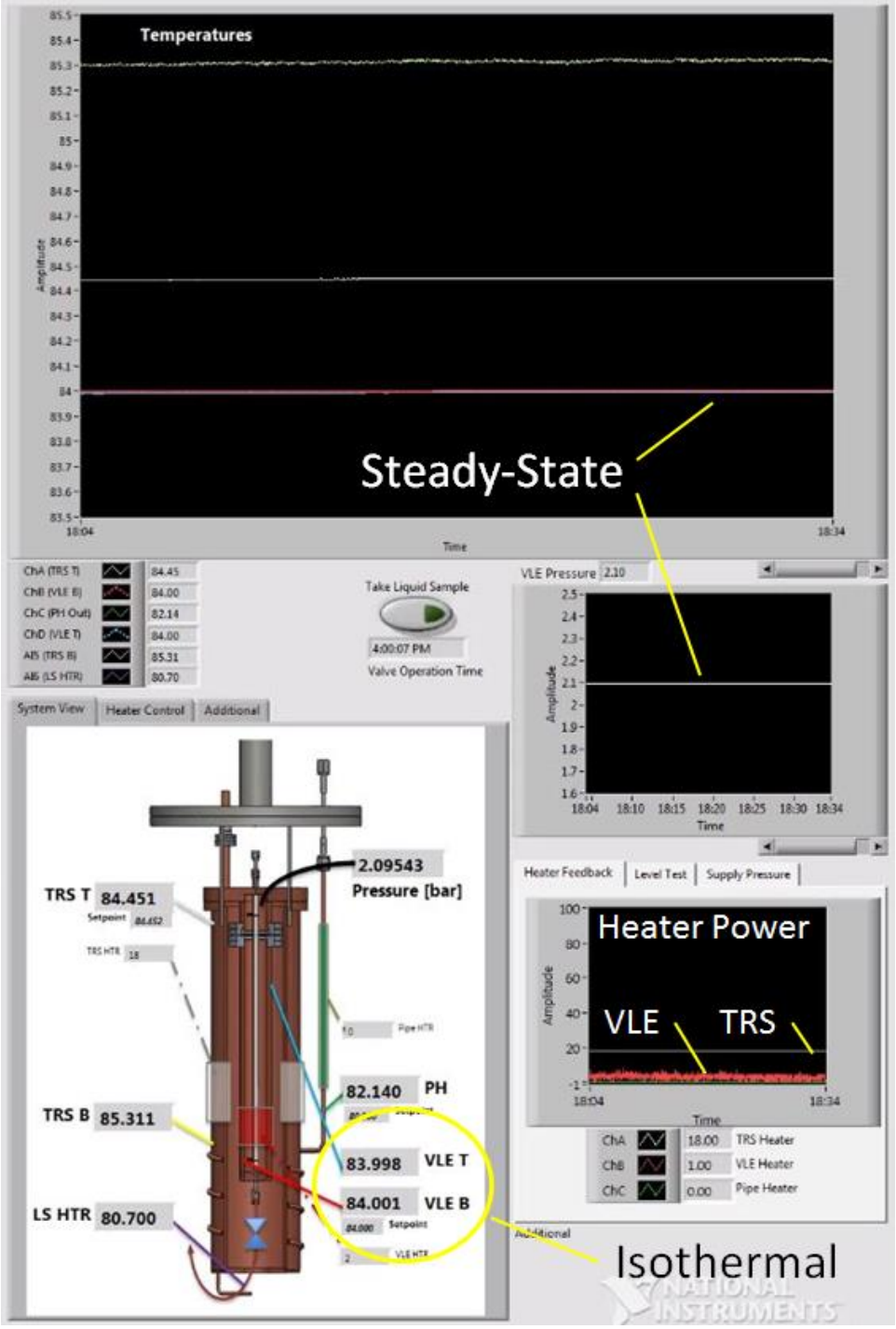

Figure 43: LabVIEW front panel when VLE is at isothermal steady-state condition

Both of the VLE temperatures, as well as the VLE pressure must be recorded before either the vapor or liquid sample is taken.

Taking a Vapor Sample

The blue shaded regions in Figure 24represent the two sample canisters. The vapor sample canister must be evacuated before taking a vapor sample. Open AV11 to make sure that this condition is met. Close AV11 once the pressure indicator on the canister reads approximately -30 inHg. Close AV2 to ensure that the vapor sample will come primarily from the VLE cell instead of the ambient piping. To take a sample, quickly open AV9 until the pressure in the canister is at least 8 psig, and then quickly close AV9. Once the sample is isolated in the vapor canister, open AV2.

Taking a Liquid Sample

Once the isothermal and steady-state requirements are met again, the liquid sample can be taken. As with the vapor sample canister, the liquid sample canister and transfer line must first be evacuated. Open AV10 and AV8 until the pressure indicator reads approximately -30 inHg. Close AV10 when this condition is met. Press the 'Take Liquid Sample' button in the LabVIEW vi. This will quickly pulse power to the solenoid valve in the cold zone which will open it for about a quarter of a second.

There is now the possibility of a new vapor-liquid equilibrium in the liquid sample (LS) transfer line. Manually turn on the LS heater by operating the switch shown below.

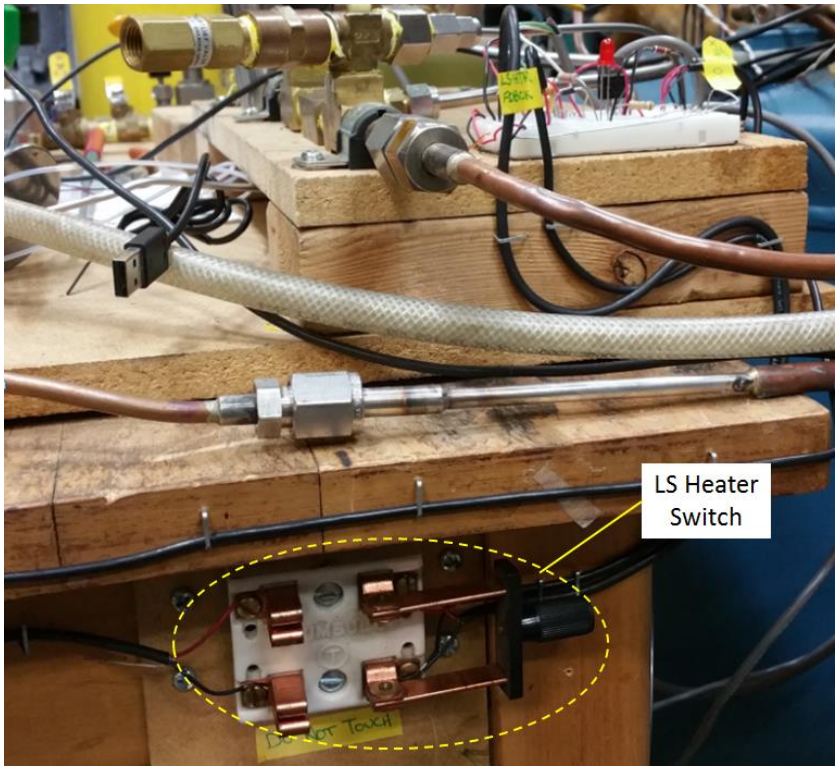

Figure 44: Switch to control liquid sample heater

The LS HTR thermometer will rise very rapidly once this 10 watt heater is on. Monitor this closely while also watching the pressure indicator on the liquid sample canister. While this heater is boiling liquid in the liquid sample line, the pressure will increase but once the liquid is all boiled off, the pressure will become steady even while the temperature is still increasing (experimentally, this occurs when the pressure in the liquid sample canister is between 25 and 40 psig). When that point is reached, turn off the LS heater and close AV8. The liquid sample, which is now a superheated vapor, is trapped in the liquid sample canister. The pressure and temperature in the liquid sample transfer line will both drop after the LS heater is turned off.

Gas Chromatograph Sampling

Consistent conditions in the sample (temperature, pressure, and volume), and in the GC (carrier gas flow rate, oven, injection, and detector temperatures) are crucial for obtaining consistent and repeatable results from the gas chromatograph. Ensure that the inlet pressure of the carrier gas into the GC is steady at 8 psig. Using the LabVIEW vi for the GC, set the oven temperature to 30°C, and the detector and injection temperatures to 150°C. Ensure that the TCD signal is steady before injecting samples into the GC.

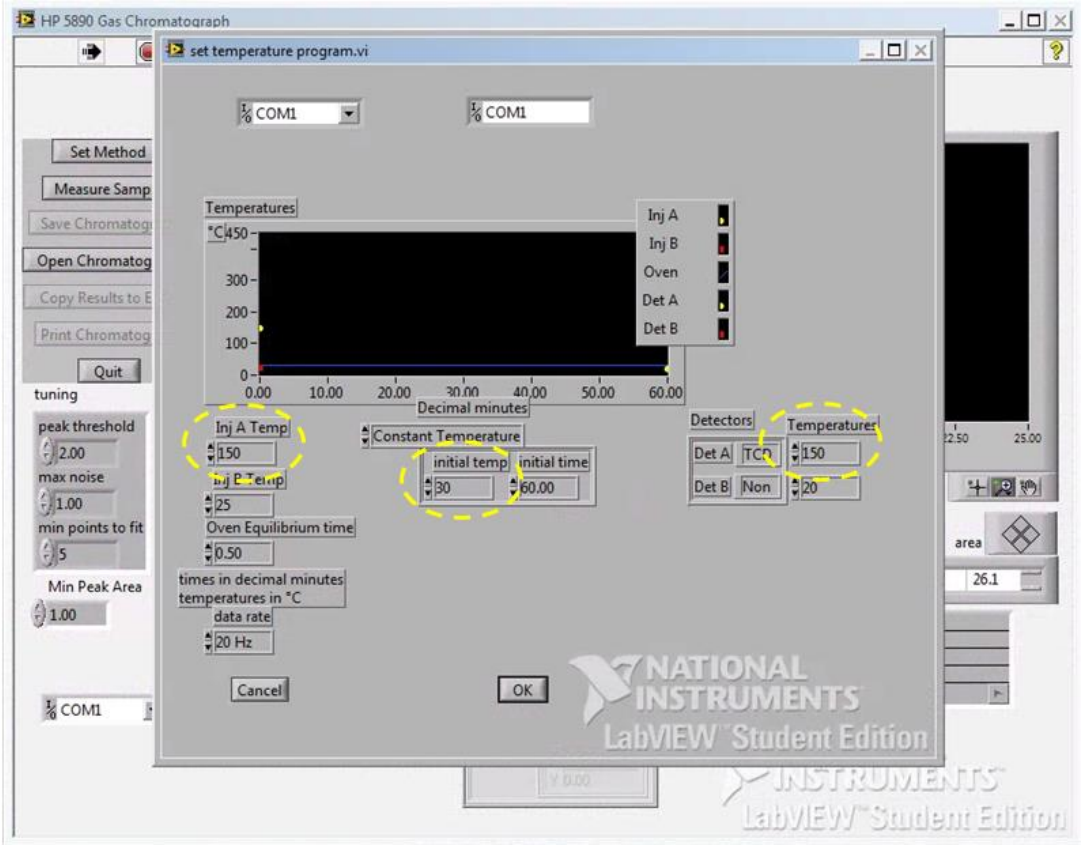

Figure 45: LabVIEW panel for setting gas chromatograph method

The temperature and pressure of the sampling canister should be consistent throughout sampling. The thermal mass of the copper will ensure that the sample is close to the ambient temperature of the lab. The pressure of the sample was arbitrarily chosen to be 5 psig. A positive pressure was chosen so that there would not be a leak into the sample canister or into the injection needle. Decrease the vapor sample canister pressure by slowly opening AV11 until the pressure indicator reads 5 psig. Similarly, decrease the liquid sample canister pressure by slowly opening AV10.

Press ‘Measure Sample’ in the GC LabVIEW vi to begin recording the TCD response. Pierce the sampling port of the canister with the injection needle, with the needle plunger all the way down. Draw approximately 150 microliters into the needle and plunge this volume back into the sample canister. Repeat this three times to ensure that the volume in the needle is purged. Draw at least 100 microliters into the needle one more time and remove the needle from the sampling port. Carefully push the plunger down so that 50 microliters of sample remain in the needle. Now pierce the GC injection port and plunge the needle volume to zero to inject the sample into the GC. Repeat this procedure five times for each composition.

The five samples can all be gathered and measured on a single chromatogram to save space on the computer. The GC LabVIEW front panel when this is done will look like the screenshot shown below.

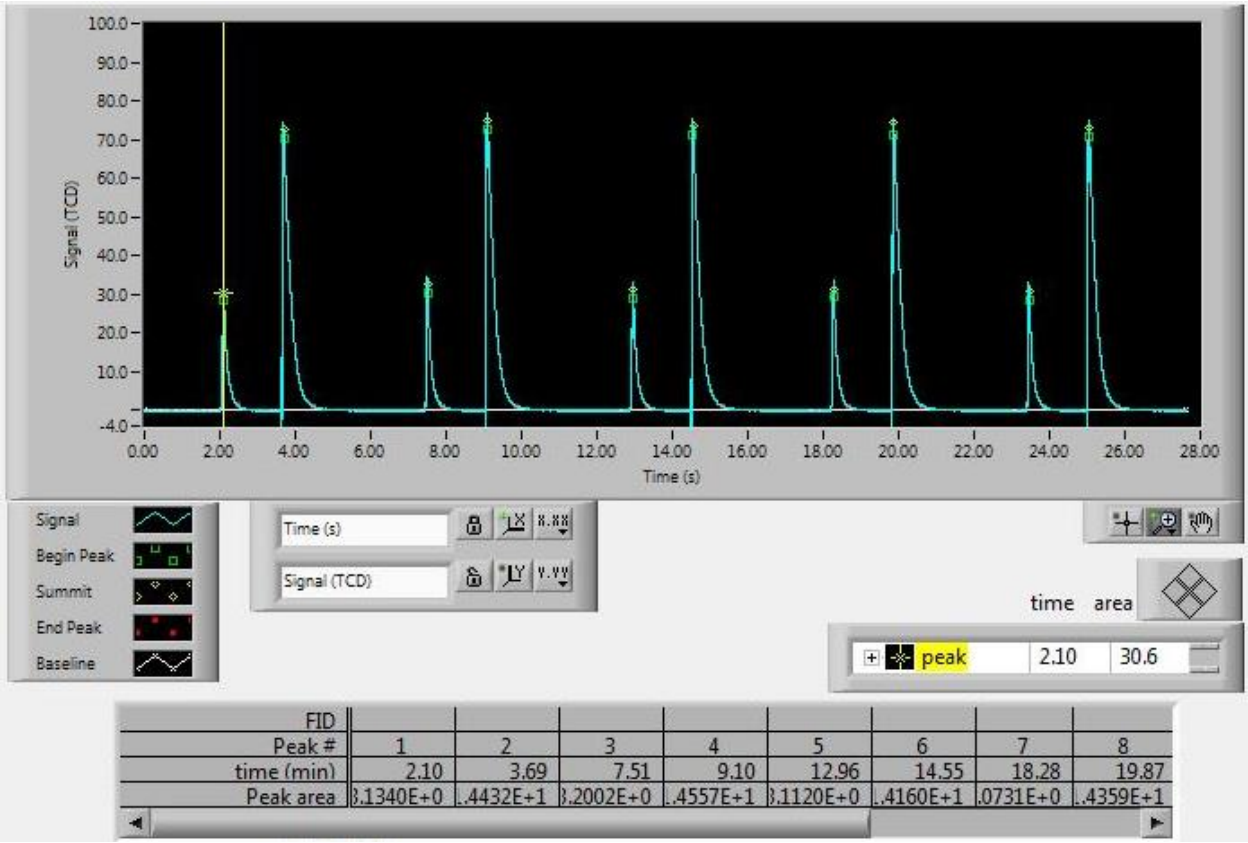

Figure 46: Gas chromatograph VI front panel after five samples have ran through the GC

The raw TCD data on the LabVIEW plot must be exported for further analysis of the peaks.

6. Results

6.1 Preliminary Results from October Experimental Run

The first time the dewar was filled with liquid nitrogen was in October 2015. Although several VLE data points were taken during this run, the primary objective of the test was to learn how to control our system. The complications and resolutions of the first run is the focus of the present section, not the VLE data points taken during the run.

Independent Control of Temperature and Pressure

From the initial stages of modeling for this experiment, it was assumed that there would be a constant flow through the VLE cell. The temperature of the VLE cell would be controlled with heaters in the cold zone, and the pressure and flow through the cell would be controlled with the two pressure regulators in the ambient plumbing. This quickly proved to be very difficult during the initial charge of the first test mixture.

The first lesson learned was that the temperature of the VLE cell determines the system pressure, and that steady state could be realized through temperature control, but not through pressure control. Also it is difficult to control the temperature of the VLE using the heaters while a flow of mixture passes through the cold zone. The plot below shows the recorded temperatures and pressure in the cold zone after initially charging the system. Several moments identified on the plot mark the times when changes were made to the system.

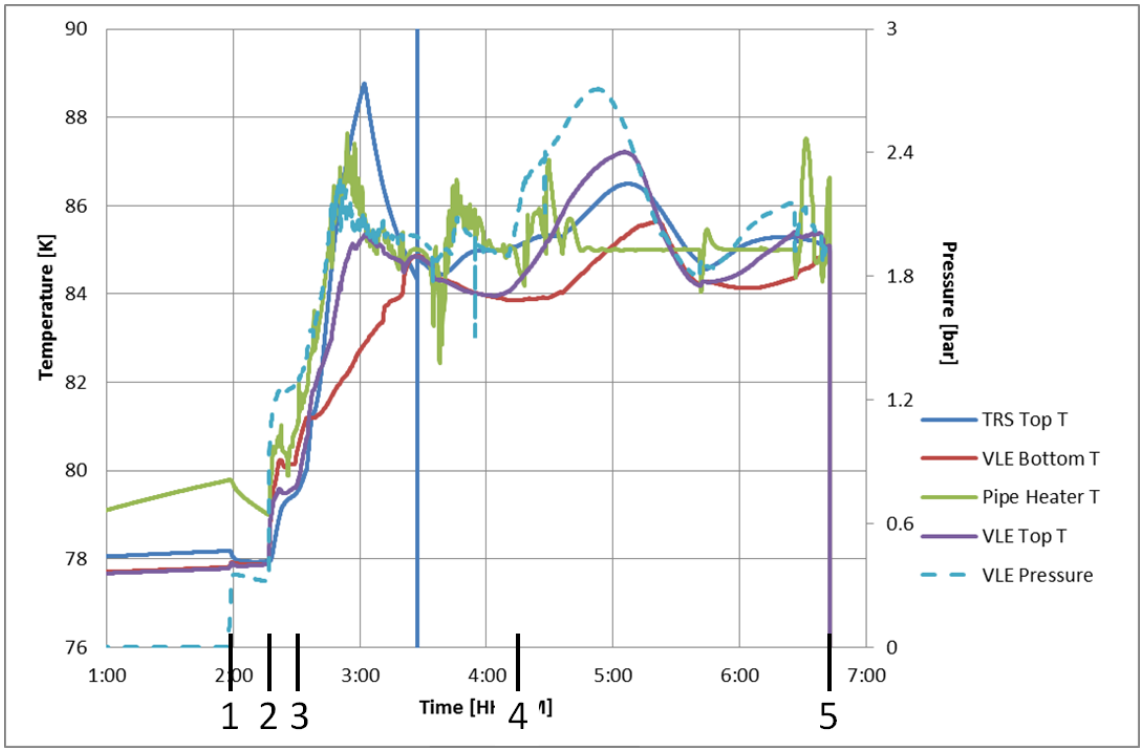

Figure 47: Temperatures and pressure versus time after first charging VLE system with mixture

At point 1, the pressure in the VLE rises above zero for the first time. This is when the ST regulator was first opened. At point 2, the VLE pressure rises again. Here, the regulator is adjusted to allow flow into the VLE cell. Point 3 marks the time when the three heaters were turned on in an attempt to control the temperature to 85 Kelvin. Between points 3 and 4, both the DNS and backpressure regulators were adjusted in an attempt to steady the VLE pressure. After point 4, manual adjustments ceased. At point five, the data acquisition was shut off in order to change the VLE temperature control setpoint from the VLE bottom temperature to the VLE top temperature.

As a result of this early trouble maintaining temperature and pressure, a flow equilibrium condition was abandoned for a static equilibrium condition. The VLE cell was isolated from the compressor once it was sufficiently charged.

Level Detector Problems

The silicon diode level detector did not give the expected response during the first run. Shown below is a screenshot of the voltage response of the two silicon diodes used for liquid detection. The voltage in the upper diode drops slightly more than the voltage in the lower diode, indicating more self-heating in the vapor region. However the expected decrease was much larger and faster.

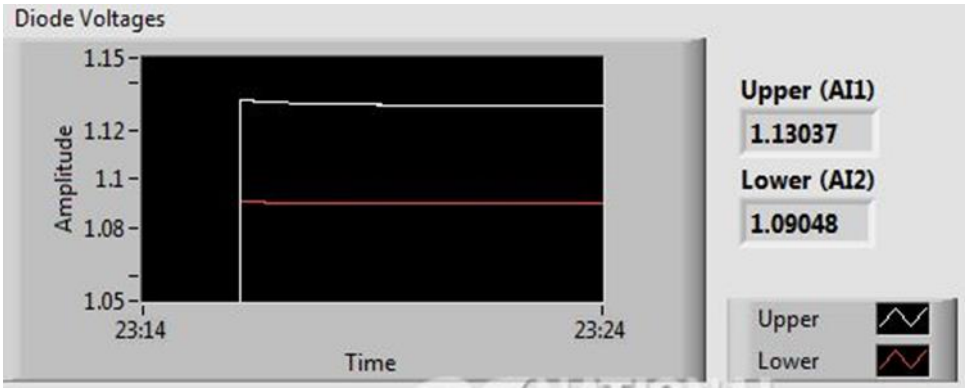

Figure 48: Unexpected liquid level detector response during October experimental run

It was later determined that a grounding issue kept the two voltage responses approximately equal to each other. The ground problem was resolved before the experiment ran again in February. Below is another screenshot of the voltage of the two silicon diodes taken during the experimental run in February.

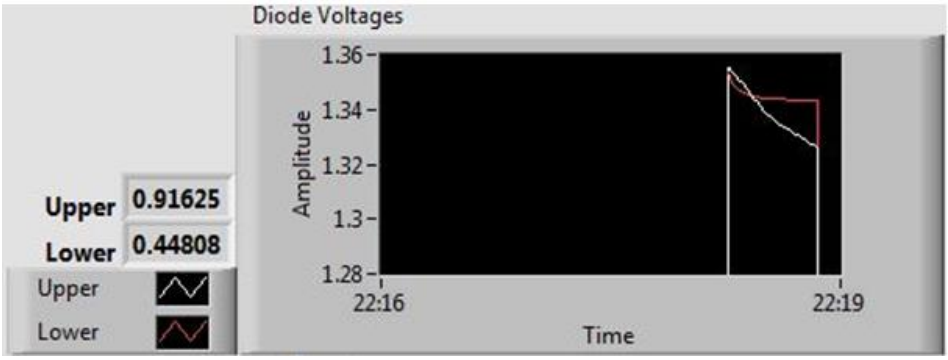

Figure 49: Expected liquid level detector response when liquid level is present (February 2016)

This screenshot shown in Figure 50 was taken in February under similar conditions as in Figure 48. However, the self-heating of the upper diode is clearly visible, while the signal from lower diode levels out indicating that it is still covered by liquid. Also, the duration of this test is less than one minute, compared to about eight minutes for the similar test in October.

VLE Cell Temperature Stratification

Shown below is a schematic that depicts where the thermometers and heaters were located during the experiment run in October.

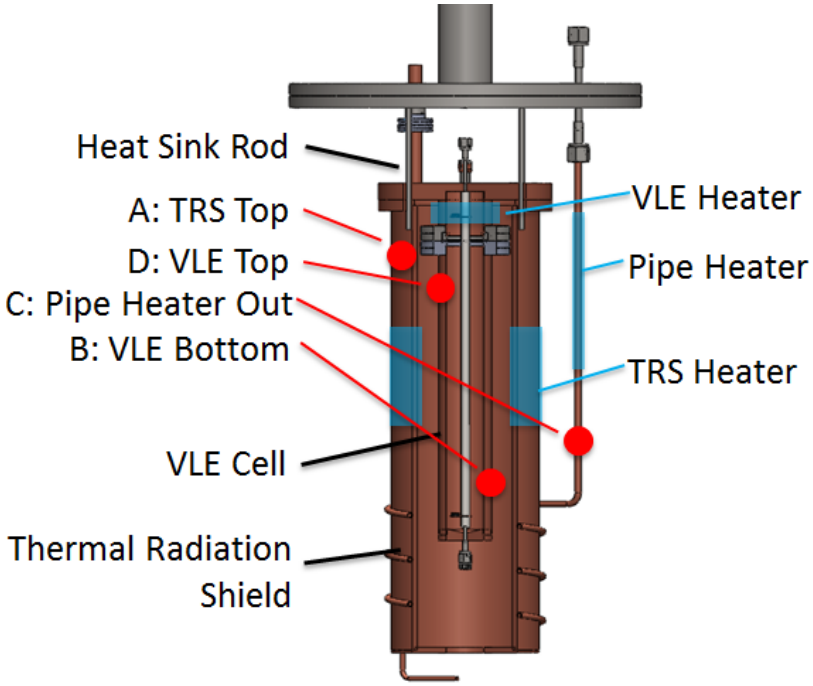

Figure 50: System thermometer and heater locations during October experimental run

Focusing on the VLE cell, the VLE heater is above both of the VLE thermometers. Without any flow of the mixture through the VLE cell, any heat load greater than zero from the VLE heater will result in a temperature gradient between the VLE top and bottom thermometers. It was possible to have all of the temperatures in the system steady, but there would always be a difference between the VLE top and bottom. In other words, an equilibrium condition existed, but it contained a temperature gradient.

The temperature difference between VLE top and bottom increased as the controlled temperature increased. Vapor and liquid samples were still taken during the October run but the unresolved problem rendered the data unusable.

The location of the VLE heater was moved much lower on the VLE cell before running again in February. The figure below shows the new location of the VLE heater with respect to the VLE thermometers.

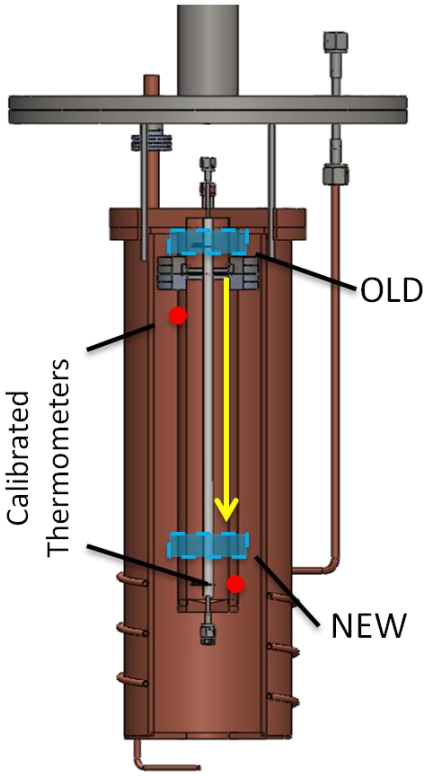

Figure 51: New heater location on VLE cell

With the new arrangement, the VLE bottom thermometer is controlled directly with the VLE heater. The VLE top thermometer is controlled indirectly by adjusting the set point of the TRS heater. The improved setup allowed for control of each thermometer, enabling the VLE cell to be isothermal.

Leak through the Liquid Sample Solenoid Valve

A leak through the solenoid valve was identified when the piping on the low pressure side was evacuated by noting a pressure increase in the liquid sample canister when it should have remained constant. The leak through the valve worsened as the experiment progressed. Subsequent inspection at room temperature revealed that the leak was caused by debris making its way in between the valve's plunger and orifice.

The solenoid valve was taken apart and inspected after the October run was concluded. Some pictures of this process are shown in the figure below.

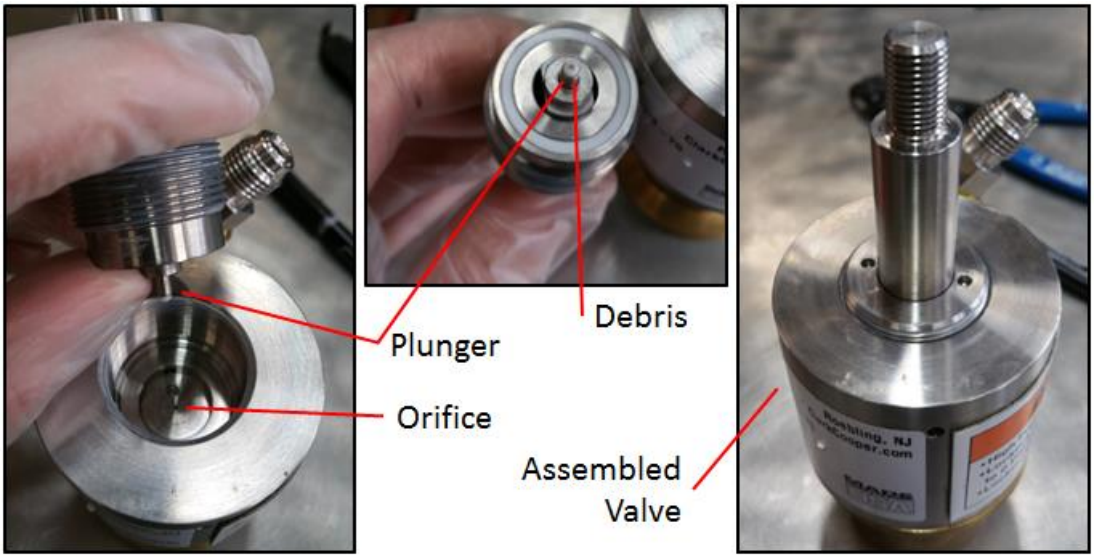

Figure 52: Pictures taken during cleaning of solenoid valve internals

Significant debris was found on the Teflon plunger of the valve. We speculated that this came from impurities in the piping connected to the VLE cell as a result of brazing. The tip of the plunger was cleaned and smoothed out using a polishing cloth. The cleaning process provided an improved seat for the plunger on top of the orifice. The high pressure side of the solenoid valve is attached to the VLE cell with a VCR connection. A gasket with a two micron mesh was added there to prevent debris from causing the same problem in the future.

Two-Phase Condition in Liquid Sample Transfer Line

The need for the liquid sample line heater has already been discussed. However, during the October experiment run, the heater was not yet installed. This means that the recorded liquid compositions may not accurately represent the composition of the liquid portion of the VLE cell.

Vapor-Liquid Equilibrium Results from October Run

Four VLE data points were taken from this run. All were out of the same base mixture of approximately 80% nitrogen, 20% argon. The temperatures, pressure and compositions of each phase are shown in the table below.

Table 6: VLE data from October experiment run

Temperature			Pressure		Vapor Composition			Liquid Composition		
Bottom	Top	Unc.	Meas.	Unc.	Ar	N2	Unc.	Ar	N2	Unc.
[K]	[K]	[±K]	[bar]	[±bar]	[%]	[%]	[±%]	[%]	[%]	[±%]
88.537	88.992	0.0187	2.838	0.0027	16.252	83.748	0.637	23.624	76.376	0.095
92.758	93.494	0.0191	4.055	0.0028	8.686	91.314	0.107	21.079	78.921	0.256
95.310	96.200	0.0194	4.915	0.0028	9.021	90.979	0.117	17.851	82.149	0.240
98.219	99.101	0.0196	5.93	0.0029	7.258	92.742	0.126	23.421	76.579	0.110

As alluded to in a previous section and reflected in the table above, the VLE cell was not isothermal while the samples were being taken. The difference in temperature ranged from about 0.4 to 0.9 Kelvin. Also, because the data was gathered without a heater on the liquid sample line, the liquid composition results may not accurately represent the VLE condition measured by the temperature and pressure.

The uncertainty in temperature is in the expected range, but does not reflect the temperature of the VLE mixture since it does not take into account the temperature difference.

Calculating the relative volatility of each VLE condition leads to the plot shown below.

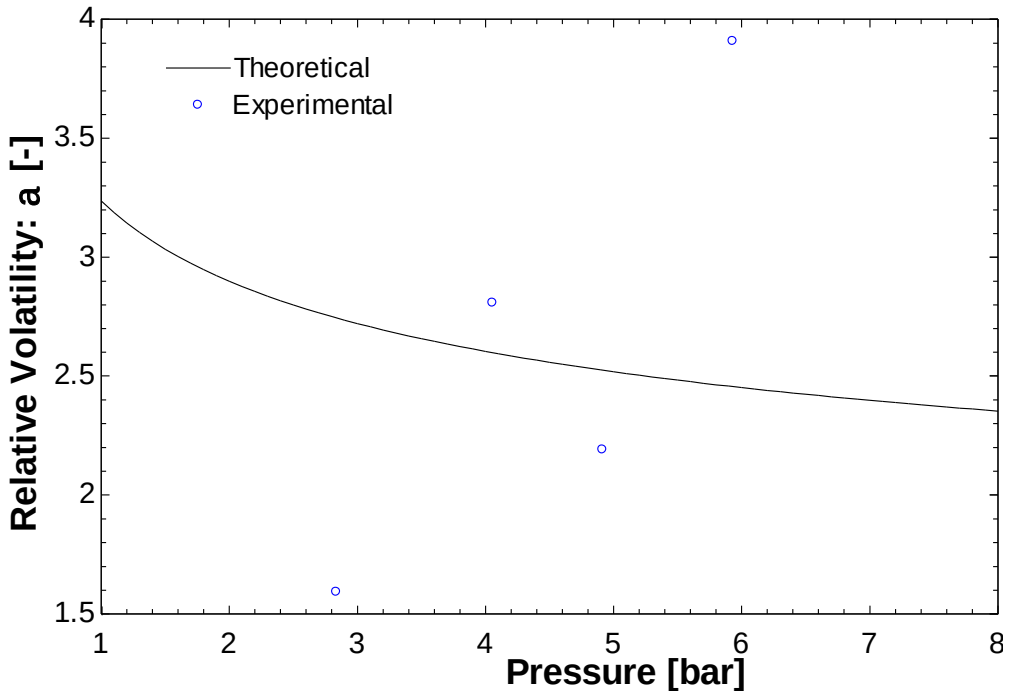

Figure 53: Relative volatility of VLE data points taken in October

The theoretical line represents the relative volatility if the liquid phase mole fraction is set at 80% nitrogen. The trend in the experimental data points is heading in the wrong direction, and the first and last points are very far away from the expectation.

6.2 Results from February Experimental Run

The second experimental run occurred in February 2016. All of the improvements discussed in the previous sections were implemented. This section discusses the results from the experimental run in February, 2016.

Pure Component Validation

As a validation of both the temperature and pressure measurements, the VLE system was charged with pure nitrogen. Isothermal conditions in the VLE were established in the same manner as if it were charged with a nitrogen-argon mixture. When the system is charged such that there is a vapor-liquid interface in the VLE cell, the resulting pressure should be equal to the saturation pressure at the controlled temperature. The temperature was controlled at increments of two Kelvin over the range of 82 to 96 Kelvin. The table below shows the results of this process.

Table 7: Experimental nitrogen saturation data

	Experimental Data				Theoretical Data			
Data Point	Temperature [K]			Pressure [bar]	Pressure		Temperature	
	VLE Bottom	VLE Top	**Averaged**		$P_{sat}(T)$ [bar]	Error [bar]	$T_{sat}(P)$ [K]	Error [K]
1	81.999	82.001	**82**	**1.71**	1.695	-0.015	82.087	0.087
2	83.998	84.001	**84**	**2.095**	2.076	-0.019	84.094	0.094
3	85.997	86.002	**86**	**2.54**	2.517	-0.023	86.096	0.096
4	87.998	88	**87.999**	**3.05**	3.025	-0.025	88.092	0.093
5	89.998	90.002	**90**	**3.633**	3.605	-0.028	90.092	0.092
6	91.997	92.001	**91.999**	**4.293**	4.261	-0.032	92.09	0.091
7	93.999	94	**94**	**5.036**	5.002	-0.034	94.087	0.087
8	96	96	**96**	**5.868**	5.832	-0.036	96.083	0.083

The experimental data shows the three points that could be measured: the temperatures on the top and bottom of the VLE cell, and the pressure attached to the VLE cell by an eighth inch pipe up to ambient. The experimental data is plotted below against the theoretical saturation line for nitrogen. The temperature used is the average of the temperatures of the top and bottom of the VLE cell.

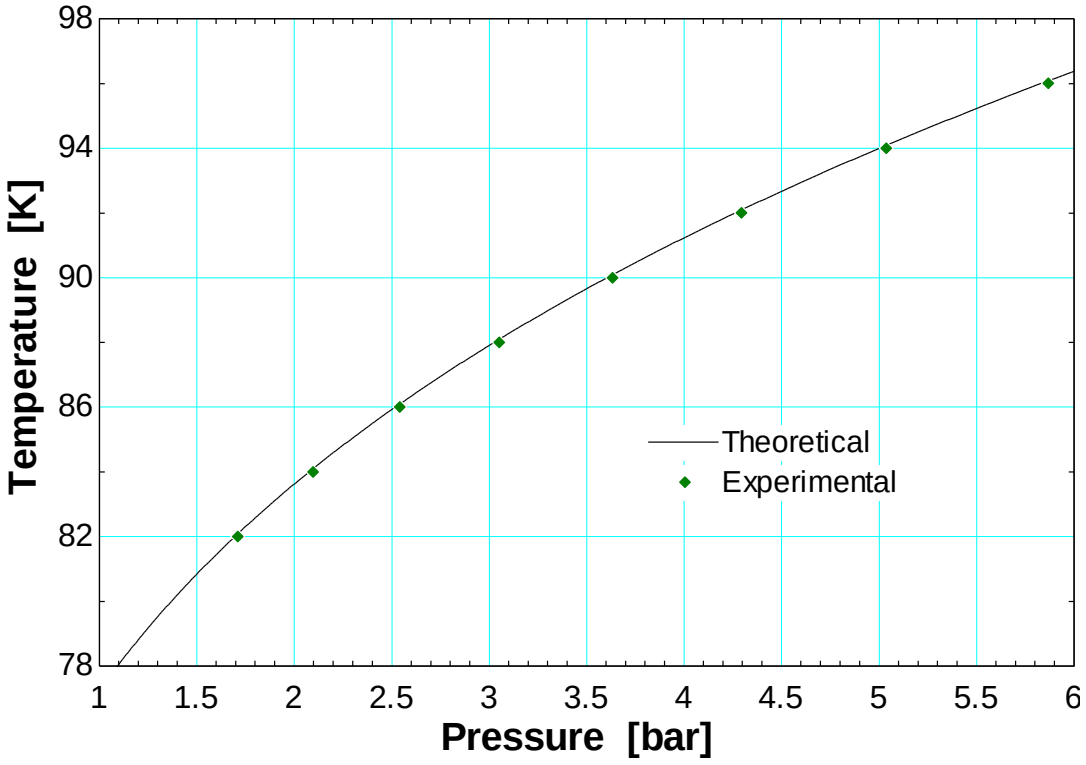

Figure 54: Nitrogen saturation curve experimental data

As shown in Figure 54, the data includes no outliers but there is a consistent offset between the experimental data and the theoretical line. The experimental temperature always is below theoretical value; similarly, the experimental pressure is always above the theoretical value. The plot below explores this more.

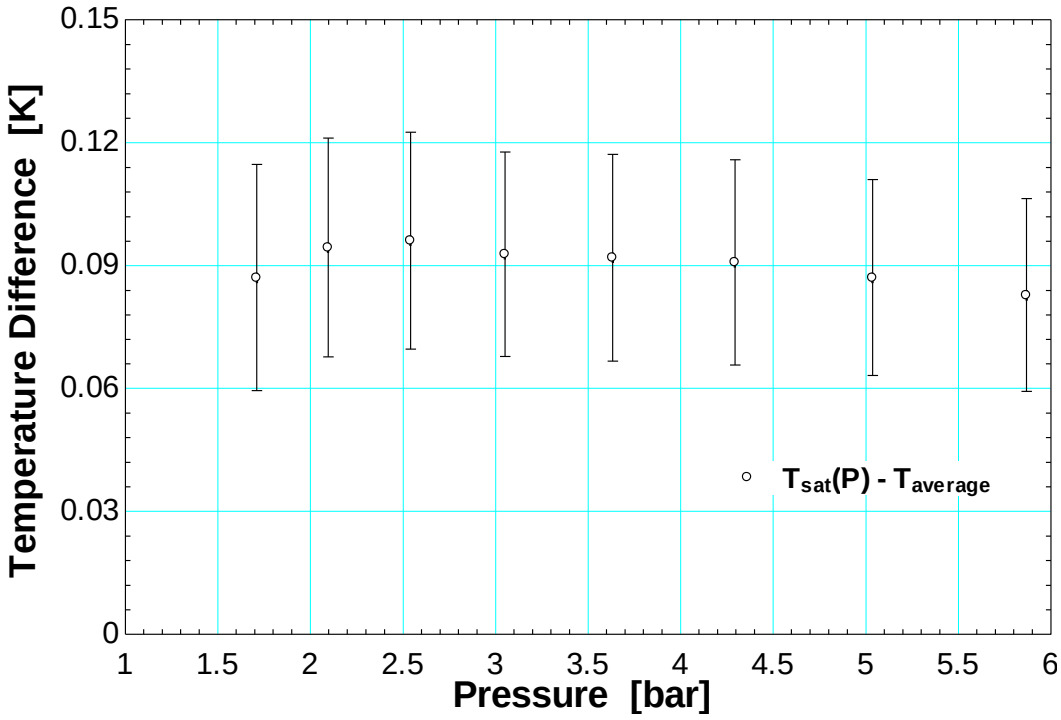

Figure 55: Difference between expected and measured saturation temperatures

As shown in Figure 55, the offset between the theoretical and experimental temperatures is consistently around 0.09 Kelvin.

$$Average(\Delta T) = 0.09037\ [K]$$

$$Std.Dev.(\Delta T) = 0.00442\ [K]$$

The uncertainty bars shown in the plot result from the uncertainty in the temperature readings, the difference in the two measured temperatures, and the pressure reading that computes the saturation temperature.

Figure 56 shows the difference between measured pressure and predicted saturation pressure based on measured temperature. As expected, the difference in pressure displays the opposite sign as the difference in temperature.

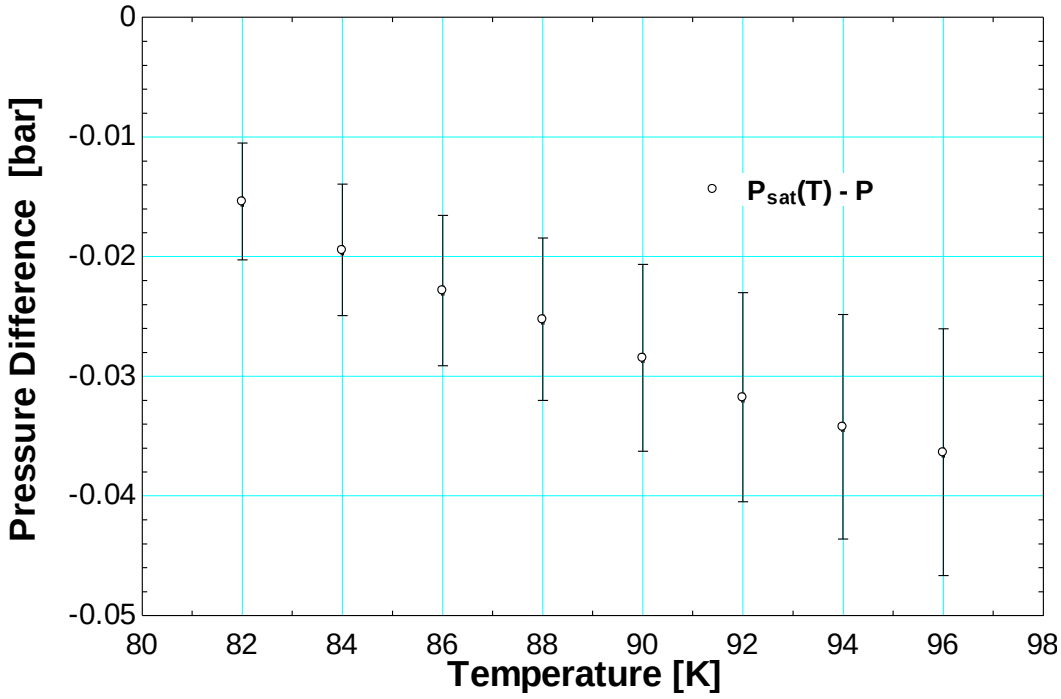

Figure 56: Difference between expected and measured saturation pressure

In other words, a measured temperature below the theoretical value corresponds to a measured pressure above the theoretical value. Note that the uncertainty bars grow as the temperature increases. Such behavior results from the slope of the theoretical saturation line for nitrogen as shown in Figure 54, decreasing as temperature is increased. The trend amplifies the pressure uncertainty at higher temperatures. The procedure for uncertainty analysis of the saturation properties, as well as additional uncertainty results, is included in Appendix Section 9.2.

Comparing the two plots to each other, both show an offset from the theoretical value that is greater than the calculated measurement uncertainty. The temperature error is relatively constant when plotted against temperature, but the pressure error worsens as temperature increases. This could make the temperature error the more likely culprit for the cause of the error.

Vapor-Liquid Equilibrium Results

One liquid and one vapor sample were taken separately at each two-degree temperature increment. Since it was much easier to add heat to the VLE cell than it was to remove it, the temperature was incremented starting at 84 Kelvin and increasing to 98 Kelvin. Once samples had been taken at all of the temperatures, the test mixture was evacuated from the system and a new one with a different composition was added in its place.

The same procedure was carried out with three separate mixtures. The data for each mixture is tabulated below.

Table 8: VLE data for low argon concentration mixture

Sample Name	Type	T_bottom	T_top	Temperature		Pressure		Compositions		
[-]	[-]	[K]	[K]	[K]	Unc. [±K]	[bar]	Unc. [±bar]	Ar	N2	Uncertainty
84V-0220-1746	Vapor	84.008	84.011	84.0095	0.030	2.037	0.002696	**0.02133**	**0.97867**	0.000907
84L-0220-2126	Liquid	84.008	84.011	84.0095	0.030	2.035	0.002696	**0.06463**	**0.93537**	0.000789
86V-0221-0104	Vapor	86	85.999	85.9995	0.030	2.469	0.002724	**0.02439**	**0.97561**	0.001590
86L-0221-0130	Liquid	86	86	86	0.030	2.466	0.002724	**0.06405**	**0.93595**	0.002651
88V-0221-1002	Vapor	88	87.999	87.9995	0.031	2.967	0.002756	**0.02303**	**0.97697**	0.000276
88L-0221-0927	Liquid	88.001	87.999	88	0.031	2.969	0.002757	**0.06188**	**0.93812**	0.002627
90V-0221-1453	Vapor	90	90	90	0.031	3.528	0.002793	**0.02671**	**0.97329**	0.000878
90L-0221-1352	Liquid	90	89.999	89.9995	0.031	3.529	0.002793	**0.05419**	**0.94581**	0.001015
92V-0221-2000	Vapor	92.001	92.001	92.001	0.031	4.175	0.002835	**0.02567**	**0.97433**	0.000671
92L-0221-1830	Liquid	92.005	92.005	92.005	0.031	4.176	0.002835	**0.05671**	**0.94329**	0.001187
94V-0222-2155	Vapor	94.004	93.918	93.961	0.031	4.884	0.002881	**0.01741**	**0.98259**	0.000595
94L-0222-1839	Liquid	94.012	93.911	93.9615	0.031	4.888	0.002881	**0.06171**	**0.93829**	0.001685
96V-0223-1450	Vapor	96.041	96.039	96.04	0.032	5.708	0.002934	**0.02366**	**0.97634**	0.000555
96L-0223-1406	Liquid	96	95.993	95.9965	0.032	5.692	0.002933	**0.05425**	**0.94575**	0.000407

Table 9: VLE data for medium argon concentration mixture

Sample Name	Type	T_bottom	T_top	Temperature		Pressure		Compositions		
[-]	[-]	[K]	[K]	[K]	Unc. [±K]	[bar]	Unc. [±bar]	Ar	N2	Uncertainty
84V-0224-2041	Vapor	84	84	84	0.030	1.885	0.002686	**0.06647**	**0.93353**	0.000268
84L-0224-2030	Liquid	83.999	84.002	84.0005	0.030	1.886	0.002686	**0.1583**	**0.8417**	0.000367
86V-0225-1207	Vapor	86	85.998	85.999	0.030	2.289	0.002712	**0.07321**	**0.92679**	0.000528
86L-0225-1155	Liquid	86.001	85.998	85.9995	0.030	2.291	0.002713	**0.16544**	**0.83456**	0.000706
88V-0225-1430	Vapor	88.001	88.004	88.0025	0.031	2.742	0.002742	**0.07019**	**0.92981**	0.000721
88L-0225-1508	Liquid	88	87.999	87.9995	0.031	2.743	0.002742	**0.16621**	**0.83379**	0.001467
90V-0225-1747	Vapor	90	90.005	90.0025	0.031	3.27	0.002776	**0.07074**	**0.92926**	0.000216
90L-0225-1806	Liquid	90	89.999	89.9995	0.031	3.262	0.002776	**0.1565**	**0.8435**	0.001204
92V-0225-2139	Vapor	91.999	92.001	92	0.031	3.856	0.002814	**0.06384**	**0.93616**	0.001146
92L-0225-2245	Liquid	92	91.997	91.9985	0.031	3.861	0.002814	**0.16333**	**0.83667**	0.000508
94V-0226-0957	Vapor	94.011	94.993	94.502	0.032	4.532	0.002858	**0.07188**	**0.92812**	0.000315
94L-0226-1041	Liquid	94.01	94.006	94.008	0.031	4.532	0.002858	**0.15597**	**0.84403**	0.001028
96V-0226-1424	Vapor	96	95.992	95.996	0.032	5.272	0.002906	**0.0752**	**0.9248**	0.000542
96L-0226-1542	Liquid	96.003	95.995	95.999	0.032	5.28	0.002906	**0.15941**	**0.84059**	0.001427
98V-0226-1758	Vapor	98.006	97.998	98.002	0.032	6.141	0.002962	**0.06528**	**0.93472**	0.000740
98L-0226-1822	Liquid	98.006	98.004	98.005	0.032	6.114	0.00296	**0.1765**	**0.8235**	0.000827

Table 10: VLE data for high argon concentration mixture

Sample Name	Type	T_bottom	T_top	Temperature		Pressure		Compositions		
[-]	[-]	[K]	[K]	[K]	Unc. [±K]	[bar]	Unc. [±bar]	Ar	N2	Unc.
84V-0227-1143	Vapor	84	83.993	83.9965	0.030	1.72	0.002676	**0.12788**	**0.87212**	0.000933
84L-0227-1202	Liquid	84.012	84	84.006	0.030	1.72	0.002676	**0.31354**	**0.68646**	0.001046
86V-0227-1351	Vapor	85.998	85.999	85.9985	0.030	2.09	0.0027	**0.13846**	**0.86154**	0.000279
86L-0227-1435	Liquid	86	85.997	85.9985	0.030	2.083	0.002699	**0.29279**	**0.70721**	0.000827
88V-0227-1533	Vapor	88	88.001	88.0005	0.031	2.512	0.002727	**0.14127**	**0.85873**	0.000200
88L-0227-1707	Liquid	88	88.003	88.0015	0.031	2.506	0.002727	**0.32268**	**0.67732**	0.000679
90V-0228-1508	Vapor	90	89.996	89.998	0.031	2.993	0.002758	**0.12628**	**0.87372**	0.000772
90L-0228-1530	Liquid	90.002	89.99	89.996	0.031	2.99	0.002758	**0.32051**	**0.67949**	0.000316
92V-0228-1715	Vapor	92	92.002	92.001	0.031	3.54	0.002794	**0.1489**	**0.8511**	0.000435
92L-0228-1754	Liquid	91.999	91.993	91.996	0.031	3.542	0.002794	**0.29067**	**0.70933**	0.001243
94V-0228-2023	Vapor	94.001	94.003	94.002	0.031	4.168	0.002834	**0.13792**	**0.86208**	0.000797
94L-0228-2049	Liquid	94	94.003	94.0015	0.031	4.15	0.002833	**0.3164**	**0.6836**	0.000438
96V-0228-2207	Vapor	96.005	96.006	96.0055	0.032	4.86	0.002879	**0.13927**	**0.86073**	0.000507
96L-0228-2243	Liquid	96.003	96.003	96.003	0.032	4.855	0.002879	**0.30197**	**0.69803**	0.001835
98V-0229-1655	Vapor	98	98	98	0.032	5.623	0.002929	**0.13582**	**0.86418**	0.000516
98L-0229-1727	Liquid	98.006	97.999	98.0025	0.032	5.617	0.002928	**0.29658**	**0.70342**	0.001124

The temperature difference between top and bottom of the VLE cell was vastly reduced compared to the results from October. In almost all data points, the two temperatures are within a hundredth of a Kelvin. More careful and consistent sampling (in addition to being more practiced at it) led to a small decrease in the uncertainty of the compositions.

Taking the data from all three mixtures, P-xy plots have been created for each of the controlled temperatures during the experiment. These are shown in the figures below.

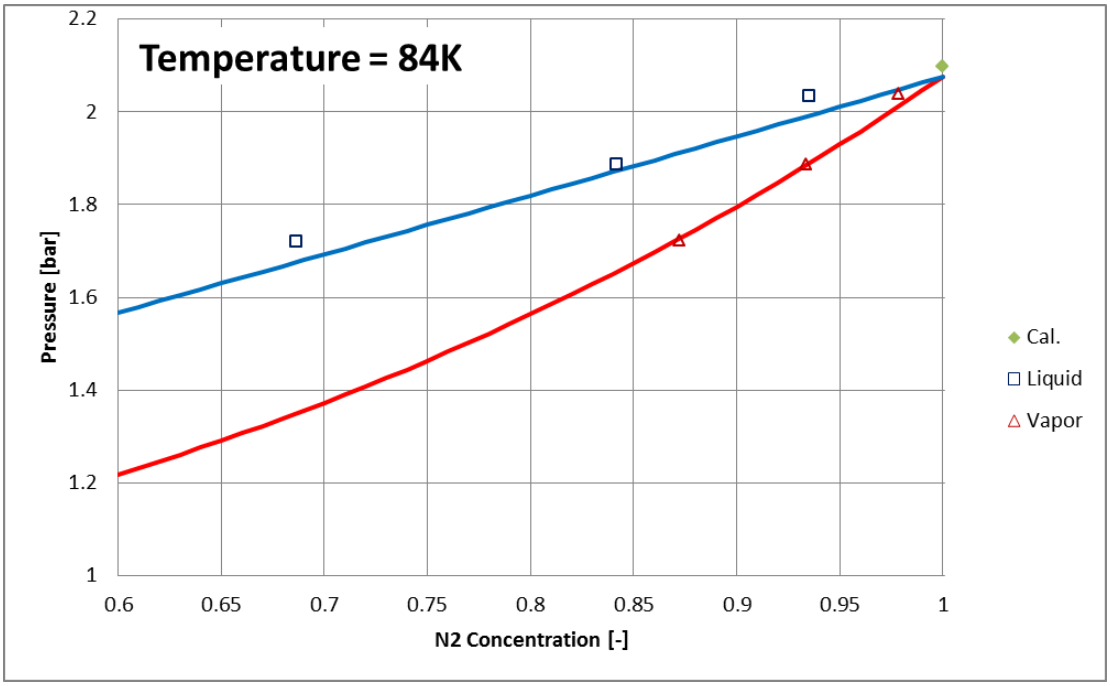

Figure 57: Experimental VLE data at 84 Kelvin

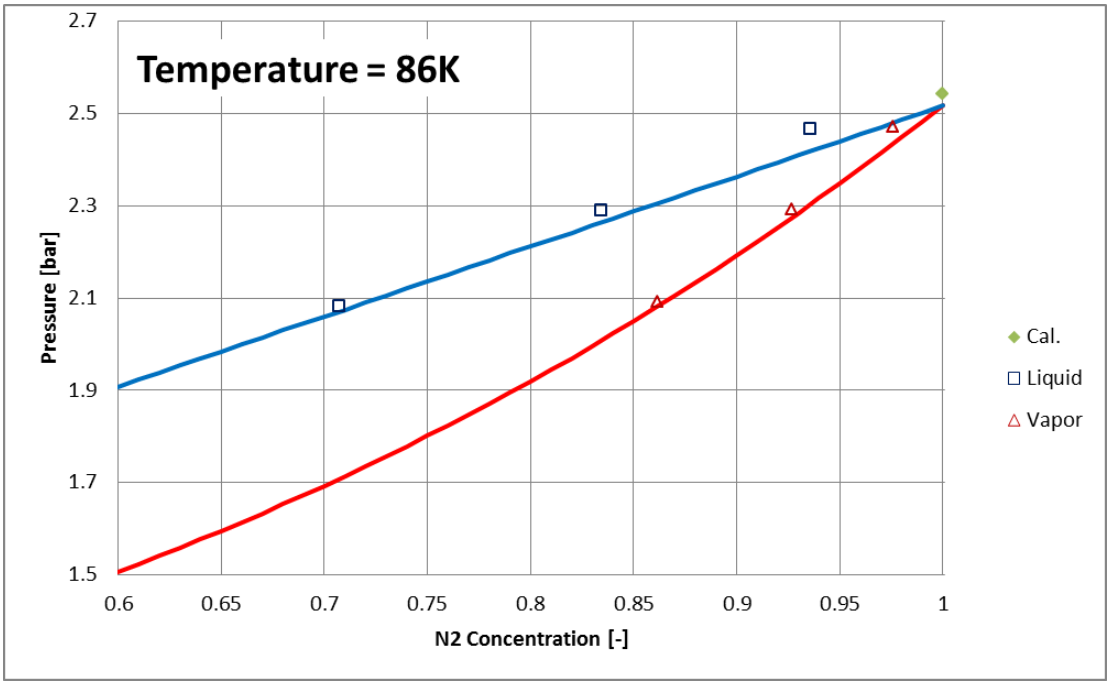

Figure 58: Experimental VLE data at 86 Kelvin

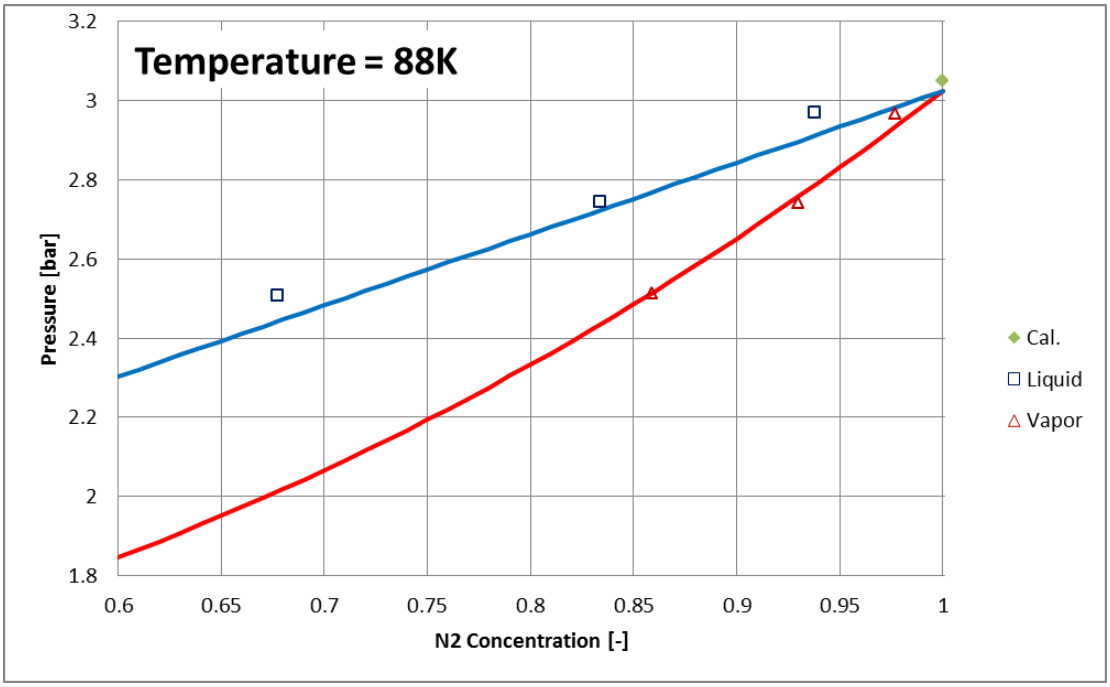

Figure 59: Experimental VLE data at 88 Kelvin

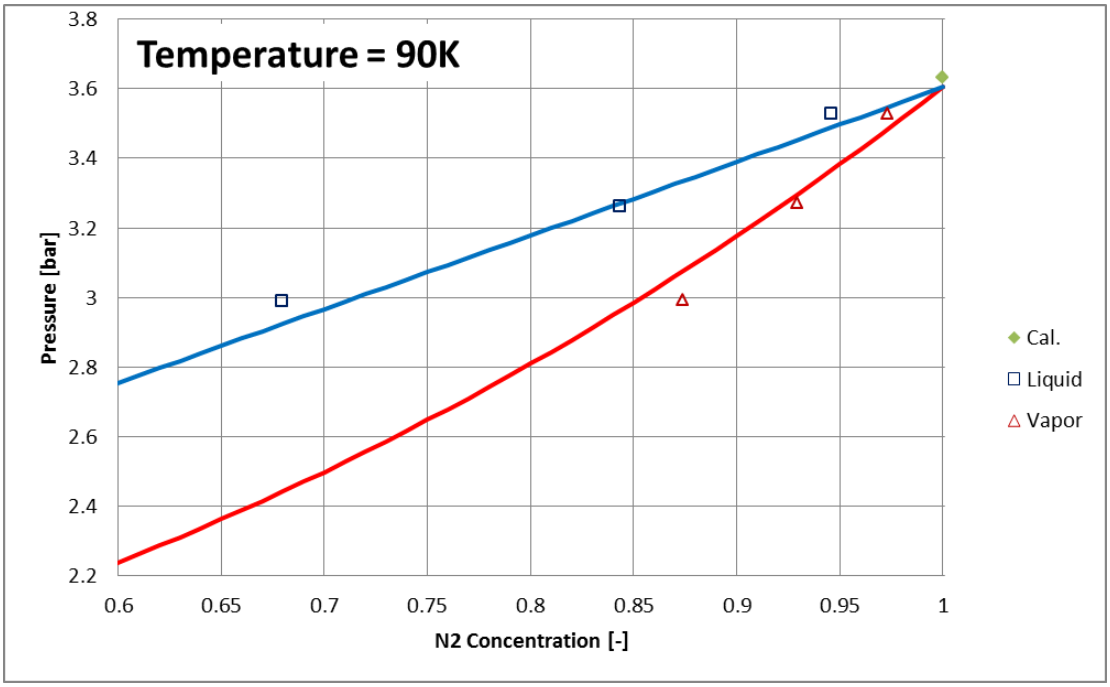

Figure 60: Experimental VLE data at 90 Kelvin

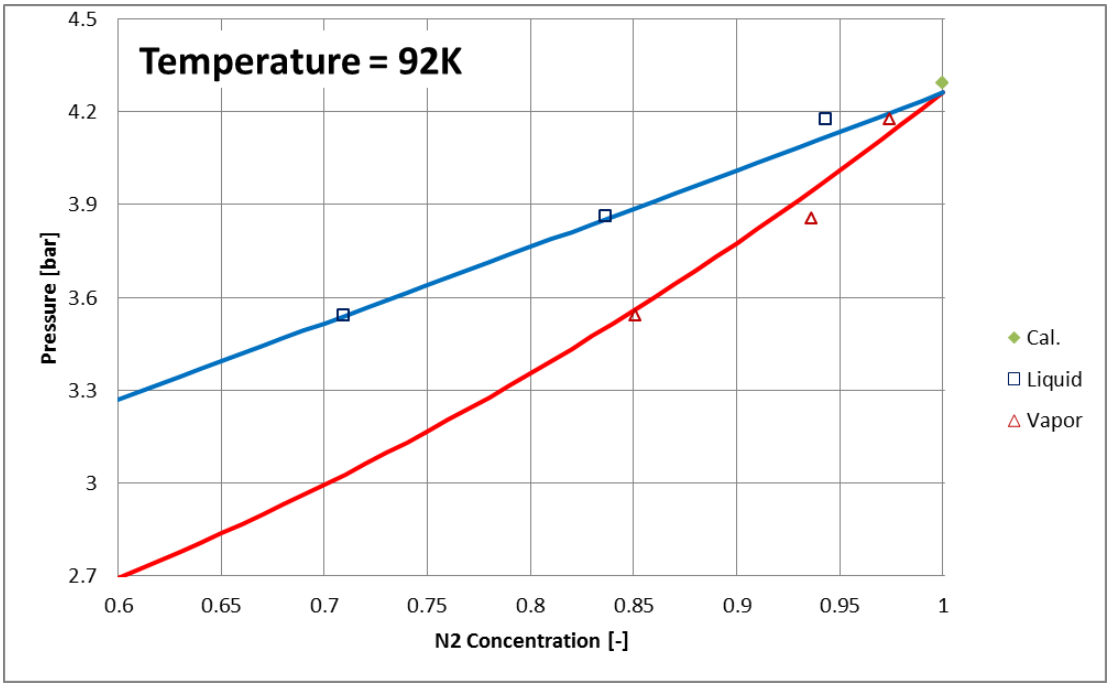

Figure 61: Experimental VLE data at 92 Kelvin

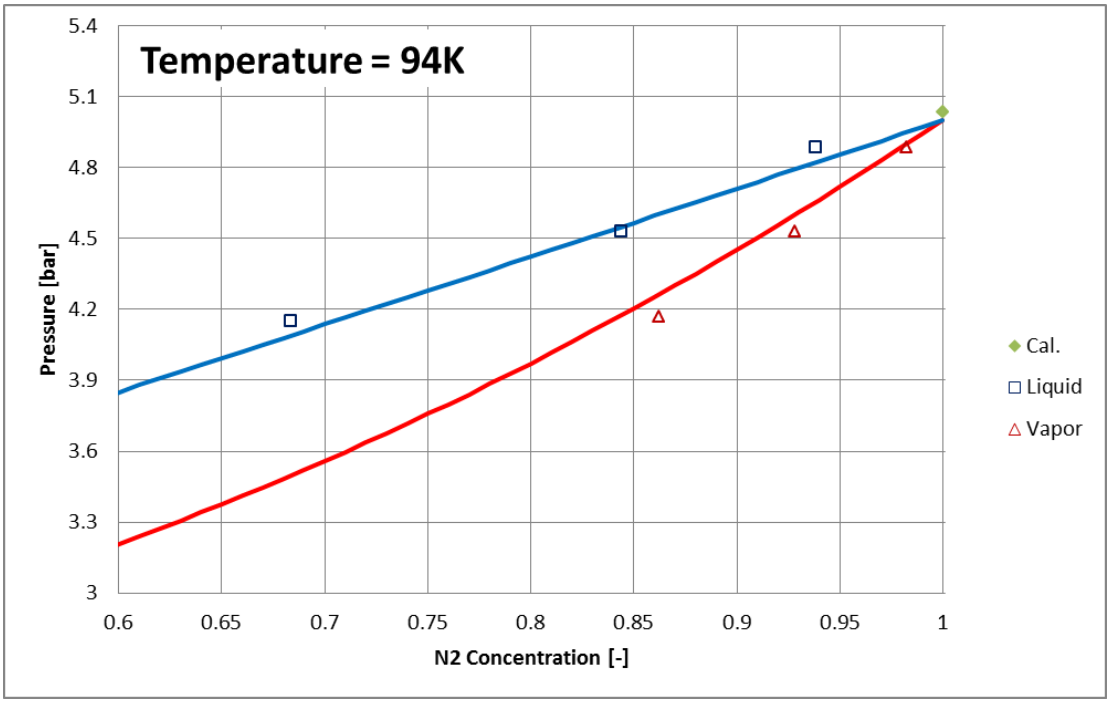

Figure 62: Experimental VLE data at 94 Kelvin

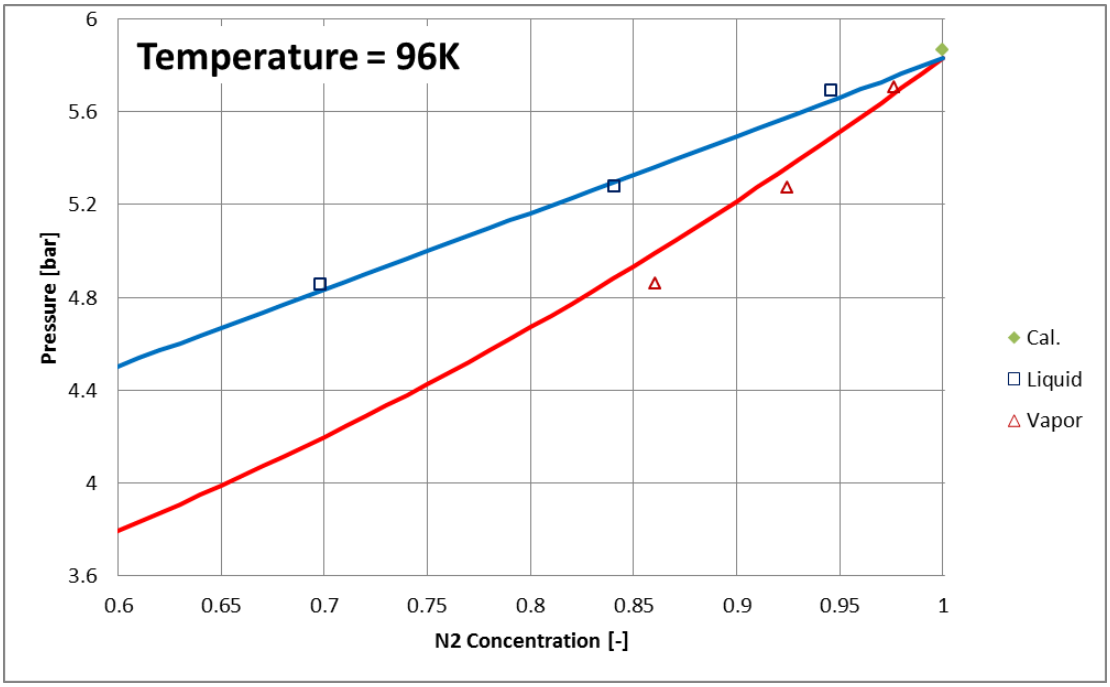

Figure 63: Experimental VLE data at 96 Kelvin

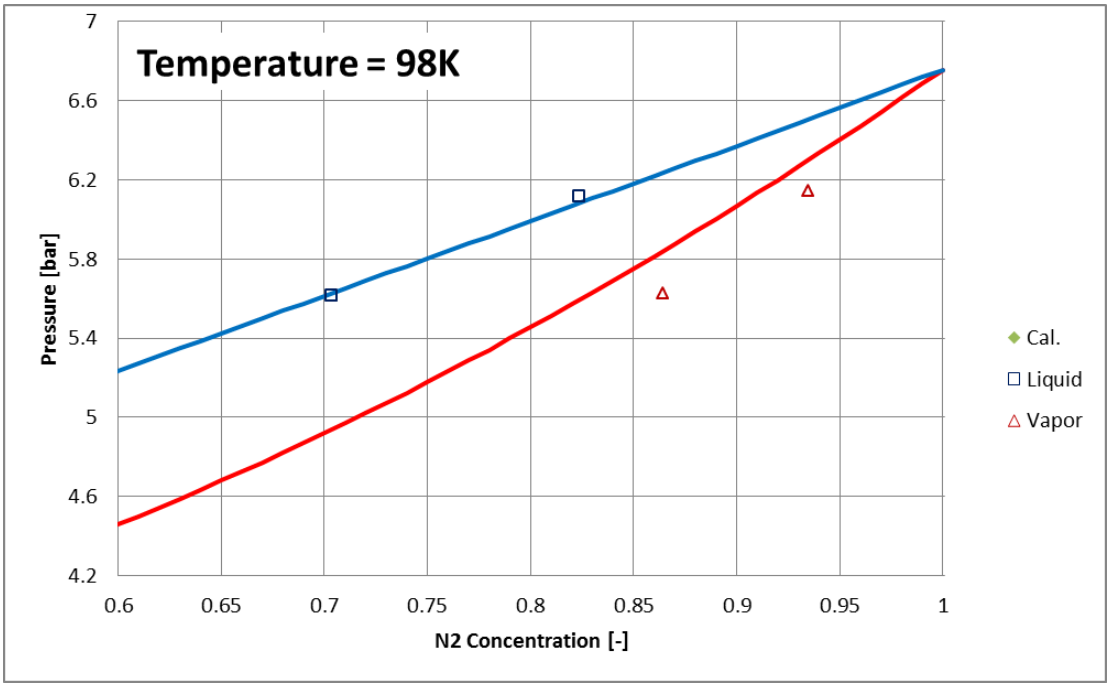

Figure 64: Experimental VLE data at 98 Kelvin

The ‘Cal’ data point is the result of the pure component validation described in the previous section. The theoretical lines on each plot indicate the composition based on temperature and pressure calculated using REFPROP and setting the temperature to what is shown on each plot.

The temperatures in each plot represent the controlled target temperatures during the experiment. The measured experimental temperature for each data point was not necessarily exactly equal to this target temperature. However, these plots still show that the experimental data generally follows the pressure-composition relationships predicted by REFPROP.

The next plots are the experimental relative volatilities versus pressure for each of the three mixtures.

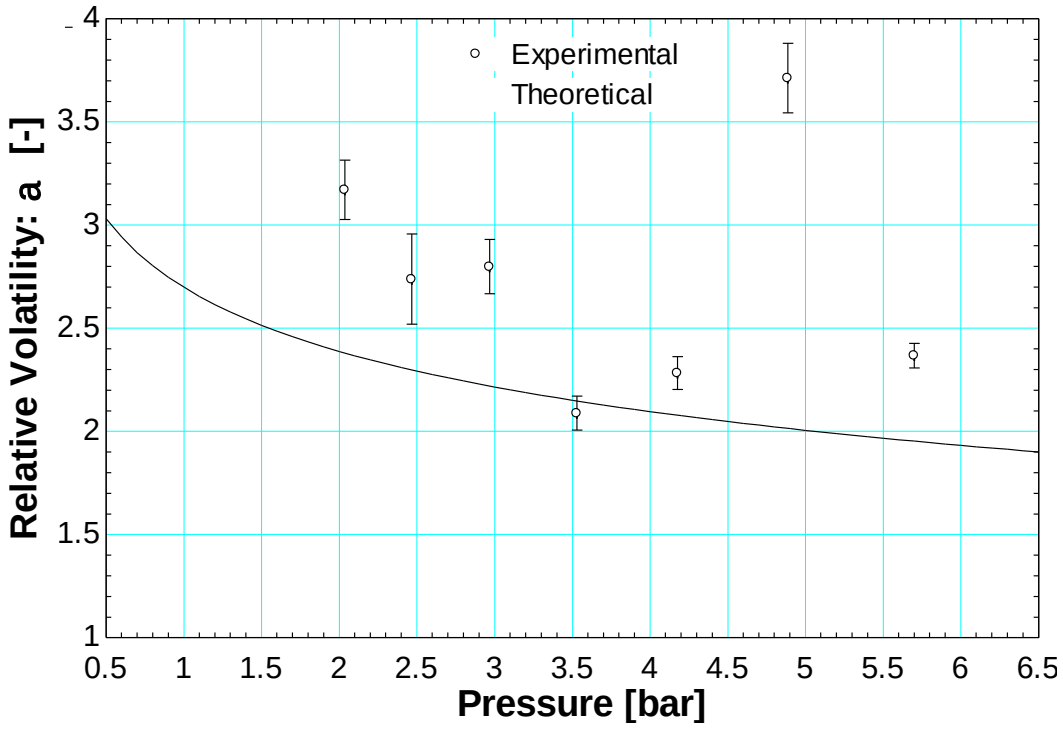

Figure 65: Relative volatility for low argon concentration mixture

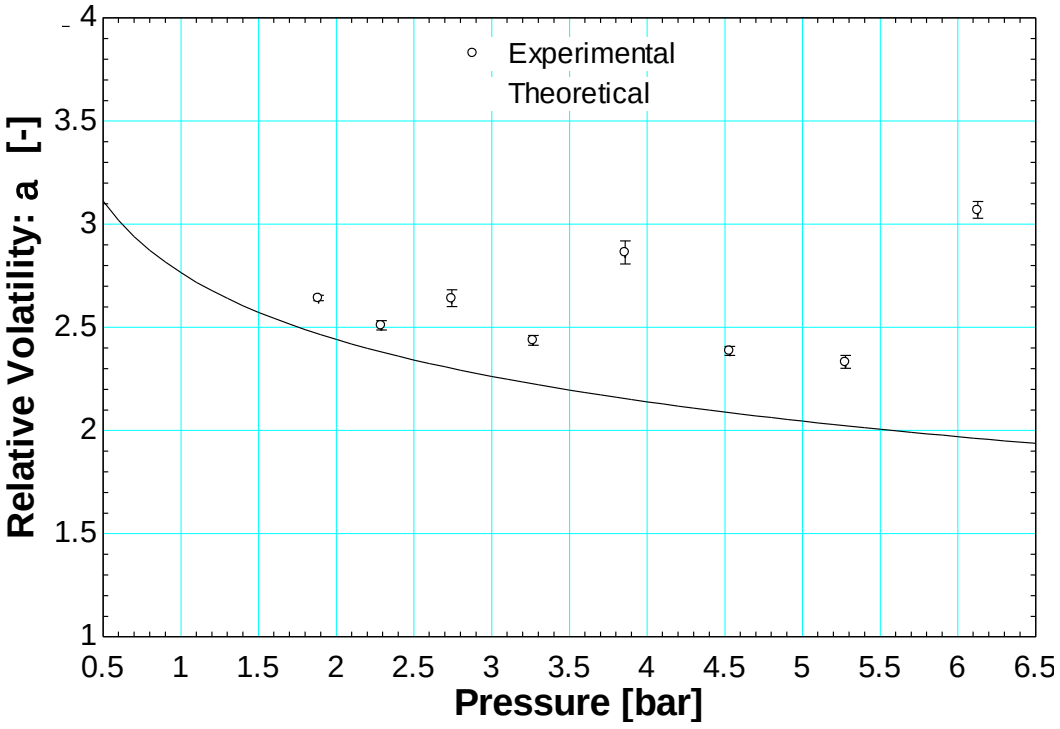

Figure 66: Relative volatility for medium argon concentration mixture

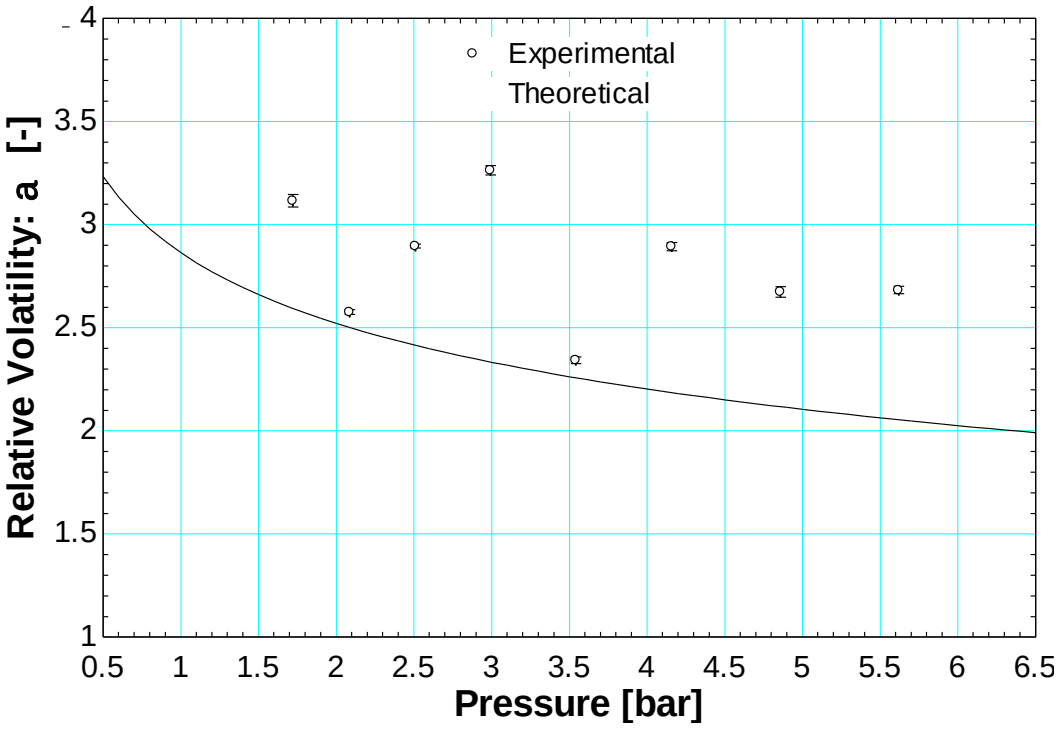

Figure 67: Relative volatility for high argon concentration mixture

In each of the three plots above, the theoretical line is determined using REFPROP. For creation of this theoretical line, the liquid phase composition was set to the average value calculated for each separate mixture and the pressure was varied.

The magnitude of the uncertainty bars in the relative volatility plots is largest in the low argon concentration mixture, and smallest in the high argon concentration mixture. The equation for relative volatility multiplies and divides the VLE compositions. For this reason, it is expected to see larger uncertainty bars in a mixture with compositions of one component approaching zero.

It is also important to note that the vapor and liquid data points were taken separately for each controlled temperature, meaning that the pressure of the second phase sampled was slightly different than the pressure of the first phase. This could help to explain some of the scatter in the relative volatility plots.

6.3 Results from April Experimental Run

The experiment was ran again briefly in April 2016. The goal of this run was to focus on the sampling technique. The only physical change made to the experiment after the February run was cleaning out the solenoid valve in the same manner that was used after the October run.

However there were some other changes. The LabVIEW code that controls the liquid sample solenoid valve was modified so that the timing of the valve open was specified to be a half of a second. Previously, this time was not quantified or consistent from sample to sample (it was based off of loop iterations within the LabVIEW VI). The sampling procedure was also modified so that the vapor and liquid samples were taken simultaneously instead of separately. The number of samples injected into the GC for each sample was varied to see how this impacted the uncertainty in the composition.

The result of this run was six separate VLE data points, all with the same base mixture and at the same target temperature. The table below summarizes the data points captured.

Table 11: VLE data from April experimental run

Temperature				Pressure		Vapor Composition				Liquid Composition			
Bottom	Top	Average	Unc.	Meas.	Unc.	Ar	N2	N_sam.	Unc.	Ar	N2	N_sam	Unc.
[K]	[K]	[K]	[±K]	[bar]	[±bar]	[-]	[-]		[±-]	[-]	[-]		[±-]
84.021	84.010	84.016	0.030	1.945	0.0027	**0.05155**	**0.94845**	**27**	0.00021	**0.13378**	**0.86622**	**26**	0.00025
83.998	84.000	83.999	0.030	1.931	0.0027	**0.05683**	**0.94317**	**11**	0.00040	**0.12505**	**0.87495**	**13**	0.00028
83.999	84.004	84.002	0.030	1.940	0.0027	**0.05254**	**0.94746**	**6**	0.00061	**0.13289**	**0.86711**	**8**	0.00067
83.999	84.000	84.000	0.030	1.944	0.0027	**0.04460**	**0.95540**	**5**	0.00065	**0.14139**	**0.85861**	**5**	0.00041
84.000	84.004	84.002	0.030	1.944	0.0027	**0.05165**	**0.94835**	**5**	0.00046	**0.14471**	**0.85529**	**5**	0.00027
84.002	84.002	84.002	0.030	1.946	0.0027	**0.04981**	**0.95019**	**5**	0.00082	**0.14936**	**0.85064**	**5**	0.00045

As expected, the pressures and compositions between samples are very close to each other. The points in this table are shown in chronological order based on when each sample was taken from

the VLE cell. An unexpected result is that the pressure does not necessarily go down after each sample is taken.

The VLE compositions are shown below in a pressure composition plot. The axes are expanded in order to magnify the differences between runs.

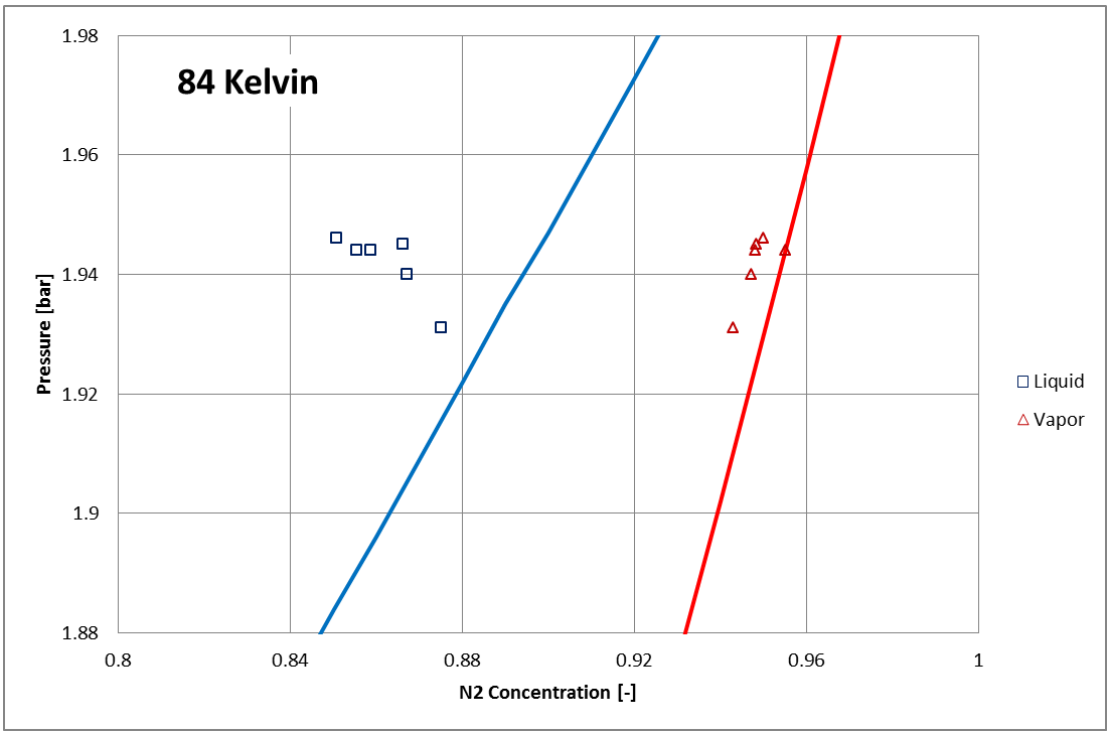

Figure 68: VLE data at 84 Kelvin for April experimental run

Examining the vapor data points, the experimental points reasonably follow the direction of the theoretical line. However, there does seem to be a systemic error resulting in a slightly high experimental pressure or a slightly low experimental temperature.

There is considerably more scatter in the liquid sample compositions. There is a slight trend in the set of liquid phase compositions, but it is heading away from, rather than toward the theoretical composition line.

Next, the relative volatilities of each VLE data point are plotted against pressure.

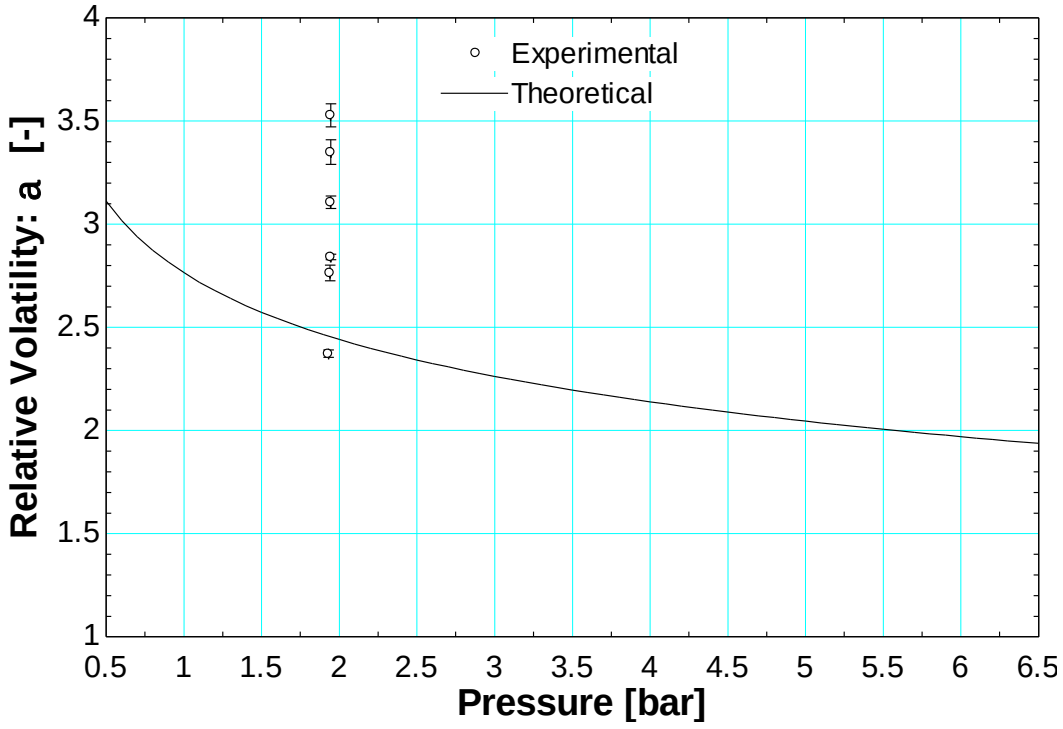

Figure 69: Relative volatilities of VLE data points at 84 Kelvin

The scatter shown in this plot comes from the inconsistent liquid phase compositions. The magnitude of the scatter shown on this plot is of the same magnitude as the scatter shown in the relative volatility plots for the February run.

Recall the equation for the relative volatility of a nitrogen–argon mixture which is shown again below.

$$\alpha = \frac{K_{N2}}{K_{Ar}} = \frac{y_{N2}/x_{N2}}{y_{Ar}/x_{Ar}}$$

If the nitrogen portion of the liquid phase is underrepresented (shown in Figure 68), the effect on the experimental relative volatility is an increase in the numerator and a decrease in the denominator. Both of these effects result in an increase in the relative volatility (shown in Figure 69).

The plot below relates the composition uncertainty to the number of samples injected through the gas chromatograph.

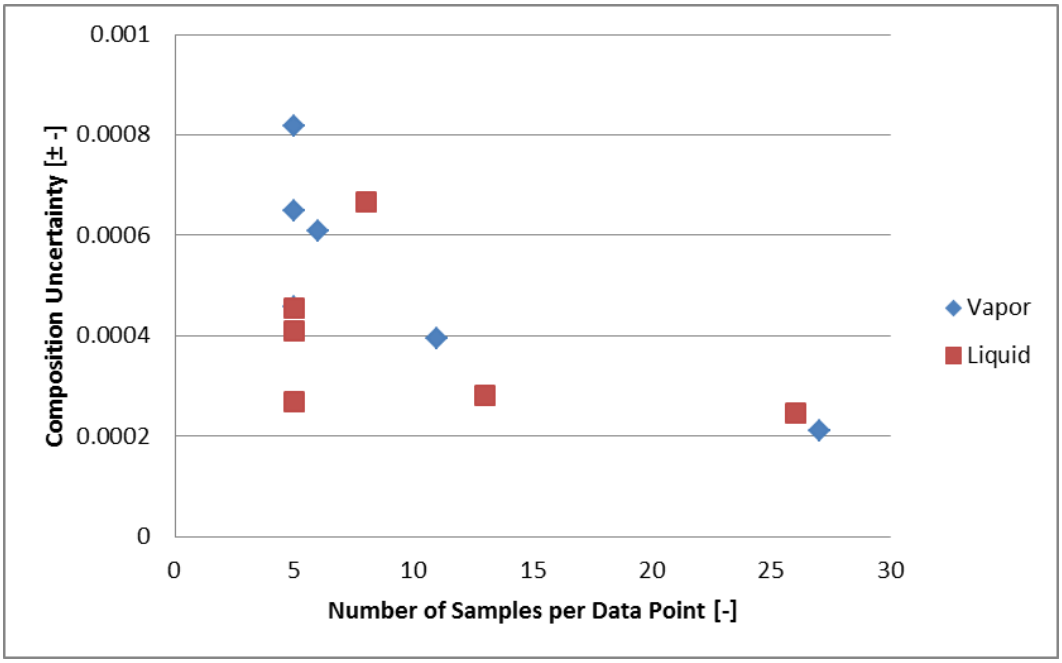

Figure 70: Composition uncertainty versus number of samples injected

As expected, the composition uncertainty is reduced as more samples are taken. However, even the maximum value of uncertainty on this plot corresponds to a composition difference of less than 0.1%. The uncertainty bars as they are do not make up the difference between experimental and theoretical for the P-xy diagrams or the relative volatility diagrams. This suggests a more systemic error in the measurements that needs to be addressed in a different way.

7. Analysis and Conclusions

7.1 Analysis

As mentioned in section 6.3, the experimental values of the relative volatility are larger than theoretically expected. However, looking at the larger set of data taken in February, the experimental relative volatility is still consistently over-predicted with our test rig. The equation for relative volatility, as well as the results presented in Section 6.3, suggests that inconsistent liquid sampling may be the reason for the high experimental values. The cryogenic solenoid valve used in this experiment did not consistently perform within specifications. With care, it could be made to be leak-tight in ambient conditions. But after cycling several times in the cold zone, it could no longer maintain vacuum on the low pressure side. The test rig used by Wilson et al. (1964) did not contain any moving parts in the cryogenic area. This may have been due to the increased maintenance requirements and decreased reliability of components like cryogenic solenoid valves.

The plot below shows the relative volatilities obtained in this experiment along with the relative volatilities computed from the data provided by Wilson et al. (1964).

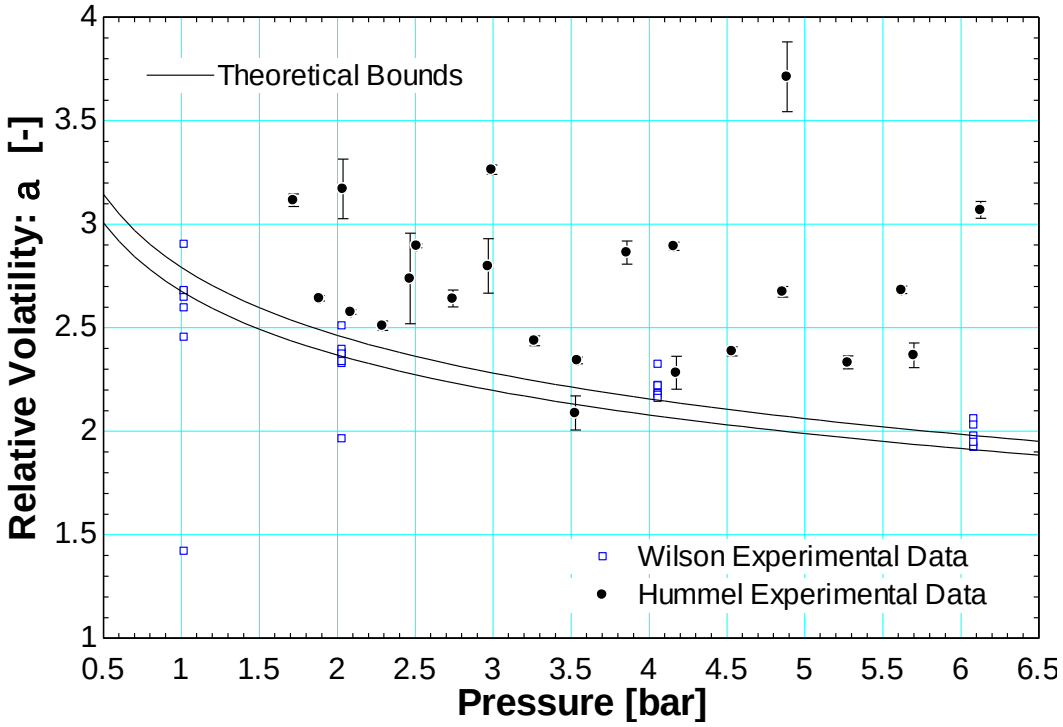

Figure 71: Experimental relative volatilities of nitrogen-argon mixtures

Both data sets have outliers. However, the Wilson data (1964) shows considerably less scatter around the theoretical bounds, and does not consistently overshoot these bounds.

The pure component validation performed in February showed a potentially systemic error in the temperature reading. All the VLE thermometers are mounted on the outside of the VLE cell. If the thermometers were moved to the inside of the VLE cell, for example by mounting the thermometers to the support for the liquid level detectors, the temperature error may be reduced.

More points of analysis include varying the time that the liquid sample solenoid valve is opened. Varying the volume of the vapor sample chamber could make the experiment more efficient. If this volume is found to have a negligible effect on the vapor composition, reducing the volume of the vapor sample chamber would be advantageous because the sampling process would have a smaller effect on the equilibrium in the cell.

The process of reaching an isothermal condition in the VLE cell was very time consuming. Moving the location of the TRS heater upwards so that it is closer to the VLE top thermometer would be a simple way to speed up this process, making it possible to obtain VLE samples more efficiently.

7.2 Conclusions

The goal of this experiment was to acquire high accuracy vapor-liquid equilibrium data for binary nitrogen-argon mixtures in the pressure range of one to six bar (resulting in 77 to 100 Kelvin).

The first objective, to design and create a system that controls and maintains steady temperature and pressure, was met. Temperature is controlled jointly by using heaters and the heat sink rod. The pressure in the VLE cell is dependent on the temperature of that cell, therefore the VLE pressure will be steady as long as the temperature is also. The compressor, bypass loop, and pressure regulators in ambient allow for several ways to add or remove mixture from the cold zone. Feedback for these ambient controls is provided by pressure and flow indicators also in ambient.

The second objective was to have the equipment and procedures that enabled high accuracy measurements. There are three measurements that go into VLE data: temperature, pressure and composition.

The combination of the platinum RTDs and the Cryo-Con Model 24C temperature controller was carefully chosen because it had the best accuracy in our temperature range of 77 to 100 Kelvin. The thermometers were calibrated, checked, and re-calibrated. A thorough analysis of the components that affect the temperature reading was conducted to quantify the total uncertainty in the temperature measurement. The uncertainty in the temperature measurement varies linearly from 29 to 33 milliKelvin in the temperature range of 75 to 105 Kelvin.

The Rosemount ‘Ultra’ performance transducer was the most accurate transducer available in our pressure range. The reading from this transducer was verified at ambient pressure using a calibrated barometric gauge in the lab. A thorough uncertainty analysis was also conducted for the components that affect the pressure measurement. The total uncertainty in the pressure measurement varies approximately linearly from 26 to 30 millibar in the pressure range of zero to six bar.

The gas chromatograph is responsible for the VLE composition data. The column and detector for our GC were specifically chosen for their ability to separate permanent gases. A reliable method for running nitrogen-argon mixtures through the GC was established early on and maintained consistently throughout the experiment. A careful calibration procedure was performed to obtain our own response factors and associated uncertainties instead of taking the theoretical RFs which were available. For each of the VLE data points, a minimum of five injections were put into the GC to provide an average composition and to ensure that our injection method was repeatable. The uncertainty in composition came from the calibration procedure and from the sample standard deviation for each data point.

The experimental run in October provided much needed insight into the complications that would come up while running this experiment. The VLE data points from this run were not reliable because of the problems that were discovered during this experimental run. Physical changes to the experiment, as well as changes to the procedure were made as a result of the October experimental run.

The experimental run in February was the longest run to date. The pure component validation was performed first and it showed that there is a systemic error in either the temperature or pressure measurements. As yet, this error is still unresolved. The experimental run in February also provided VLE data points for three separate mixtures at a range of controlled temperatures. Outliers in this data were not immediately apparent after creating T-xy diagrams for each temperature. The data from the February run was then characterized as a whole using experimental values for relative volatility. Considerable scatter, and a consistent over-prediction of the relative volatility was found, indicating room for improvement in the sampling procedure.

The experimental run in April sought to find how repeatable the sampling technique actually was. Several VLE data points of the same mixture at the same controlled temperature were taken and analyzed. The change in pressure between samples was very small. The vapor compositions taken in the April run were very close to each other and while they were not on top of the theoretical line, they displayed the same trend as the theoretical line. However, the liquid compositions showed considerably more scatter when compared to the vapor. The nitrogen content of the liquid phase was consistently under-represented. Characterizing the April data with relative volatility showed the same over-prediction of the value seen in February.

Further work on the experiment outlined in this thesis should include analysis of the liquid sampling technique to see if improvements in the VLE data, characterized by the relative volatility, are possible. The systemic error shown by the pure component validation should also be analyzed. Moving the VLE thermometers to the inside of the VLE cell may provide a more accurate representation of the equilibrium taking place, and reducing the systemic measurement error. Other improvements to reduce the time required to reach equilibrium in the VLE cell would enable more efficient analysis of VLE data.

8. References

Clark Cooper. (2014). Specialty Valves: Clark Cooper. Retrieved from clarkcooper.com/sv/specialtyvalves.html

Courts, S. S. (2002). A new cryogenic diode thermometer. *AIP Conference Proceedings*, *613*, 1620–1627. http://doi.org/10.1063/1.1472198

Cryogenic Control Systems. (2016). *User's Guide Model 24C Cryogenic Temperature Controller* (4a ed.). Rancho Santa Fe, CA.

Elliott, J. R., & Lira, C. T. (2012). *Introductory Chemical Engineering Thermodynamics, Second Edition*. Prentice Hall. Retrieved from http://books.google.co.uk/books?id=1fM0uPLZZfEC

Emerson Process Management. (2014). *Rosemount 3051S Series Product Data Sheet*. Chanhassen, MN. Retrieved from http://www2.emersonprocess.com/siteadmincenter/pm rosemount documents/00813-0100-4801.pdf

Eugene. Rosie, D. M. B. (1971). Response Prediction of the Thermal Conductivity Detector with Light Carrier Gases. *Journal of Chromatography*, *59*, 269–279.

Gislason, J., & Wharry, S. M. (2000). Relative molar response factors for thermal conductivity detectors. *Journal of Chromatographic Science*, *38*(3), 129–32. Retrieved from http://www.ncbi.nlm.nih.gov/pubmed/10702921

Grob, R. L., & Barry, E. F. (2004). *Modern Practice of Gas Chromatography* (4th ed.). Hoboken, New Jersey: John Wiley & Sons.

Klein, S., & Nellis, G. (2012). *Thermodynamics*.

Lake Shore Cryotronics. (2016). Platinum RTDs | Product Overview. Retrieved April 30, 2016, from http://lakeshore.com/products/Cryogenic-Temperature-Sensors/Platinum-RTDs/Models/Pages/Overview.aspx

Lemmon, E. W., Huber, M. L., & Mclinden, M. O. (2010). NIST Reference Fluid Thermodynamic and Transport Properties — REFPROP 9.0 user's guide.

Malanowski, S. (1982). Experimental methods for vapour-liquid equilibria. Part I. Circulation methods. *Fluid Phase Equilibria*, *8*(2), 197–219. http://doi.org/10.1016/0378-3812(82)80035-6

Myers, R. H., & Myers, S. L. (2007). *Probability & Statistics for Engineers & Scientists*. (S. Yagan, Ed.), *Education* (Vol. 6). Upper Saddle River, New Jersey: Pearson Prentice Hall. http://doi.org/10.2307/2288012

Perry, R. H., & Green, D. W. (2008). *Perry's Chemical Engineers' Handbook*. *The effects of brief mindfulness intervention on acute pain experience: An examination of individual difference* (Vol. 1). http://doi.org/10.1017/CBO9781107415324.004

Rarey, J. R., & Gmehling, J. (1993). Computer-operated differential static apparatus for the measurement of vapor-liquid equilibrium data. *Fluid Phase Equilibria*, *83*(C), 279–287. http://doi.org/10.1016/0378-3812(93)87031-U

Snow, N. (2016). Introduction to Capillary GC injection techniques. Retrieved from http://www.chromedia.org/chromedia?waxtrapp=wlqdcDsHqnOxmOlIEcClBwFjE&subNav=rwhpbjDsHqnOxmOlIEcClBwFjEQ

Wichterle, I., Linek, J., Wagner, Z., Fontaine, J. C., Sosnkowska-Kehiaian, K., & Kehiaian, H. V. (2004). *Vapor-Liquid Equilibrium in Mixtures and Solutions*. (H. V. Kehiaian, Ed.) (Vol. 13). Springer.

Wilson, G. M., Silverberg, P. M., & Zellner, M. G. (1964). *Argon-Oxygen-Nitrogen Three Component System Experimental Vapor-Liquid Equilibrium Data*. Allentown, PA.

9. Appendix

9.1 Background

Wilson et al. Nitrogen-Argon VLE Data

Table 12: Binary nitrogen-argon VLE data from Wilson et al. (1964)

Pressure	Run Number	Temperature	Liquid Mole Fraction		Vapor Mole Fraction			K_N2	K_Ar	alpha
[atm]	[-]	[°R]	N2	Ar	N2	Ar		[-]	[-]	[-]
1	1651	139.7	0.9928	0.0072	0.9973	0.0027		1.0045	0.3750	2.6788
1	1650	140	0.9822	0.0178	0.9938	0.0062		1.0118	0.3483	2.9049
1	1649	140.2	0.9623	0.0377	0.9843	0.0157		1.0229	0.4164	2.4562
1	1648	140.4	0.9373	0.0627	0.9749	0.0251		1.0401	0.4003	2.5982
1	1647	141	0.879	0.121	0.9506	0.0494		1.0815	0.4083	2.6489
1	1646	141.5	0.8457	0.1543	0.9363	0.0637		1.1071	0.4128	2.6818
1	1641	143	0.8514	0.1486	0.8907	0.1093		1.0462	0.7355	1.4223
2	1567	151.2	0.9949	0.0051	0.9974	0.0026		1.0025	0.5098	1.9665
2	1941	151.2	0.993	0.007	0.9972	0.0028		1.0042	0.4000	2.5106
2	1568	151.4	0.981	0.019	0.9919	0.0081		1.0111	0.4263	2.3717
2	1569	151.5	0.9719	0.0281	0.988	0.012		1.0166	0.4270	2.3805
2	1570	151.7	0.9529	0.0471	0.9798	0.0202		1.0282	0.4289	2.3975
2	1571	151.8	0.941	0.059	0.9738	0.0262		1.0349	0.4441	2.3304
2	1572	152.2	0.9001	0.0999	0.9547	0.0453		1.0607	0.4535	2.3391
2	1573	152.9	0.845	0.155	0.9283	0.0717		1.0986	0.4626	2.3749
4	1372	165	0.9872	0.0128	0.9941	0.0059		1.0070	0.4609	2.1847
4	1371	165.1	0.9775	0.0225	0.9902	0.0098		1.0130	0.4356	2.3257
4	1370	165.3	0.9632	0.0368	0.9828	0.0172		1.0203	0.4674	2.1831
4	1369	165.4	0.9529	0.0471	0.9778	0.0222		1.0261	0.4713	2.1771
4	1368	165.6	0.9373	0.0627	0.9708	0.0292		1.0357	0.4657	2.2240
4	1367	165.9	0.9181	0.0819	0.9614	0.0386		1.0472	0.4713	2.2218
4	1366	166.9	0.8444	0.1556	0.9214	0.0786		1.0912	0.5051	2.1602
6	1309	174.4	0.961	0.039	0.9807	0.0193		1.0205	0.4949	2.0621
6	1308	174.6	0.9522	0.0478	0.9759	0.0241		1.0249	0.5042	2.0328
6	465	174.8	0.9373	0.0627	0.9666	0.0334		1.0313	0.5327	1.9359
6	466	175.3	0.9035	0.0965	0.9474	0.0526		1.0486	0.5451	1.9237
6	467	175.8	0.8728	0.1272	0.9314	0.0686		1.0671	0.5393	1.9787
6	468	176.3	0.8395	0.1605	0.9107	0.0893		1.0848	0.5564	1.9497

9.2 Analysis of Instrumentation and Measurement Accuracy

Uncertainty in composition measurement as a result of GC calibration

The table below shows the injection volumes and integrated areas for nitrogen and argon acquired from the GC calibration.

Table 13: GC calibration results

Injection Volume [µL]	Integrated Area	
	Nitrogen	Argon
10	3115.06	3275.95
	3176.72	3285.56
	3194.10	3307.19
	3158.54	3307.15
	3285.85	3344.42
	3154.85	3246.39
	3309.73	3357.05
	3197.70	3275.32
	3210.08	3329.62
	3238.61	3322.94
20	6088.38	6321.09
	6085.85	6341.16
	5999.22	6406.91
	5939.72	6251.56
	6131.23	6389.67
	6024.20	6409.88
	6146.18	6293.81
	6042.83	6249.72
	6068.76	6240.75
	6236.81	6334.02
30	9117.89	9292.37
	8860.62	9344.86
	8931.20	9455.61
	8851.37	9370.21
	8884.90	9338.23

Injection Volume [µL]	Integrated Area	
	Nitrogen	Argon
30 (Continued)	8775.37	9412.35
	8867.30	9223.81
	8801.80	9423.88
	8926.73	9389.39
	8972.12	9324.10
40	11677.12	12169.21
	11619.34	12236.33
	11756.84	12198.65
	11795.39	12148.66
	11803.29	12260.22
	11785.45	12211.33
	11664.30	12271.21
	11661.10	12324.86
	11768.80	12272.90
	11931.26	12402.82
50	14568.83	15248.03
	14499.02	15040.33
	14607.01	15234.45
	14718.39	15152.36
	14481.67	15243.57
	14493.87	15244.83
	14514.77	15044.71
	14534.50	15162.29
	14561.68	15124.65
	14510.41	15094.47

The plot below shows the final result of a linear regression analysis.

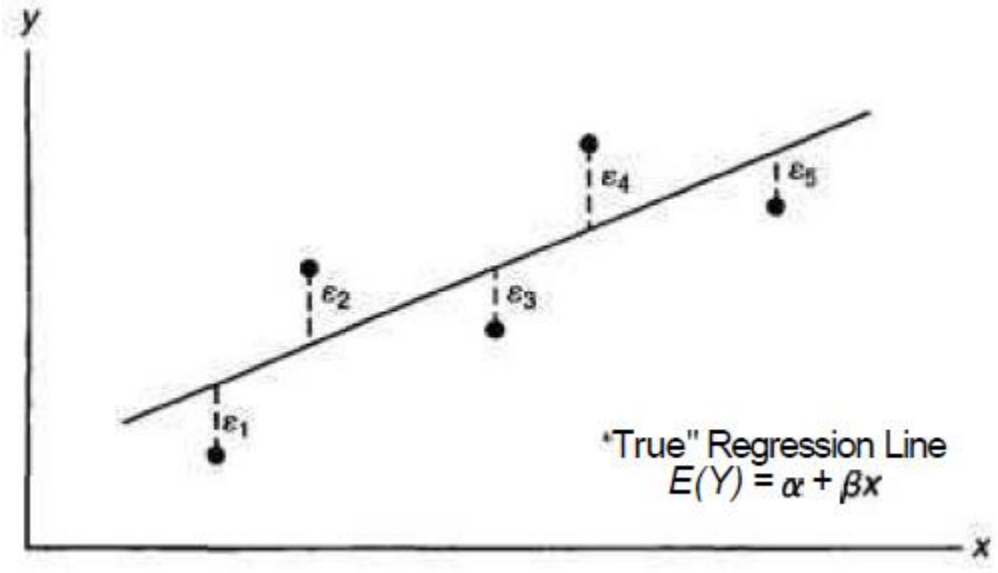

Figure 72: Linear best fit of data points from regression (Myers & Myers, 2007)

For our data, when injection volume is plotted on the y-axis, and integrated area is plotted on the x-axis, the slope of that line is equal to the response factor for each gas. From linear regression, the slope is equal to 'β'. The equations required for computation of 'β' and 'α' are shown below. A caret symbol has been added to these variables so that they are not confused with other variables discussed in this thesis.

$$\hat{\beta} = \frac{\sum_{i=1}^{N}(x_i - \bar{x})(y_i - \bar{y})}{\sum_{i=1}^{N}(x_i - \bar{x})^2}$$

$$\bar{x} = \frac{\sum_{i=1}^{N} x_i}{N} \quad ; \quad \bar{y} = \frac{\sum_{i=1}^{N} y_i}{N}$$

$$\hat{\alpha} = \bar{y} - \hat{\beta}\bar{x}$$

The code used to calculate the response factors for nitrogen and argon is shown below.

```
N = 50 [-]                                  "Number of calibration data points per component"
  "Pull calibration data from lookup table"
Duplicate i = 1, N
  vol[i] = lookup('Calibration', i, 'Vol')  "Injection volume"
    y[i] = vol[i]                           "'y' term in regression equations"
  N2Area[i] = lookup('Calibration', i, 'N2Area')  "Integrated area for nitrogen"
    x_N[i] = N2Area[i]                      "'x' term for N2 in regression equations"
  ArArea[i] = lookup('Calibration', i, 'ArArea')  "Integrated area for argon"
    x_A[i] = ArArea[i]                      "'x' term for Ar in regression equations"
End
```

```
x_bar_N = average(x_N[1..N])                    "Average value of N2 area"
x_bar_A = average(x_A[1..N])                    "Average value of Ar area"
y_bar = average(Vol[1..N])                      "Average value of injection volume"

  "Equation for slope of best fit line"
BETA_N = sum(Numerator_N[1..N])/sum(Denominator_N[1..N])
BETA_A = sum(Numerator_A[1..N])/sum(Denominator_A[1..N])
Duplicate i = 1, N
  Numerator_N[i] = (x_N[i] - x_bar_N)*(y[i] - y_bar)
  Denominator_N[i] = (x_N[i] - x_bar_N)^2
  Numerator_A[i] = (x_A[i] - x_bar_A)*(y[i] - y_bar)
  Denominator_A[i] = (x_A[i] - x_bar_A)^2
End

  "Equation for intercept of best fit line"
alpha_N = y_bar - BETA_N*x_bar_N
alpha_A = y_bar - BETA_A*x_bar_A

$CHECKUNiTS off                                 "Response factor is equal to best fit slope"
  RF_N2 = BETA_N
  RF_Ar = BETA_A
$CHECKUNITS on
```

The injection volume uncertainty of 0.5 microliters was added to every single volume data point. This uncertainty was propagated through to find the uncertainty in each response factor.

$$RF_{N2} = 0.003524745 \pm 0.000017627$$

$$RF_{Ar} = 0.003373385 \pm 0.000016870$$

By artificially setting and varying an area percentage for nitrogen, the error in response factors can be fully propagated through to the composition measurement for a full range of binary nitrogen-argon compositions data.

```
$ifnot parametric
  AP_N2 = 0.5 [-]                               "Set N2 area percentage"
$endif
AP_N2 + AP_Ar = 1.0 [-]                         "Area percentages must sum to unity"

  "Conversion of area percentage to composition"
Composition_N2 = (RF_N2*AP_N2)/(RF_N2*AP_N2 + RF_Ar*AP_Ar)
Composition_Ar = (RF_Ar*AP_Ar)/(RF_N2*AP_N2 + RF_Ar*AP_Ar)
```

An uncertainty propagation table was created varying the nitrogen area percentage from zero to one. The results from this table are shown in Figure 32.

9.3 Experimental Procedure

Prediction of liquid level in VLE cell based on pressure drop in supply tank

9.4 Results

Pure component validation – uncertainty propagation results

First, the uncertainty in each temperature measurement was propagated to find the uncertainty in the average temperature reported. The uncertainty in the average temperature came from the measurement uncertainty in each VLE thermometer, discussed in Section 4.2. The equations are results are shown below.

```
T_BOT = 81.999 [K]                          "VLE bottom temperature"
T_TOP = 82.001 [K]                          "VLE top temperature"

T = average(T_BOT, T_TOP)                   "Temperature - average of top and bottom"
u_T = .000140911*T + .018331340 [K]   "Linear fit of absolute error in the temperature measurement"
```

Parametric Table

Experimental

1..8	T_{BOT} [K]	T_{TOP} [K]	u_T [K]	T [K]
Run 1	81.9990±0.0299	82.0010±0.0299	0.02989	82±0.02113
Run 2	83.9980±0.0302	84.0010±0.0302	0.03017	84±0.02133
Run 3	85.9970±0.0304	86.0020±0.0304	0.03045	86±0.02153
Run 4	87.9980±0.0307	88.0000±0.0307	0.03073	88±0.02173
Run 5	89.9980±0.0310	90.0020±0.0310	0.03101	90±0.02193
Run 6	91.9970±0.0313	92.0010±0.0313	0.0313	92±0.02213
Run 7	93.9990±0.0316	94.0000±0.0316	0.03158	94±0.02233
Run 8	96.0000±0.0319	96.0000±0.0319	0.03186	96±0.02253

Figure 73: Uncertainty in VLE temperature measurement

The uncertainty in the pressure measurement is discussed in Section 4.3. The equation and results of the pressure uncertainty are shown below.

```
P_VLE = 1.710 [bar]                         "VLE pressure"
u_P = 6.485E-5*(P_VLE) + 0.002564 [bar]     "Linear fit of absolute error in pressure measurement"
```

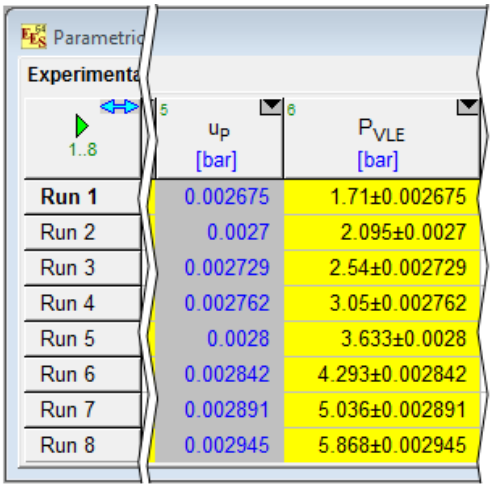

Figure 74: Uncertainty in VLE pressure measurement

The experimental values of temperature and pressure are used to find theoretical values of pressure and temperature. There is uncertainty in each of these theoretical predictions. Lastly, the experimental results are subtracted from the theoretical predictions to create the plots shown in Figures Figure 55 and Figure 56 in Section 6.2.

```
P_sat = p_sat(Nitrogen, T = T)                "Predicted sat. pressure based on avg VLE temperature"
T_sat = t_sat(Nitrogen, P = P_VLE)            "Predicted sat. temperature based on VLE pressure"

DELTAT = T_sat - T                            "Temperature difference from theoretical"
DELTAP = P_sat - P_VLE          "Pressure difference from theoretical"
```

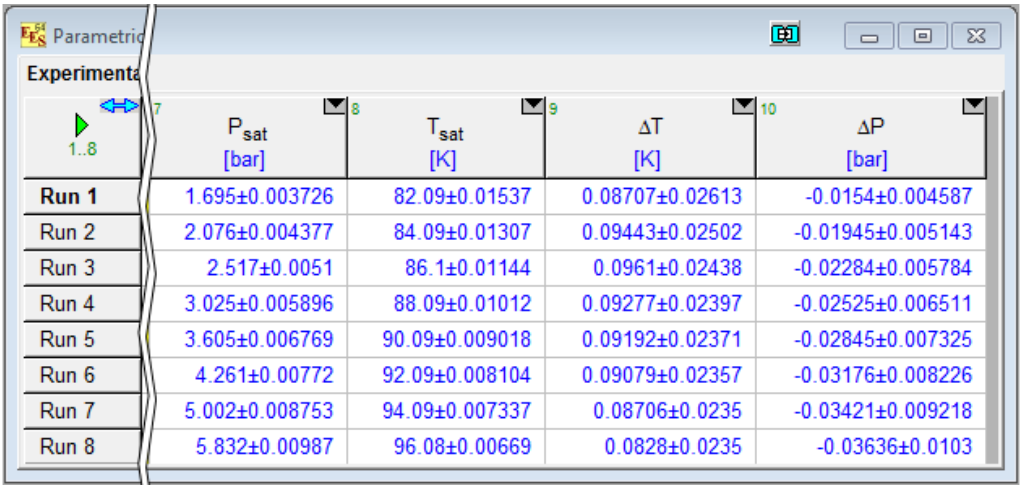

Figure 75: Uncertainty in relating experimental and theoretical saturation results

The figures below show the uncertainty break down of uncertainties in for a low temperature (or pressure) saturation value as well as a high temperature (or pressure) saturation value.

Unit Settings: SI K bar J mass deg

Variable±Uncertainty	Partial derivative	% of uncertainty
ΔP = -0.0154±0.004586 [bar]		
P_{VLE} = 1.71±0.002675 [bar]	$\partial\Delta P/\partial P_{VLE}$ = -1	34.01 %
T_{BOT} = 81.9990±0.0299 [K]	$\partial\Delta P/\partial T_{BOT}$ = 0.0882	32.99 %
T_{TOP} = 82.0010±0.0299 [K]	$\partial\Delta P/\partial T_{TOP}$ = 0.0882	32.99 %
ΔT = 0.08707±0.02595 [K]		
P_{VLE} = 1.71±0.002675 [bar]	$\partial\Delta T/\partial P_{VLE}$ = 5.634	33.71 %
T_{BOT} = 81.9990±0.0299 [K]	$\partial\Delta T/\partial T_{BOT}$ = -0.5000	33.15 %
T_{TOP} = 82.0010±0.0299 [K]	$\partial\Delta T/\partial T_{TOP}$ = -0.5000	33.15 %

Figure 76: Uncertainty results at low temperature

Unit Settings: SI K bar J mass deg

Variable±Uncertainty	Partial derivative	% of uncertainty
ΔP = -0.02636±0.0103 [bar]		
P_{VLE} = 5.858±0.002944 [bar]	$\partial\Delta P/\partial P_{VLE}$ = -1	8.17 %
T_{BOT} = 96.0000±0.0319 [K]	$\partial\Delta P/\partial T_{BOT}$ = 0.2191	45.92 %
T_{TOP} = 96.0000±0.0319 [K]	$\partial\Delta P/\partial T_{TOP}$ = 0.2191	45.92 %
ΔT = 0.06007±0.0235 [K]		
P_{VLE} = 5.858±0.002944 [bar]	$\partial\Delta T/\partial P_{VLE}$ = 2.275	8.12 %
T_{BOT} = 96.0000±0.0319 [K]	$\partial\Delta T/\partial T_{BOT}$ = -0.5000	45.94 %
T_{TOP} = 96.0000±0.0319 [K]	$\partial\Delta T/\partial T_{TOP}$ = -0.5000	45.94 %

Figure 77: Uncertainty results at high temperature